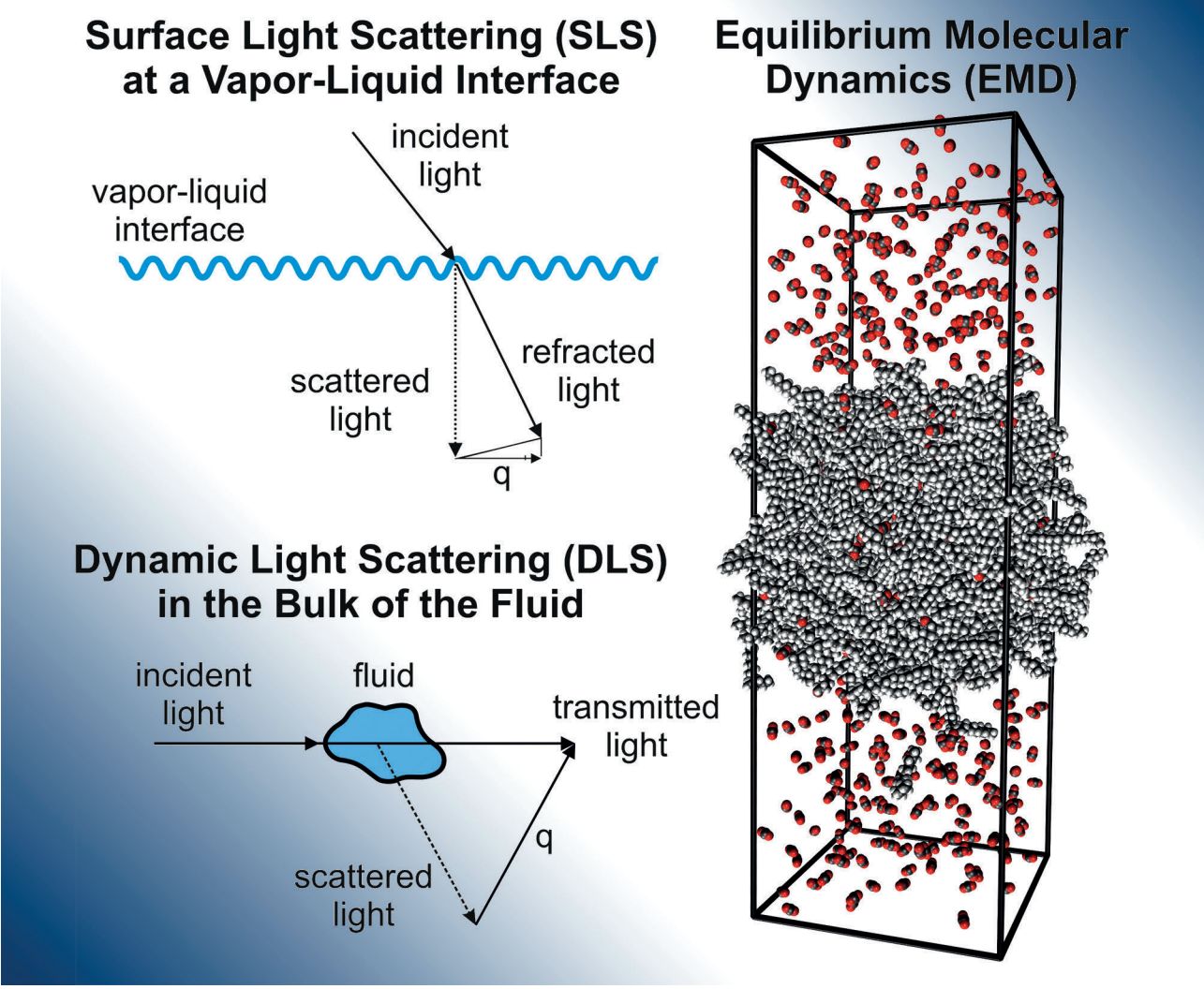

FAU Studies Chemical and Biological Engineering 1

Tobias Klein

Thermophysical Properties of Liquids with Dissolved Gases as Working Fluids in Chemical and Energy Engineering

FAU University Press

Tobias Klein

Thermophysical Properties of Liquids with Dissolved Gases as Working Fluids in Chemical and Energy Engineering

FAU Studies Chemical and Biological Engineering

Band 1

Herausgeber/-innen:

Prof. Dr. Kathrin Castiglione
Prof. Dr.-Ing. habil. Andreas Paul Fröba

Tobias Klein

Thermophysical Properties of Liquids with Dissolved Gases as Working Fluids in Chemical and Energy Engineering

Erlangen
FAU University Press
2023

Bibliografische Information der Deutschen Nationalbibliothek:
Die Deutsche Nationalbibliothek verzeichnet diese Publikation in der Deutschen Nationalbibliografie; detaillierte bibliografische Daten sind im Internet über http://dnb.d-nb.de abrufbar.

Bitte zitieren als
Klein, Tobias. 2023. *Thermophysical Properties of Liquids with Dissolved Gases as Working Fluids in Chemical and Energy Engineering.* FAU Studies Chemical and Biological Engineering Band 1. Erlangen: FAU University Press. DOI: 10.25593/978-3-96147-646-6.

Das Werk, einschließlich seiner Teile, ist urheberrechtlich geschützt.
Die Rechte an allen Inhalten liegen bei ihren jeweiligen Autoren.
Sie sind nutzbar unter der Creative-Commons-Lizenz BY.

Der vollständige Inhalt des Buchs ist als PDF über den OPUS-Server der Friedrich-Alexander-Universität Erlangen-Nürnberg abrufbar:
https://opus4.kobv.de/opus4-fau/home

Verlag und Auslieferung:
FAU University Press, Universitätsstraße 4, 91054 Erlangen

Druck: Docupoint

ISBN: 978-3-96147-645-9 (Druckausgabe)
eISBN: 978-3-96147-646-6 (Online-Ausgabe)
ISSN: 2940-6986
eISSN: 2940-6994
DOI: 10.25593/978-3-96147-646-6

Thermophysical Properties of Liquids with Dissolved Gases as Working Fluids in Chemical and Energy Engineering

Thermophysikalische Stoffeigenschaften von Flüssigkeiten mit darin gelösten Gasen als Arbeitsfluide in der Chemie- und Energietechnik

Der Technischen Fakultät der
Friedrich-Alexander-Universität Erlangen-Nürnberg

zur Erlangung des Doktorgrades Dr.-Ing.

vorgelegt von
Tobias Klein, M. Sc.,

Als Dissertation genehmigt
von der Technischen Fakultät
der Friedrich-Alexander-Universität Erlangen-Nürnberg (FAU)
Tag der mündlichen Prüfung: 28.01.2022

Gutachter: Prof. Dr.-Ing. habil. Andreas Paul Fröba
Prof. Dr.-Ing. habil. Jadran Vrabec

Acknowledgement

The present thesis was conducted at the Institute of Advanced Optical Technologies - Thermophysical Properties (AOT-TP) in the Department of Chemical and Biological Engineering (CBI) and the Erlangen Graduate School in Advanced Optical Technologies (SAOT) of the Friedrich-Alexander-Universität Erlangen-Nürnberg (FAU). It was financially supported by the German Research Foundation through the projects FR 1709/11-1 and FR 1709/15-1. Furthermore, I want to gratefully acknowledge support by the Erlangen Graduate School in Advanced Optical Technologies (SAOT) funded by the Bavarian State Ministry for Science and Art and the computing resources and support provided by the Erlangen Regional Computing Center (RRZE).

First of all, I would like to thank my doctoral advisor Prof. Dr.-Ing. habil. Andreas Paul Fröba for the possibility to perform my doctoral thesis at his research institute. During this time, he supported me by motivating and challenging me and provided the scientific opportunities and freedoms for my research activities. I would also like to thank Dr.-Ing. Thomas M. Koller, who was my advisor during the first years of my time as a doctoral candidate and has taught me many things, while giving me enough freedom to bring in my own ideas. Furthermore, I want to thank Dr.-Ing. Michael H. Rausch for his help and guidance, who has greatly contributed to the scientific outcome through his great experience.

I am very grateful for all team members of AOT-TP, who have helped to create a pleasant atmosphere. I would like to specially thank Maritta Lechler for her support over the years and Frances D. Lenahan, who has not only contributed to various scientific project, but also became a great friend. A special thank you goes also to all students, who have contributed to the various scientific project over the years.

I would like to thank Prof. Dr.-Ing. habil. Jadran Vrabec for agreeing to review my thesis.

Finally, a very special thank you goes Lara, Henry, and my parents for supporting and motivating me in my professional and private dreams and passions.

Abstract

The present thesis aims to get a fundamental understanding of how the molecular characteristics of a solute and solvent influence the thermophysical properties of mixtures consisting of a liquid and a dissolved gas. Due to their relevance as working fluids in chemical and energy engineering, accurate data for the viscosity, interfacial tension, and mutual diffusion coefficient are required for the efficient design and optimization of related processes. In this work, light scattering experiments, which can determine the thermophysical properties in macroscopic thermodynamic equilibrium, are combined with equilibrium molecular dynamics (EMD) simulations at temperatures up to 573 K. EMD simulations are able to predict multiple thermophysical properties by the analysis of the molecular motion in macroscopic thermodynamic equilibrium. The combination of EMD simulations with light scattering experiments allows for the validation of simulations as well as an interpretation of the results by studying the influence of molecular characteristics and the fluid structure on the thermophysical properties.

The solvents investigated in this work by the experiments and simulations include linear and branched alkanes and alcohols as well as ionic liquids. The solutes include different gases with varying molecular size, weight, and polarity. For the pure solvents, a force field (FF) from the literature was modified on the basis of experimental density data, to improve the predictive capabilities of EMD simulations up to temperatures of 573 K. Using the modified FF, the viscosity and interfacial tension could be predicted with an average absolute relative deviation (AARD) from experimental correlations of (17 and 11)%. The influence of the solute characteristics on the viscosity and interfacial tension is investigated through experiments for six systems consisting of n-hexadecane with a dissolved gas. EMD simulations using the modified FF could predict the influence of the dissolved gas over the entire temperature range for the interfacial tension, when compared to the interfacial tension of *n*-hexadecane from EMD simulations. However, there was a consistent offset from the experimental results. For the viscosity, predicting the influence of the gas at low temperatures failed due to the inability of the FF to accurately predict the viscosity. Structure-property relationships, for example between the surface enrichment of the gases and the interfacial tension of the mixture, could help to get a fundamental understanding of how the solvent and solute characteristics influence the thermophysical properties. In the case of the mutual diffusion coefficient,

the results from the simulations and experiments for mixtures consisting of a liquid with a dissolved gas agree with an AARD of about 14% and are often within combined uncertainties. Here, the results from experiments and simulations were used for the development of a prediction model for the mutual diffusion coefficient at the limit of infinite dilution of the dissolved gas, which was able to predict the diffusion coefficient with an AARD of 12%.

Kurzdarstellung

Die vorliegende Arbeit hat das Ziel, zu einem grundlegenden Verständnis beizutragen, wie molekulare Eigenschaften gelöster Stoffe und Lösungsmittel die thermophysikalischen Eigenschaften von Mischungen aus einer Flüssigkeit und gelöstem Gas beeinflussen. Aufgrund ihrer Bedeutung als Arbeitsfluide in der Chemie- und Energietechnik sind genaue Daten zu Viskosität, Grenzflächenspannung und Diffusionskoeffizienten für die effiziente Auslegung und Optimierung von Prozessen erforderlich. In dieser Arbeit werden Lichtstreuexperimente und molekulardynamische Simulationen im makroskopischen thermodynamischen Gleichgewicht (equilibirum molecular dynamics simulations, EMD simulations) zur Bestimmung thermophysikalischer Eigenschaften kombiniert und bei Temperaturen bis zu 573 K angewandt. Mittels EMD-Simulationen können mehrere thermophysikalische Eigenschaften durch die Analyse der Molekülbewegungen im makroskopischen thermodynamischen Gleichgewicht vorhergesagt werden. Die Kombination von EMD-Simulationen mit Lichtstreuexperimenten ermöglicht einerseits die Validierung der Simulationen, andererseits die Interpretation der Ergebnisse hinsichtlich des Einflusses der molekularen Eigenschaften und der Fluidstruktur auf die thermophysikalischen Eigenschaften.

Die in dieser Arbeit untersuchten Lösungsmittel umfassen lineare und verzweigte Alkane und Alkohole sowie ionische Flüssigkeiten. Die gelösten Stoffe umfassen verschiedene Gase mit unterschiedlicher Molekülgröße, Masse und Polarität. Für die reinen Lösungsmittel wurde ein Kraftfeld (FF) aus der Literatur auf Basis experimenteller Dichtedaten modifiziert, um die Vorhersagefähigkeit von EMD-Simulationen für Temperaturen bis 573 K zu verbessern. Mit dem modifizierten FF konnten Viskosität und Grenzflächenspannung mit einer mittleren absoluten relativen Abweichung (average absolute relative deviation, AARD) von den experimentellen Korrelationen von (17 und 11)% vorhergesagt werden. Mit Experimenten an sechs Systemen bestehend aus *n*-Hexadekan mit darin gelösten Gasen wurde der Einfluss der Eigenschaften des gelösten Stoffes auf die Viskosität und Grenzflächenspannung untersucht. Im Fall der Grenzflächenspannung waren EMD-Simulationen mit dem modifizierten FF in der Lage, den Einfluss des gelösten Gases im Vergleich zur Grenzflächenspannung von n-Hexadekan über den gesamten Temperaturbereich vorherzusagen. Sie zeigten jedoch eine systematische Abweichung zu den experimentellen Ergebnissen. Die Viskosität konnte durch das FF nur mit einer Unsicherheit

von circa 25% vorhergesagt werden, weswegen keine Vorhersage des Einflusses des Gases bei niedrigen Temperaturen möglich war. Mit Hilfe von EMD-Simulationen war es möglich, Struktur-Eigenschafts-Beziehungen, beispielsweise zwischen der Oberflächenanreicherung der Gase und der Grenzflächenspannung des Gemisches, zu aufzustellen, um ein grundlegendes Verständnis für den Einfluss der Molekülgeometrie auf die Stoff–eigenschaften zu entwickeln. Die Ergebnisse für den Diffusionskoeffizienten für Gemische bestehend aus einer Flüssigkeit mit einem darin gelösten Gas aus Simulationen stimmen mit den Experimenten mit einem AARD von etwa 14% überein und liegen oft innerhalb kombinierter Unsicherheiten. Die Ergebnisse aus den Experimenten und Simulationen wurden zur Entwicklung eines Vorhersagemodells für den Diffusionskoeffizienten im Bereich der unendlichen Verdünnung des gelösten Gases verwendet. Dieses Modell ist in der Lage den Diffusionskoeffizienten mit einem AARD von 12% vorherzusagen.

Table of Contents

Symbols, Indices, and Abbreviations

Latin symbols

A	unit area	m^2
a	thermal diffusivity	$m^2 \cdot s^{-1}$
a_g	fitting parameter for correlation function (CF)	
b_o	equilibrium bond length	m
b_g	fitting parameter for CF	
c	concentration	$mol \cdot m^{-3}$
c_S	speed of sound	$m \cdot s^{-1}$
c_g	fitting parameter for CF	
d	distance	m
D_1	self-diffusion coefficient of component 1	$m^2 \cdot s^{-1}$
D_{11}	binary diffusion coefficient	$m^2 \cdot s^{-1}$
$Đ_{12}$	Maxwell-Stefan diffusion coefficient	$m^2 \cdot s^{-1}$
F	force	N
G	Gibbs energy	J
$g^{(2)}(t)$	normalized second-order CF of the scattered light intensity	
$g_{ij}(r)$	radial distribution function between species i and j	
$H_{i,j}$	Henry constant	MPa
I	light intensity	$W \cdot m^{-2}$
j	molar flux density	$mol \cdot m^{-2} \cdot s^{-1}$
k_I	modulus of wave vector of the transmitted light	m^{-1}
k_S	modulus of wave vector of the scattered light	m^{-1}
L	length	m

M	molar mass	$kg \cdot mol^{-1}$
N	number of atoms or molecules	
N_A	Avogadro constant	mol^{-1}
k	coverage factor	
p	pressure	MPa
q	modulus of the scattering vector	m^{-1}
q_i	partial charge of atom i	C
r	position	m
r_{ij}	distance between species i and j	m
T	temperature	K
t	time	s
U	potential energy	J
V	volume	m^3
v	velocity	$m \cdot s^{-1}$
x	x-coordinate	
x_i	mole fraction of component i	
y	y-coordinate	
z	z-coordinate	

Greek symbols

Γ	damping coefficient	s^{-1}
Γ_{11}	thermodynamic factor	
$\Gamma_i^{(j)}$	adsorption of component i relative to component j	$mol \cdot m^{-2}$
γ	activity coefficient	
λ	thermal conductivity	$W \cdot m^{-1} \cdot K^{-1}$
ε_{ii}	energy parameter of LJ potential	$J \cdot mol^{-1}$
ε_o	permittivity in vacuum	$J \cdot V^{-2} \cdot m^{-1}$

η	dynamic viscosity	Pa·s
Θ	angle	rad
Θ_I	incident angle	rad
Θ_S	scattering angle	rad
Θ_o	equilibrium bending angle	rad
λ	wavelength	m
ν	kinematic viscosity	$m^2 \cdot s^{-1}$
ρ	density	$kg \cdot m^{-3}$
ρ_N	number density	m^{-3}
σ	surface tension	$N \cdot m^{-1}$
σ_{ij}	size parameter of LJ potential	m
τ	time	s
τ_{xy}	shear stress	Pa
τ_C	correlation time	s
χ	dihedral angle	rad
ω	angular frequency	$rad \cdot s^{-1}$

Abbreviations

AA	all-atom
AARD	average absolute relative deviation
CF	correlation function
CG	coarse grained
DLS	dynamic light scattering
DMIM	1-decyl-3-methylimidazolium
EMD	equilibrium molecular dynamics
EMIM	1-ethyl-3-methylimidazolium
FF	force field

GROMACS	Groningen Machine for Chemical Simulations
HMIM	1-hexyl-3-methylimidazolium
HMN	heptamethylnonane
IL	ionic liquid
L-OPLS	Optimized Potential for Liquid Simulations for Long Hydrocarbons
LJ	Lennard-Jones
MC	Monte-Carlo
MD	molecular dynamics
MSD	mean square displacement
NMR	nuclear magnetic resonance
NTf_2	bis(trifluoromethylsulfonyl)imide
OPLS	Optimized Potential for Liquid Simulations
PME	particle mesh Ewald
QM	quantum mechanics
SLS	surface light scattering
TraPPE	Transferable Potential for Phase Equilibria
UA	united atom
VLE	vapor-liquid equilibrium
VLLE	vapor-liquid-liquid equilibrium

Indices

o	time origin
c	related to concentration fluctuations
calc	calculated
exp	experiments
t	related to temperature fluctuations

1 Introduction

Systems consisting of liquids with dissolved gases are important working fluids in many areas of chemical and energy engineering. Such systems are formed whenever a liquid phase comes into contact with a vapor or gas phase, and the gas molecules are absorbed into the liquid. Prominent examples can be found in applications related to the utilization of synthesis gas, i.e. a mixture of hydrogen (H_2) and carbon monoxide (CO). Synthesis gas is used, for example, for the synthesis of methanol [1] or dimethyl ether [2]. When the synthesis gas is produced from renewable primary energy sources, green fuels in the form of liquid hydrocarbons can be synthesized via the catalytic Fischer-Tropsch process [3]. For all examples, the catalytic reaction in the liquid phase has many benefits, such as a good control of the catalyst temperature [1-2,4]. The working fluids for such processes, however, are multicomponent mixtures that consist of liquids with dissolved gases. Other applications where liquids with dissolved gases are important working fluids, can be found in the separation of gases, e.g., CO_2 separation from flue gas using supported ionic liquid (IL) membranes [5], refrigeration applications using absorption refrigerators [6], fuel injection and combustion where fuels contain dissolved gases to improve the atomization behavior of the injected fuel [7], or enhanced oil recovery technologies where light gases such as CO_2 are injected into an oil reservoir to increase the amount of recoverable oil [8].

For the evaluation and design of such applications, detailed knowledge of the thermophysical properties of the working fluids is required. This includes the equilibrium and transport properties of the pure components and their mixtures with and without dissolved gases over a wide range of thermodynamic states. In particular, transport properties like viscosity and mutual diffusivity, but also equilibrium properties like surface or interfacial tension are of interest for the design of applications and apparatuses, as shown by their frequent occurrence in dimensionless numbers describing heat and mass transfer as well as fluid dynamics. Viscosity, which is used to describe momentum transport, influences heat and mass transfer, as well as the flow behavior of fluids, and determines the power requirements of pumps and mixers. In particular, the occurrence of the dimensionless Reynolds number can be mentioned here, where the viscosity of the fluid, besides the flow speed and the characteristic length, determines whether a fluid has a laminar or turbulent flow profile. The interfacial tension influences heat and mass transfer across phase boundaries and is required in

many technical applications such as wetting, coating, and drying processes. In engineering applications, such as spray injection or bubble column reactors, the interfacial tension enters the dimensionless Bond number used to describe the size distribution of gas bubbles [9], or the Weber number used to study the break-up of sprays into smaller bubbles. The mutual diffusion coefficient is used to describe mass transport due to a concentration or chemical potential gradient. Especially in chemical reactions, where large concentration profiles occur due to the conversion of reactants into products, diffusive mass transport has been shown to be a limiting factor for the overall reaction rate [4].

Experimental data for the above properties are still scarce for mixtures consisting of liquids with dissolved gases and are often limited to small compounds and to a moderate temperature range. For the example of linear *n*-alkanes, more than 110 datasets are available for the liquid viscosity of *n*-hexane (*n*-C_6H_{14}) [10]. However, only nine of these datasets exceed a temperature of 450 K, which is the lower limit of the low-temperature Fischer-Tropsch process [3]. For the longer *n*-alkane *n*-octacosane (*n*-$C_{28}H_{58}$), only three experimental datasets are available in the literature [11-13], and for *n*-tetracontane (*n*-$C_{40}H_{82}$), the experimental data for liquid viscosity are presented for the first time in this work [14]. For the viscosity of systems consisting of liquids with dissolved gases, the data situation is even more scarce. For the solvent *n*-hexane, only the dataset of Berstad [15], who studied mixtures of *n*-hexane with dissolved methane, is available in the literature, aside from the data for a binary mixture of *n*-hexane with dissolved CO_2 shown in this work [16]. For interfacial tension, the data situation is comparable to that for liquid viscosity with most experimental studies for short molecules [17], few data for larger molecules [14], and only exemplary studies for liquids with dissolved gases [18]. For the mutual diffusion coefficient, most experimental studies focus on binary liquid mixtures of alkanes [19], 1-alcohols [20], or binary mixtures of alkanes or 1-alcohols with toluene [21-22]. For systems consisting of liquids with dissolved gases, most experimental studies have been performed for binary mixtures of IL with CO_2 [23-24], ammonia (NH_3) [25], and refrigerants [26].

The current data situation clearly shows that there is still a lack of experimental data for systems consisting of liquids with dissolved gases. In addition, there are few data for higher temperatures above about 450 K, which are relevant for many technical applications. Due to the large number of different combinations of liquids with dissolved gases, together with a large range of thermodynamic states, which are of interest for different technical applications, the experimental investigations have to be combined with

modeling approaches such as simulations and prediction models. Although prediction models for viscosity [27-28], interfacial tension [29-30], and mutual diffusion coefficient [31-32] exist, they are limited by the database of available experimental data used to develop and test the predictive models. For example, the correlation developed by Wilke and Chang [31] predicted the 155 binary diffusion coefficients in dilute solutions with an average absolute relative deviation (AARD) of 12%. However, when applied to systems of *n*-alkanes with dissolved gases at infinite dilution, which was not available in 1955 when the original model was developed, an AARD of over 100% from experimental data was found [33]. This shows that in order to develop a model that can be applied to a wide range of different solute and solvent classes, a database with a systematic variation of solute and solvent molecules is required.

In addition to empirical or semi-empirical prediction models, molecular or atomistic, simulation approaches have been developed in recent years, driven by the constant increase in computing capacities. Here, one can distinguish between ab-initio quantum calculations at the electron level [34], atomistic models [35], and united-atom approaches [36-37] that combine multiple atoms within a virtual interaction site. Molecular dynamics (MD) simulations, based on either atomistic or united-atom approaches to describe inter- and intramolecular interactions between atoms or interaction sites, model the discrete-time motion of atoms and molecules using pairwise potential functions between atoms or interaction sites, called force field (FF), in combination with Newton's equations of motion [38-40]. By analyzing the spatially and temporally resolved position of atoms and molecules, multiple thermophysical properties can be accessed simultaneously, making MD simulations a valuable tool in thermophysical properties research today. However, the accuracy of the predicted properties strongly depends on the underlying FF. Since many of the FFs available in the literature were developed for small molecules and temperatures close to ambient conditions, the predicted properties may show large deviations from experimental reference data when the FF is transferred to larger compounds or high temperatures [33,41-42]. Moreover, only equilibrium properties are often considered in the development of such FFs [35-36,43-46], which leads to very large deviations up to more than 60% for transport properties such as viscosity [41,44,47-48]. However, to improve the predictive power of MD simulations by modifying the underlying FFs, reliable experimental data with low uncertainties are required. The study of systems consisting of liquids with dissolved gases is currently limited by the amount of literature data available to verify the simulations. Therefore, most

studies focus on the determination of the self-diffusion coefficient [47-51] or viscosity [52-54] of mainly CO_2 in alkanes, ILs, or water (H_2O). In addition to predicting thermophysical properties, MD simulations provide insight into the fluid structure at the molecular level [38-39]. This can be used to gain a fundamental understanding of how the fluid structure affects thermophysical properties, for example, by analyzing the composition at the vapor-liquid interface of a binary mixture, which directly affects the interfacial tension [55-57].

This overview clearly shows that accurate experimental data are needed for systems consisting of liquids with dissolved gases. To gain a fundamental understanding of how the dissolved gases affect the thermophysical properties of the liquids, a systematic variation of both the solute and solvent molecules, as well as a wide range of temperatures, are particularly required but are still lacking in the literature. Furthermore, such a database is essential for the development and verification of theoretical models for the prediction of thermophysical properties. To predict thermophysical properties using a computational approach such as MD simulations, the underlying FFs for the solvent molecules still need to be refined for the transferability to large molecule sizes and high temperatures. Therefore, experimental results on the thermophysical properties of the pure solvents are also needed. To verify the simulations for systems consisting of liquids with dissolved gases, additional experimental data for the mixtures are required. MD simulations, on the other hand, are a valuable addition to experiments in thermophysical property research since they can be applied to extreme thermodynamic states, such as large temperature and pressures, or in the presence of potentially harmful substances where experiments can only hardly be realized.

This cumulative dissertation aims to develop a fundamental understanding how the molecular characteristics of the solvent and solute molecules influence the thermophysical properties of liquids with dissolved gases that are relevant as working media in chemical and energy engineering. Therefore, the viscosity, surface tension, and mutual diffusion coefficient of systems consisting of liquids with dissolved gases, the pure solvents, as well as the solvent mixture, is determined by light scattering experiments and MD simulations. Linear and branched hydrocarbons, including alcohols, and ILs, which are typical working fluids in technical applications, with a systematic variation of the molecule size, branching, and polarity, in combination with gaseous solutes with varying molecular size, weight, and polarity are studied as model systems. The thermophysical properties are used to develop and verify the simulations and improve the data in the literature.

Based on the experimental and simulation results, structure-property relationships should be derived and used in the development of simple predictive models based on the pure component properties of the solute and solvent. Due to the cumulative nature of this thesis, the results and discussion of this work are based on publications. A list of the publications used in this thesis, with a short explanation of the author's contribution, as well as other publications, is given below. In the following, first an overview of the current status of thermophysical property research on systems consisting of liquids with dissolved gases with focus on the properties viscosity, mutual diffusion coefficient and interfacial tension is given. After an introduction to dynamic light scattering and EMD simulations, which were applied as part of this work, the main findings are summarized with the help of the following publications.

Publications

A. Giraudet, C.; Klein, T.; Zhao, G.; Rausch, M. H.; Koller, T. M.; Fröba, A. P. *Thermal, Mutual, and Self-Diffusivities of Binary Liquid Mixtures Consisting of Gases Dissolved in n-Alkanes at Infinite Dilution*. J. Phys. Chem. B **2018**, *122*, 3163-3175.

Author's contribution: The author was responsible for the planning, execution, and evaluation of the simulations. The experimental investigations in this work were carried out by C. Giraudet and G. Zhao. The author wrote all parts of the publication related to the simulations and participated in the planning and writing of the entire publication.

B. Klein, T.; Wu, W.; Rausch, M. H.; Giraudet, C.; Koller, T. M.; Fröba, A. P. *Influence of Liquid Structure on Fickian Diffusion in Binary Mixtures of n-Hexane and Carbon Dioxide Probed by Dynamic Light Scattering, Raman Spectroscopy, and Molecular Dynamics Simulations.* J. Phys. Chem. B **2018**, *122*, 7122-7133.

Author's contribution: The author was responsible for the planning, execution, and evaluation of the simulations. The experimental investigations in this work were carried out by W. Wu. The author wrote all parts of the publication related to the simulations and participated in the planning and writing of the entire publication.

C. Klein, T.; Cui, J.; Kalantar, A.; Chen, J.; Rausch, M. H.; Koller, T. M.; Fröba, A. P. *Liquid Viscosity and Interfacial Tension of Binary and*

Ternary Mixtures Containing n-Octacosane by Surface Light Scattering. J. Chem. Eng. Data **2019,** *64*, 817-826.

Author's contribution: The author was responsible for the planning, execution, and evaluation of the experimental investigations. The experimental investigations were supported by J. Cui. The author wrote all parts of the publication related to the experimental procedure and data analysis and participated in the planning and writing of the entire publication.

D. Koller, T. M.; Yan, S.; Steininger, C.; Klein, T.; Fröba, A. P. *Interfacial Tension and Liquid Viscosity of Binary Mixtures of n-Hexane, n-Decane, or 1-Hexanol with Carbon Dioxide by Molecular Dynamics Simulations and Surface Light Scattering*. Int. J. Thermophys. **2019,** *40*, 79.

Author's contribution: The author was responsible for the planning, execution, and evaluation of the experimental investigations. The experimental investigations were supported by S. Yan. The author was also responsible for coordinating and processing the simulations performed by C. Steininger. The author wrote all parts of the publication related to the procedure and data analysis of the simulations and experiments and participated in the planning and writing of the entire publication.

E. Klein, T.; Yan, S.; Cui, J.; Magee, J. W.; Kroenlein, K.; Rausch, M. H.; Koller, T. M.; Fröba, A. P. *Liquid Viscosity and Surface Tension of n-Hexane, n-Octane, n-Decane, and n-Hexadecane up to 573 K by Surface Light Scattering*. J. Chem. Eng. Data **2019,** *64*, 4116-4131.

Author's contribution: The author was responsible for the planning, execution, and evaluation of the experimental investigations and the processing of the results. The experimental investigations were supported by J. Cui and S. Yan. As the corresponding author, the author was responsible for planning and writing the entire publication.

F. Wu, W.; Klein, T.; Kerscher, M.; Rausch, M. H.; Koller, T. M.; Giraudet, C.; Fröba, A. P. *Diffusivities in 1-Alcohols Containing Dissolved H_2, He, N_2, CO, or CO_2 Close to Infinite Dilution.* J. Phys. Chem. B **2019,** *123*, 8777-8790.

Author's contribution: The author was responsible for the planning, performing, and evaluation of the simulations and the processing of the results. The experimental investigations in this work were carried out by W. Wu and M. Kerscher. The author wrote all parts of the publication related to the simulations and participated in the planning and writing of the entire publication.

G. Wu, W.; Klein, T.; Kerscher, M.; Rausch, M. H.; Koller, T. M.; Giraudet, C.; Fröba, A. P. *Mutual and Thermal Diffusivities as well as Fluid-Phase Equilibria of Mixtures of 1-Hexanol and Carbon Dioxide.* J. Phys. Chem. B **2020,** *124*, 2482-2494.

Author's contribution: The author was responsible for the planning, execution, and evaluation of the simulations and the processing of the results. The experimental investigations in this work were carried out by W. Wu and M. Kerscher. The author wrote all parts of the publication related to the simulations and participated in the planning and writing of the entire publication.

H. Klein, T.; Piszko, M.; Lang, M.; Mehler, J.; Schulz, P. S.; Rausch, M. H.; Giraudet, C.; Koller, T. M.; Fröba, A. P. *Diffusivities in Binary Mixtures of [AMIM][NTf_2] Ionic Liquids with the Dissolved Gases H_2, He, N_2, CO, CO_2, or Kr Close to Infinite Dilution.* J. Chem. Eng. Data **2020,** *65*, 4116-4129.

Author's contribution: The author was responsible for the planning, execution, and evaluation of the simulations and the processing of the results. The experimental investigations in this work were carried out by M. Piszko and M. Lang. As the corresponding author, the author was responsible for planning and writing the entire publication.

I. Klein, T.; Lenahan, F. D.; Kerscher, M.; Rausch, M. H.; Economou, I. G.; Koller, T. M.; Fröba, A. P. *Characterization of Long Linear and Branched Alkanes and Alcohols for Temperatures up to 573.15 K by Surface Light Scattering and Molecular Dynamics Simulations.* J. Phys. Chem. B **2020**, 124, 4146-4163.

Author's contribution: The author was responsible for the planning, execution, and evaluation of the experimental investigations, simulations, and the processing of the results. The experimental investigations in this work were carried out by F. Lenahan and M. Kerscher. As the corresponding

author, the author was responsible for planning and writing the entire publication.

J. Klein, T.; Piszko, M.; Kankanamge, C. J.; Kasapis, G.; Fröba, A. P. *Fick Diffusion Coefficient in Binary Mixtures of [HMIM][NTf_2] and Carbon Dioxide by Dynamic Light Scattering and Molecular Dynamics Simulations.* J. Phys. Chem. B **2021,** 125, 5100-5113.

Author's contribution: The author was responsible for the coordination of the experimental investigations, simulations, and the processing of the results. The experimental investigations in this work were carried out by M. Piszko and G. Kasapis. The simulations were performed by C. Kankanamge. As the corresponding author, the author was responsible for planning and writing the entire publication.

K. Klein, T.; Lenahan, F. D.; Kerscher, M.; Jander, J. H.; Rausch, M. H.; Koller, T. M.; Fröba, A. P. *Viscosity and Interfacial Tension of Binary Mixtures of n-Hexadecane with Dissolved Gases Using Surface Light Scattering and Equilibrium Molecular Dynamics Simulations.* J. Chem. Eng. Data **2021**, 66, 3205-3218.

Author's contribution: The author was responsible for the coordination of the experimental investigations and the processing of the results and carried out all simulations. The experimental investigations in this work were carried out by F. Lenahan, M. Kerscher, and J. Jander. As the corresponding author, the author was responsible for planning and writing the entire publication.

2 State of the Art

In this chapter, a characterization of systems consisting of liquids with dissolved gases as a function of the thermodynamic state is first given by linking temperature, pressure, and composition using solubility data. The importance of the thermophysical properties viscosity, interfacial tension, and mutual diffusivity of systems consisting of liquids with dissolved gases for technical applications is then highlighted, and an overview of the currently available data for these properties is given. After a brief definition and theoretical basis of the properties, different approaches to determine or predict the three mentioned properties, divided into experiments, simulations, and predictive models, are discussed. The focus lies on the advantages and disadvantages of applying the approaches to systems consisting of liquids with dissolved gases.

Systems consisting of liquids with dissolved gases are defined by at least two components. One component, i.e. the solvent, is characterized by a partial pressure equal to or higher than its pure-component vapor pressure at the same temperature T and a melting point lower than the given temperature. The second component, i.e. the solute, is characterized by the fact that its partial pressure at the given temperature is lower than the vapor pressure. By bringing the gas into contact with the liquid phase, the gas molecules are absorbed into the liquid phase according to their solubility. The solubility, which determines the concentrations of the gas molecules in the liquid phase, is usually strongly dependent on the type of gas and liquid as well as on the thermodynamic state. In 1802, William Henry [58] experimentally studied the amount of a gas absorbed by water as a function of temperature and pressure and established for the first time the linear relation between the partial pressure p_i of the gas i and the mole fraction x_i of gas absorbed [58], which is widely used in the form of Henry's Law,

$$H_{i,j}(T) = \frac{p_i}{x_i} \tag{2.1}$$

$H_{i,j}(T)$ is Henry's constant for the binary system of a solvent j and the dissolved gas i at a given T. However, this relation holds only for a limited range of x_i between the limit of infinite dilution ($x_i \rightarrow 0$) and an upper limit between x_i = (0.1 and 0.3), depending on the system [59]. To obtain the relationship between p_i and x_i over a wide compositional range, vapor- and liquid-phase compositional studies must be performed at vapor-liquid

equilibrium (VLE). The relationship between p_i and x_i over a wide composition range is exemplified for the binary mixture of 1-hexanol and CO_2 at temperatures of (303.15 and 313.15) K in Figure 2.1 based on the results from experimental studies illustrated by Secuianu et al. [60].

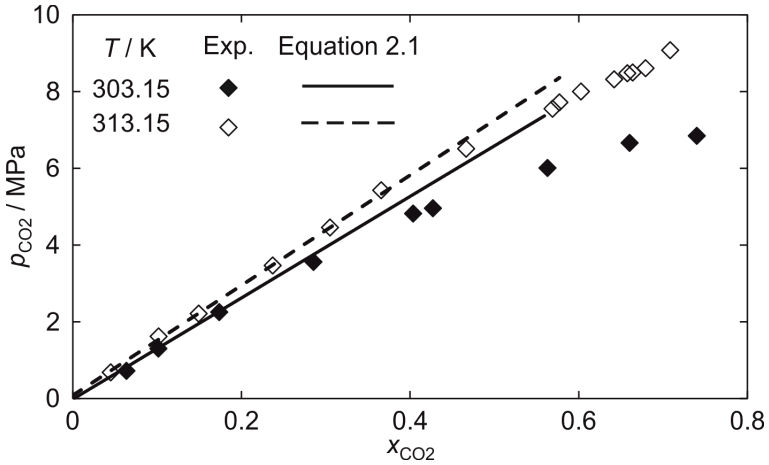

Figure 2.1: Phase equilibria of the binary mixture of 1-hexanol and CO_2 at (303.15 and 313.15) K using the experimental data of Secuianu et al.[60]. Experimental data up to x_{CO_2} = 0.2 were used to calculate the relationship between p_{CO_2} and x_{CO_2} according to Equation 2.1.

The experimental data in Figure 2.1 show that at pressures below 6.86 MPa, a system within the boundaries of the two-phase region decomposes into a liquid phase and a vapor phase in thermodynamic equilibrium. The composition of the vapor and liquid phase is determined by the dew point and bubble point line at the given pressure, respectively. At a pressure of 6.86 MPa, the system transitions from a VLE to a vapor-liquid-liquid equilibrium (VLLE) [60]. At pressures above 6.68 MPa, the system is characterized by a liquid-liquid equilibrium (LLE) until the two-phase region disappears at a pressure of 7.87 MPa [60]. At temperatures above the critical temperature of CO_2, a transition from VLE to VLLE and then to LLE can no longer be observed, and the two-phase region is characterized by a VLE. The binary mixture of 1-hexanol and CO_2 is therefore characterized by a Type III phase behavior, according to the classification of van Konynenburg and Scott [61].

To compare the composition of the liquid phase with Henry's law, the experimental data of Secuianu et al. [60] with a CO_2 mole fraction below 0.2 were used to calculate $H_{CO_2,1\text{-hexanol}}$. The partial pressure of CO_2 was calcu-

lated by subtracting the vapor pressure of 1-hexanol [62] from the total pressure, and the linear relation was calculated with the boundary condition $x_{CO_2} = 0$ at the vapor pressure of 1-hexanol at the given temperature, according to Eq. 2.1. For both temperatures, a systematic deviation between Henry's law and the VLE data is observed at x_{CO_2} above 0.2.

This shows that accurate solubility data are required for the characterization of systems consisting of liquids with dissolved gases. This is also necessary to assign the evaluated property to the correct thermodynamic state. Compared to pure fluids, where the thermodynamic state along the saturation line is defined by either temperature or pressure due to the connection between temperature and pressure along the saturation line, the thermodynamic state for a binary system consisting of a liquid with a dissolved gas under saturation conditions is defined by the temperature, pressure, and composition, where pressure and composition are connected via solubility data.

2.1 Thermophysical Properties of Liquids with Dissolved Gases

This section provides an overview of the relevance and availability of thermophysical properties for liquids with dissolved gases. First, an overview of technical applications and processes in which systems consisting of liquids with dissolved gases are used as working fluids or reactants and products in chemical reactions. The importance of thermophysical properties for design and optimization is discussed on the basis of selected applications examples. Then an overview of the available thermophysical properties of liquids with dissolved gases is given by experiments and simulations.

2.1.1 Relevance of Thermophysical Properties of Liquids with Dissolved Gases for Technical Applications

Systems consisting of liquids with dissolved gases play an important role in many different technical applications in chemical and energy engineering. Reliable thermophysical properties, including viscosity, interfacial tension, and mutual diffusion coefficient, are of interest in this work for efficient design and modeling of corresponding processes and devices. This will be illustrated in the following by means of some specific examples.

One application is the use of synthesis gas, a mixture of H_2 and CO, for the synthesis of various chemical components, as shown in Figure 2.2. In the conversion of synthesis gas, which is often exothermic, liquid phase reactions have the advantage that they can easily dissipate heat and thus realize

isothermal conditions at optimum temperature for the catalyst. An example is the production of methanol and DME in liquid phase reactors.

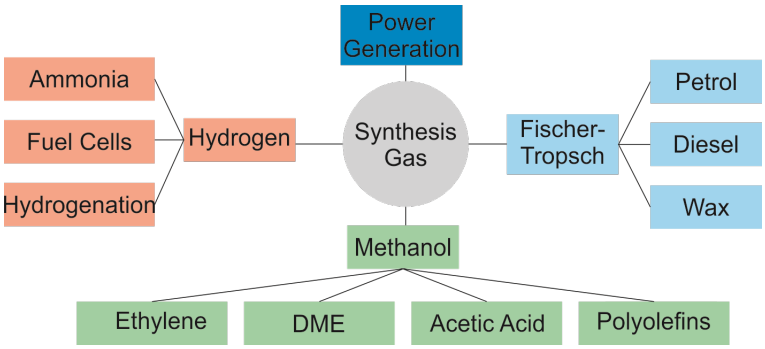

Figure 2.2: Technical processes related to the utilization of synthesis gas.

For the synthesis of methanol, the following reaction equations describe the conversion of synthesis gas to methanol.

$$CO_2 + 3H_2 \Leftrightarrow CH_3OH + H_2O$$
$$CO + H_2O \Leftrightarrow CO_2 + 3H_2 \qquad (2.2)$$

Lee and Sardesai investigated the synthesis of methanol from synthesis gas consisting of H_2, CO, CO_2, and CH_4 using a catalyst composed of copper oxide, zinc oxide, and aluminum oxide dispersed in mineral oil in a slurry reactor. In order to get a better understanding of the process, and thus enable an optimized process design, the experimental data were compared with a theoretical model for the entire mass transfer in the reactor. Here, Parameswaran et al. [63] identified a eleven-step model to describe the mass transfer in liquid phase heterogeneous catalysis. The different steps describe consecutively the transport of the reactant from the gas phase into the liquid phase, through the liquid phase and the solid-liquid boundary layer to the catalyst surface. Afterwards, the diffusion of the reactant within the pores of the catalyst to the active site and the adsorption of the reactants follow. After the reaction has taken place, the product follows the same steps backwards, starting with the desorption of the product. Taking advantage of the fact that the mass transfer in each step must be identical in a steady-state application of the process, the authors were able to empirically correlate the overall mass transfer coefficient of the process with the thermophysical properties. The liquid density, the viscosity of the gas and

liquid phases, the interfacial tension, and the diffusion coefficient of hydrogen dissolved in the liquid phase were determined since they are required to describe the overall mass transfer coefficient in this process [63]. In the absence of experimental data for the thermophysical properties of the binary mixtures, the authors had to neglect the influence of dissolved hydrogen on the liquid density, viscosity, and interfacial tension and use a prediction model for the binary diffusion coefficient. When comparing the total mass transfer from the developed correlation with the experimental results of the study for 21 different process conditions, the authors found very good agreement at operating conditions similar to those for which the empirical correlation was developed, but also discrepancies up to 30% at other operating conditions. This shows that accurate thermophysical properties for mixtures consisting of liquids with dissolved gases, as well as their dependency on the thermodynamic state, are required but are still lacking in the literature. This also applies to other processes related to the use of synthesis gas, e.g. the preparation of linear alkanes or alkenes by the Fischer-Tropsch process [4,64] or the synthesis of dimethyl ether [1,65-66].

Another example of processes where the thermophysical properties of liquids with dissolved gases are required is the bubble column reactor. This type of reactor is used because of its advantages, such as a large gas-liquid contact area, good temperature control, large heat transfer rate, and low pressure drop [67]. Bubble column reactors are used in a wide range of technical applications, such as in the oxidation of ethylene to acetaldehyde [68], the oxidation of acetaldehyde to acetic acid [69], or the production of microalgae in photobioreactors [70]. In the bubble column reactor, gas is added at the bottom of the reactor, which is filled with a liquid, and rises in the form of bubbles, to form a gas-liquid interface. Due to the solubility of the gas in the liquid, the gas is partially absorbed in the liquids phase. Figure 2.3 shows the schematic structure of a bubble column reactor.

For the design and optimization of a bubble column reactor, one of the most important parameters is the bubble size distribution. To gain a basic understanding of the factors affecting bubble size, the coalescence and breakup mechanisms for the gas bubbles in the liquid phase must be understood. Therefore, the various forces acting on the gas bubbles must be calculated. Here, it was found that mainly the drag force, which can be calculated using the viscosity and density of the liquid [71], leads to a breakup of bubbles. In addition, the bubble is acted upon by the Basset force, which is an additional drag force due to the vortices and can also be calculated using the liquid viscosity and density of the liquid [71]. Finally, considering the force acting on the gas bubble due to the gas-liquid interface, which

can be calculated using the interfacial tension [9], a theoretical model for the bubble size distribution can be developed. To describe the mass transfer between the gas bubble and the surrounding liquid, as well as the lifetime of a gas bubble, additional knowledge about the solubility and the binary diffusion coefficient is required [72-73].

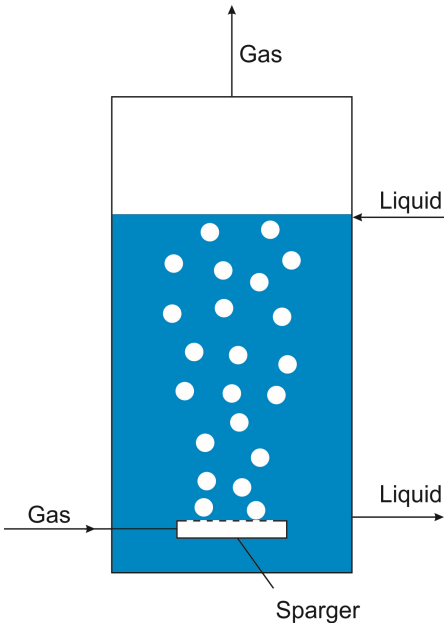

Figure 2.3: Schematic design of a bubble column reactor.

Other applications that require thermophysical properties of liquids with dissolved gases for the design and optimization include gas-saturated diesel combustion [7], absorption refrigerators [6], wastewater treatment [74], or lubrication [75].

The above examples show that accurate thermophysical properties of liquids with dissolved gases are required in many areas of chemical and energy engineering. Among them, the transport properties viscosity and diffusion coefficient are important since they are needed to calculate the mass and momentum transfer and influence the heat transfer. In addition, surface tension is needed because it affects gas absorption in liquids and is used to determine the size and shape of bubbles and droplets as well as the wetting behavior of fluids on surfaces.

2.2 Review of Thermophysical Property Research on Systems Consisting of Liquids with Dissolved Gases

In the following chapter, an overview of the current status of research on thermophysical properties of liquids with dissolved gases is given, focusing on viscosity, interfacial tension, and diffusion coefficient in the liquid phase. Experiments, computer simulations, as well as theoretical prediction models, will be discussed.

2.2.1 Experiment

Most of the research on the study of thermophysical property research of systems consisting of liquids with dissolved gases is focused on VLE. This is understandable since the study of all other properties requires precise knowledge of the composition of the fluid phase. For gases with low solubility, e.g. H_2 or He, solubilities near the limit of infinite dilution of the gas are given in terms of the Henry constant [26,58,76-80]. For highly soluble gases, such as CO_2 or CH_4, the solubility data are given numerically in terms of the liquid composition at a given temperature and pressure. Moreover, authors often use an equation of state (EoS) to correlate their experimental solubility data, which allows the interpolation or extrapolation to thermodynamic states that have not been studied experimentally [60,81-85]. A good overview of the available solubility data for gases dissolved in different solvents is provided by the IUPAC-NIST Solubility Database [86], which contains over 100 volumes with solubilities for a given solute or solvent molecule or type. With the increasing interest in ILs over the last two decades, a wide range of solubility data is also available for systems consisting of gases dissolved in ILs. The Ionic Liquid Database – ILThermo (v2.0) [87-88] contains at the moment 241 datasets for binary mixtures of gases dissolved in ILs.

Viscosity

As described in Chapter 2.1.1, viscosity is an important transport property for the design and optimization of technical processes. The viscosity of a material is a measure of the irreversible dissipation of energy in a fluid flowing with an inhomogeneous velocity profile, caused by the underlying intermolecular interactions. This can be visualized with a simple thought experiment. The schematic diagram in Figure 2.4 shows a fluid of thickness d confined between two parallel plates. The upper plate moves in the x-direction relative to the lower plate with a constant velocity v_x. Here, F_x denotes the force required to move the top plate with v_x, and τ_{zx} denotes the

stress caused by the force in the *x*-direction on the surface area *A* with a normal vector in the *z*-direction.

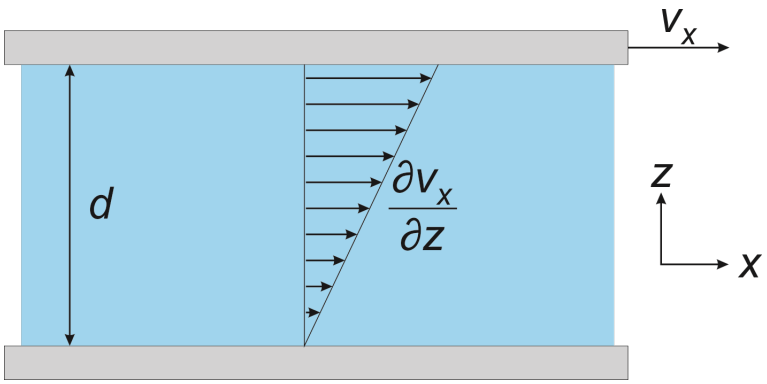

Figure 2.4: Visualization of the viscosity using the velocity profile in a fluid between two parallel plates.

The dynamic viscosity η, which can be related to the kinematic viscosity ν via the density ρ ($\eta = \rho\nu$), connects τ_{zx} to the linear velocity profile $\partial v_x/\partial z$ by η according to Newton's equation [59]

$$\tau_{zx} = -\eta \frac{\partial v_x}{\partial z}. \qquad (2.3)$$

In the liquid phase, viscosity is strongly influenced by temperature and decreases with increasing temperature. For example, when the temperature is increased from (303 to 448) K, the viscosity of squalane decreases by a factor of about 19 [89-90]. With increasing pressure, the viscosity also increases. The effect of pressure on viscosity is weaker than the effect of temperature, as shown by a 10% increase in the viscosity of squalene by increasing the pressure *p* by a factor of 5 [89-90].

For the viscosity of systems consisting of liquids with dissolved gases, the data situation in the literature is still sparse. The first systematic study was carried out in 1925 by Lewis [91] and included experimental viscosities for binary mixtures consisting of the solute sulfur dioxide, hydrogen sulfide, or chlorine gas, assumed to be hydrogen chloride, dissolved in 12 different solvents. Depending on the solubility of the gas, the experimental investigations were carried out in a wide composition range with molar fractions of the dissolved gas of up to 0.88. Much of the further research on the viscosity

of systems consisting of liquids with dissolved gases is focused on and motivated by systems related to the extraction of oil from reservoirs. Here, the influence of dissolved natural gases like CH_4 and ethane (C_2H_6) on the viscosity of *n*-alkanes or technical petroleum mixtures was studied [92-94]. Since CO_2 can be injected into petroleum reservoirs to increase recovery, commonly referred to as enhanced oil recovery, the influence of dissolved CO_2 on the viscosity of petroleum and alkanes is also discussed in the literature [89-90,93-97]. Other systems for which the influence of dissolved gas on the viscosity of the solvent has been studied experimentally are based on CO_2 as a solute in water [98], water with dissolved salts (brines) [99], and primary alcohols [100-103]. For systems consisting of ILs with dissolved gases, there are eight publications in the literature, most of which investigate the effect of dissolved CO_2 [104-108] on the viscosity of imidazolium-based ILs. Other solutes under investigation are sulfur dioxide (SO_2) [109], methyl methacrylate [110], or various refrigerants [111].

There are many different methods for the experimental investigation of viscosity. An overview of these methods is summarized in the work by Nieto de Castro et al. [112]. In general, experimental methods are divided into primary and secondary measurement techniques. A measurement method is considered primary if it is based on a physically sound working equation that relates viscosity to experimentally measured quantities, and no calibration parameters are required [112]. Since there is currently no primary measurement technique, Nieto de Castro et al. [112] have introduced the category of quasi-primary techniques, which includes instruments where each calibration parameter has a clear physical meaning. Secondary methods, on the other hand, are techniques whose calibration parameters have no clear physical meaning. In the following, the various measurement methods are briefly described, and their application to systems consisting of liquids with dissolved gases is indicated, as well as their classification into primary and secondary methods.

The most common technique for systems consisting of liquids with dissolved gases is the vibrating-wire instrument [89-90,94,97-99]. This method is based on the deformation of a metal wire immersed in a fluid. In the transient mode of operation, these distortions cause periodic oscillations whose damping can be related to the viscosity of the fluid [113]. In the steady-state mode of operation, the resonance curve for the oscillations of the wire can be related to the viscosity of the fluid [114]. For both transient and steady-state operations, additional knowledge of the density of the fluid is required. For highly accurate viscosity measurements, the average wire radius is calibrated using a reference fluid of known viscosity and

density. The vibrating-wire technique is therefore considered a quasi-primary technique. Typical uncertainties for the measured viscosity are 2%, based on a confidence level $k = 2$. The oscillating body technique is characterized by an axially symmetric body suspended on a torsion wire in a fluid enclosed between two fixed plates. This body can be a cylinder, a sphere, or a disc. With a solid mathematical description of the observed oscillation of the immersed body, the viscosity of the fluid can be determined from the period and damping of the oscillations. This technique was applied, for example, by Kariznovi et al. [100], who used an oscillating piston viscometer to determine the viscosity of a binary mixture of 1-butanol with various dissolved gases with typical uncertainties of 4% ($k = 2$). Other authors report uncertainties better than 1% ($k = 2$) for the determination of the viscosity of pure fluids [115]. For an accurate determination of the viscosity, oscillating body viscometers are calibrated to the dimensions of the apparatus, as well as to the edge effects of the immersed body; they are considered a quasi-primary measurement technique. The method of a torsional oscillating quartz crystal is based on the excitation of a quartz crystal, which leads to a microscopic torsional vibrating motion. Since the quality factor must be calibrated against a reference fluid, this technique is considered a quasi-primary technique. So far, the technique of torsional oscillating crystals has not been applied to systems consisting of liquids with dissolved gases. The surface light scattering (SLS) method [116] measures the viscosity of a fluid in macroscopic thermodynamic equilibrium without the need for calibration. It is based on the study of light scattered from a microscopic surface fluctuation at the interface between two fluids. The dynamics of these fluctuations, which are contained and accessible in the evaluation of the scattered light in the frequency or time domain, the viscosity, and often the surface tension can be derived using a physically sound working equation, the dispersion equation [117-118]. Since thermophysical properties, such as the density of both phases, as well as the viscosity of the upper phase, which is the gas phase in gas-liquid systems, are additionally required to solve the working equation, SLS is considered a quasi-primary measurement technique [112]. Depending on the system and the uncertainty of the above thermophysical properties that enter the working equation, typical uncertainties of less than 2% ($k = 2$) can be achieved [116,119-120]. So far, the SLS technique has not been applied to systems consisting of a liquid with a dissolved gas. Besides SLS, the viscosity of a fluid can also be determined using dynamic light scattering (DLS) by adding particles with a known particle size. Here, the light scattered by particles in a liquid is used to determine the particle diffusion coefficient [121]. Einstein's equation [122] can be used to calculate the dynamic viscosity of the fluid using the particle diffusion

coefficient and particle size, which can be calibrated with a reference fluid [121]. Therefore, this method can be considered as a quasi-primary measurement technique. This technique has been applied to determine the viscosity of pure liquids with typical uncertainties of less than 2% (k = 2) [123], but has not been applied to systems consisting of liquids with dissolved gases. The rotational viscometer, the capillary viscometer, and the falling-body viscometer belong to the secondary measurement methods since their calibration parameters have no clear physical meaning. Rotational viscometers are usually used in the form of a Stabinger Viscometer [124]. Here, the sample fluid is in a tube rotating at a constant speed. The kinematic viscosity of the sample can be determined from the measurement of the velocity and momentum of an axially symmetric measuring rotor immersed in the fluid. This instrument has been used to determine the viscosity of pure liquids and liquid mixtures with specified uncertainties below 1% (k = 2) [124-128] but has not been used for systems consisting of liquids with dissolved gases. Capillary flow viscometers have been widely used to determine the viscosity of liquids for over 100 years. One of their main advantages is their simple design and operation. Based on the Hagen-Poiseuille equation of fluid dynamics, capillary flow viscometers relate the kinematic viscosity to the volume flow of the liquid through a capillary tube. For systems consisting of liquids with dissolved gases, Lewis [91] constructed a capillary flow viscometer specifically designed for this type of system. Modern capillary flow viscometers are usually of the Ubbelohde type and allow the determination of viscosity with uncertainties between (0.1 and 2)%, depending on the viscosity range [112]. The rolling-body or falling-body viscometer measures the time it takes for a usually spherical body to fall a certain distance or roll down a section of an inclined plane. At very low Reynold's numbers (Re < 2.0), the time required for the object to traverse a given distance in linearly correlated with the viscosity of the fluid. Besides the advantages, such as simple construction and small fluid sample, problems in the fabrication of the passing object, such as the sphericity and surface finish of a sphere and the alignment of the falling axis with the axis of the outer tube, in the case of a falling-body viscometer, still limit the applicability of the instrument. Specifically for systems consisting of liquids with dissolved gases, Sage [129-130] has developed and tested a rolling-body viscometer with a specified uncertainty of 2.0%.

Interfacial Tension

The terms interfacial tension and surface tension are often used synonymously in the literature. However, the surface tension refers to the property

between a liquid phase consisting of a single component in equilibrium with its own vapor phase. The surface tension of a substance is therefore determined by the temperature and the corresponding vapor pressure. However, for substances with very low vapor pressure, the experimental investigations are often carried out under an inert gas atmosphere at a pressure greater than the vapor pressure of the substance. Such experimental values should be referred to as interfacial tension. In this work, the term "interfacial tension" is used for the property measured for systems of liquids with dissolved gases as well as for pure substances. The interfacial tension σ is defined by the differential change in Gibbs energy G per unit area A at a given temperature and pressure [59]

$$\sigma = \left(\frac{\partial G}{\partial A} \right)_{p,T} . \tag{2.4}$$

While the interfacial tension can be expressed quantitatively in various ways, the notation in Equation 2.4 directly explains a widely known phenomenon at interfaces, namely the tendency of a system to minimize its surface energy. Since the equilibrium system tends to a state of minimum Gibbs energy at a certain temperature and pressure, the product σA also tends to a minimum, which can lead to an enrichment of certain components of a multicomponent mixture at the interface. The interfacial tension is inversely proportional to the temperature and converges to zero at the critical point of a substance or mixture, a fact often used for predictions and correlations [131].

Similar to viscosity, early research on the interfacial tension of liquids with dissolved gases was motivated by the recovery of oil from reservoirs [132-134]. Due to modern technologies for the extraction of crude oil and natural gas recovery from oil deposits, such as enhanced oil or gas recovery, the interfacial tension of systems containing CO_2, petroleum, and natural gas components such as CH_4 is still being studied today [135-139]. Moreover, the possible geological storage of CO_2 has stimulated research on the interfacial tension of systems consisting of CO_2 dissolved in water or brines [136,140-142]. While many scientific publications focus on a single binary system [55,137-138], a systematic variation of the solute and solvent molecules is necessary to develop a fundamental understanding of how the solute gas affects the interfacial tension. A systematic analysis of the influence of dissolved gases on the interfacial tension of a liquid with varying solute and solvent molecules was first performed by Uhlig [143] for binary mixtures of solutes CH_4, oxygen (O_2), N_2, H_2, CO, and ethene (C_2H_4) dissolved

in seven different solvents, including water, hydrocarbons, ethers, and carbon tetrachloride. Based on the experimental data, Uhlig [143] was also able to develop a linear relationship between the logarithm of the solubility of the dissolved gas and the interfacial tension. Rice [144] studied the effect of pressure on the interfacial tension of H_2 or CO_2 dissolved in ethanol or ethyl ether but was unable to determine the solute concentration in the liquid phase as a function of pressure. Another systematic study that should be mentioned here is the work of Li et al. [145], who measured the interfacial tension of eleven binary mixtures consisting of CO_2 dissolved in *n*-alkanes for pressures up to 12 MPa. For binary mixtures of ILs with dissolved gases, 63 datasets are currently available in the ILThermo database [87-88]. Most of these experimental studies deal with the influence of dissolved water on the interfacial tension of ILs, followed by studies of ILs with dissolved CO_2 or primary alcohols.

The experimental techniques for the determination of interfacial tension can be divided, according to Drelich et al. [146], into five categories. These categories are direct measurement using a microbalance, measurement of capillary pressure, analysis of capillary-gravity forces, gravity-distorted droplets, and amplified distortion of droplets. Methods of direct measurement with a microbalance, often referred to as detachment methods, include the Wilhelmy plate method and the Du Noüy ring method. Either method, in detachment mode, measures the force required to lift the ring or plate off a vapor-liquid surface. The Wilhelmy plate method can also be used in static mode, where the plate remains in contact with the liquid throughout the interfacial tension measurement. The wetting of the body forms a meniscus along the surface of the body, which affects the force required to either hold the plate in place or to lift the body off the interface, depending on the mode of operation. Together with the exact weight and dimensions of the body used, as well as the densities of the two phases and the contact angle between the body and the liquid, the force can be related to the interfacial tension of the system. Due to a deformation of the ring in the Du Noüy ring method, a calibration of the setup with a reference is required [146]. Both methods can determine the interfacial tension with an absolute expanded uncertainty of approximately 0.2 $mN \cdot m^{-1}$ [147-148]. So far, this method has not been applied to systems consisting of liquids with dissolved gases. Within the category of capillary pressure measurements, the maximum bubble pressure method is the most commonly used. The method is based on immersing a capillary tube in a liquid and determining the maximum pressure required to force a gas bubble out of the capillary tube into the liquid. The interfacial tension can then be determined from

the maximum pressure using the dimensions of the capillary tube and the depth of immersion of the capillary tube in the liquid. While the maximum bubble pressure method has been used to determine the interfacial tension of systems consisting of liquids with dissolved gases, reported measurements using this technique for pure liquids give typical uncertainties of 0.2 $mN \cdot m^{-1}$ [149].

From the group of capillary gravity analysis methods, the capillary rise method is the most commonly used. Due to the ease of use of this technique, the capillary rise method is also one of the oldest techniques for the experimental determination of the interfacial tension and has already been applied by Beecher et al. [132] in 1926 to study the effect of dissolved natural gas on the interfacial tension of various oils. The method is based on the equilibrium between capillary and gravitational forces acting on a liquid in a capillary tube. When the liquid wets the inside of the capillary tube, a meniscus is formed, and due to the pressure difference according to the Young-Laplace equation, the liquid rises in the tube. Based on the difference in density between the liquid and the corresponding gas or vapor phase, the diameter of the capillary tube, as well as the contact angle, the interfacial tension can be determined from the height that the liquid rises in the tube. Since the determination of the contact angle is quite difficult, a perfect wetting of the capillary tube and thus a contact angle of 0 is often assumed when using this method [150]. Since the inner diameter of the capillary tube has a strong influence on the calculated interfacial tension, it is often calibrated with a reference fluid [150]. Recent applications of this technique can be found in the work of Ghatee and Zolghadr [150], who succeeded in determining the interfacial tension of ILs with specified uncertainties between (0.2 and 0.3) $mN \cdot m^{-1}$. In the category of measurements based on gravity-distorted drops, the pendant-drop method and sessile-drop method should be mentioned. Since the pendant-drop method is the most commonly used technique today, it is briefly introduced below. It is based on the analysis of the shape of a droplet hanging from a solid object in the gravitational field. The shape of such a pendant drop is influenced by gravitational and capillary forces. Using the Young-Laplace equation, the interfacial tension can be determined from the shape of the droplet, which is recorded with a camera during the experiments, and the difference between the liquid density and vapor or gas density. For high-precision measurements, calibration of the setup is required [151]. The pendant-drop method has been applied to numerous systems consisting of liquids with dissolved gases [55,135,152-153] with typical absolute uncertainties ($k = 2$) of 0.1 $mN \cdot m^{-1}$. In the last category of interfacial tension measurements, namely

enhanced drop deformation, the spinning drop method can be found. This technique is based on a horizontal tube that rotates along its longitudinal axis and contains a drop of liquid. Due to the centrifugal forces, the droplet is stretched and assumes a cylindrical shape. From the cylindrical shape and centrifugal force acting on the droplet, the surface tension can be determined using a modified Young-Laplace equation [154]. So far, this technique has not been applied to systems consisting of liquids with dissolved gases. Finally, the SLS technique, which is not included in the classification of Drelich et al. [146] should be mentioned for the determination of the interfacial tension. As described in the previous section, the SLS technique is able to determine the viscosity and interfacial tension from the dynamics of surface fluctuations between two fluid phases in macroscopic thermodynamic equilibrium using a theoretical description of the surface free waves. If these surface waves show an oscillatory behavior, the simultaneous determination of both properties is possible. However, if the surface waves exhibit overdamped behavior, the ratio of viscosity to interfacial tension is directly accessible with this technique, and the interfacial tension can only be determined if the viscosity of both phases is known. SLS can be used to determine the interfacial tension with typical uncertainties below 2% (k = 2) [119,155-156].

Diffusion Coefficient

In addition to viscosity, the mutual diffusion coefficient is an important transport property required in the modeling and design of technical applications, as described in the previous chapter. In general, several diffusion coefficients can be determined, namely the tracer and self- and mutual diffusion coefficients. However, only the mutual diffusion coefficient is a true transport property and can be associated with the transport of mass due to a concentration or chemical potential gradient. Since for a binary mixture at the infinite dilution limit, the self- or tracer diffusion coefficient of the component that is at infinite dilution can be directly related to the mutual diffusion coefficient; some studies focus only on determining the tracer or self-diffusion coefficient. The theoretical relations that allow a correlation between the self-diffusion coefficient of the component at infinite dilution are given in the following chapter, which describes the determination of thermophysical properties using computer simulations.

The first experimental studies on diffusion in gases [157] and liquids [158] were carried out in the 19th century by Thomas Graham. On the basis of Graham's experiments, Adolf Fick [159] was able to develop Fick's first law of diffusion

$$j_1 = -D_{11} \frac{\partial c_1}{\partial z}, \tag{2.5}$$

which relates the one-dimensional, area-normalized molar flux j_1 of component 1 in a binary nonelectrolyte mixture to the concentration gradient in the z-direction ($\partial c_1/\partial z$) via the transport property D_{11}. Here, D_{11} is the mutual diffusion coefficient and is often referred to as the Fick diffusion coefficient or binary diffusion coefficient. Although the binary diffusion coefficient is sometimes referred to as D_{12} to emphasize the fact that it describes diffusive mass transfer in a binary mixture of components 1 and 2, the notation D_{11} follow a notation consistent with the general notation for diffusive mass transport in multicomponent mixtures, where a matrix of diffusion coefficients is required to describe the molar flux of each component. The subscript in D_{11} can therefore be read as the specific mole flux of component 1 due to a concentration gradient of component 1, which is consistent with the general description of diffusion [160]. It is important to note that for a N-component mixture, N-1-independent mass fluxes can be defined, which means that for a binary nonelectrolyte mixture, only one Fick diffusion coefficient is required to describe the diffusive mass transfer. Special care should be taken if one or more of the components is an electrolyte. Electrolytic components are characterized by the fact that at temperatures above the melting point, they dissociate into two species, namely anions and cations, either in solution or in pure form. In a binary mixture of a nonelectrolyte component and an electrolyte component, three species can be found according to a species-based description, i.e. the anion, the cation, and the nonelectrolyte component, and three different mass fluxes can be defined, only two of which are independent. However, since the motion of the anions and cations is coupled due to the electroneutrality condition, the number of independent fluxes is further reduced by one, so that only one independent mass flux and one Fick diffusion coefficient can be defined [161].

In addition to the Fick diffusion coefficient, the Maxwell-Stefan diffusion coefficient $Đ$ can also be used to describe diffusive mass transfer [162]. In contrast to Fick's law of diffusion, the Maxwell-Stefan approach relates diffusive mass transport to a chemical potential gradient. Further details on the Maxwell-Stefan approach to mutual diffusion, which is often used in the computational determination of diffusion coefficients, and the relationship between the Fick and Maxwell-Stefan diffusion coefficient are described in the following chapter.

In this section, experimental studies are discussed for the determination of the mutual diffusion coefficient, either by its direct determination or by the determination of the self- or tracer diffusion coefficient of the component that is in infinite dilution. In general, the available experimental data for the mutual diffusion coefficient for systems consisting of liquids with dissolved gases can be divided into three different categories based on the solvent molecules. These are systems based on water as a solvent, hydrocarbons, and ILs. The first category includes systems composed mainly of light gases, including N_2, O_2, and CO_2, dissolved in either pure water [163-169] or brine [170] and mostly motivated by carbon capture and storage applications. Similar to the literature review on viscosity and interfacial tension, thermophysical property research with respect to the mutual diffusion coefficient of liquids with dissolved gases is often motivated by oil recovery and enhanced oil recovery applications. Here, the binary diffusion coefficients of either natural gas constituents or light gases such as H_2, CO, or CO_2 dissolved in bitumens [171-172] or hydrocarbons [168,173-178] are studied. In the last category, mutual diffusion coefficients can be found for systems consisting of ILs with dissolved gases. The reason for such studies is the relatively good solubility of gases in ILs compared to other liquids, such as hydrocarbons, and the resulting applications where ILs can be used for gas separation. Most experimental studies deal with ILs in combination with dissolved CO_2 [49,169,179-181], refrigerants [76,182-183], or water [184-186]. While the experimental studies of the first two categories are mostly limited to the infinite dilution range and do not investigate the concentration dependence of the mutual diffusion coefficient, IL-based systems with dissolved gases are more often studied over a wide concentration range. This is most likely due to the relatively good solubility of gases in ILs and their application in gas separation processes, where a wide composition range is of interest.

In gas absorption techniques, the time-dependent absorption of gas into the liquid, which is affected by solubility and mutual diffusion coefficient, is analyzed to determine the mutual diffusion coefficient. Fick's second law of diffusion can be used to calculate the mutual diffusion coefficient, which links the time-dependent change in concentration of a component to its spatially resolved concentration profile via the mutual diffusion coefficient. Equation 2.6 presents Fick's second law of diffusion for a binary system with a one-dimensional concentration gradient in z-direction

$$\frac{\partial c_1}{\partial t} = D_{11} \frac{\partial^2 c_1}{\partial z^2}. \tag{2.6}$$

There are several experimental methods for determining gas absorption, including the absorption of a gas in a laminar liquid jet [187], the one-dimensional absorption at a planar gas-liquid interface either at constant pressure [175] or in a closed system with a constant volume [188], the time-dependent shrinking of a gas bubble rising in liquid [163], or the gas flow required to maintain a constant size of a bubble suspended in a liquid [165]. The spatially and temporally resolved concertation required to solve Fick's second law of diffusion is often determined using optical methods, such as planar laser-induced fluorescence with inhibition (PLIFI), where the concentration of the gas can be calculated from the fluorescence intensity [163]. Alternatively, the amount of absorbed gas in the liquid phase can be determined, e.g., by measuring the mass of gas required to maintain the size of a bubble suspended in a liquid [165] or by determining the time-dependent change in volume due to swelling of the liquid phase [172]. A common limitation of the above methods is that the mutual diffusion coefficient is not determined at a specific concentration but is averaged over the concentration range covered in the experiment. Although this means that the concentration dependence of the diffusion coefficient cannot be determined in this way from a single experiment, Khalifi et al. [175] have presented concentration-dependent mutual diffusion coefficients from a gas absorption experiment at constant pressure, where the absorption process was started with pre-saturated liquids of different composition. Typical uncertainties for the mutual diffusion coefficient are around 3%. However, the uncertainties are often based on replicate measurements and do not include error propagation of the full working equation [175]. Another method for determining the mutual diffusion coefficient of a system consisting of liquids with dissolved gases is the Taylor dispersion method [164,173-174,189]. This method is based on the evaluation of the dispersion of a solute plug injected into a solvent flowing laminarly through a tube. Due to the parabolic flow profile of the solvent, the introduced solute plug is distributed in the longitudinal direction. Furthermore, diffusive mass transfer leads to further dispersion of the solute plug due to the concentration gradient between the solute plug and the solvent. The mutual diffusion coefficient can be calculated from the solute distribution, which can be detected with a differential refractive index detector [189] in the fully developed flow after a sufficiently long time. Using this method, the mutual diffusion coefficient can be determined with a relative expanded uncertainty between (1.6 and 2.6)% (k = 2) [173,189].

Nuclear magnetic resonance (NMR) spectroscopy was used to measure the mutual diffusion coefficient of systems consisting of CO_2 dissolved in water

[170], brines [170] and various hydrocarbons [190-191]. Therefore, pulsed-field gradient NMR experiments were applied to the mixtures, consisting of the solvent and $^{13}CO_2$ as the solvent, and the attenuation of the NMR signal in a spatially varying magnetic field was demonstrated. Since the attenuation is directly affected by the translational diffusion of the components, the self-diffusion coefficient of $^{13}CO_2$ can be determined. However, at the limit of infinite dilution of the solute, this diffusion coefficient is equal to the mutual diffusion coefficient of the system [170,191]. The relative uncertainties of the self-diffusion coefficient range from about (1 to 9)% (k = 2).

Another method for determining the mutual diffusion coefficient in binary mixtures, including mixtures consisting of liquids with dissolved gases, is the dynamic light scattering (DLS) method. With this method, the mutual diffusion coefficient can be retrieved non-invasively in macroscopic thermodynamic equilibrium, which means that no macroscopic concentration gradient needs to be imposed [192-193]. Since no macroscopic concentration gradient has to be applied, the determination of the mutual diffusion coefficient is possible for a well-defined composition. Since microscopic fluctuations exist in macroscopic thermodynamic equilibrium, the light scattered by such microscopic fluctuations contains information about their temporal behavior. Based on the principle that the relaxation of microscopic fluctuations follows the same laws as macroscopic fluctuations [194-195], DLS is can infer the associated transport properties by studying the temporal behavior of the scattered light intensity. While the mutual diffusion coefficient in a binary mixture can be determined from the microscopic fluctuation in concentration, it is often possible to simultaneously access the thermal diffusivity caused by microscopic temperature fluctuations [176-177,193]. Typical uncertainties for the determination of the mutual diffusion coefficient in systems consisting of liquids with dissolved gases are strongly dependent on the concentration of the dissolved gas and can therefore range from 5% (k = 2) for mole fractions of the dissolved gas above 0.1 to 30% (k = 2) near-infinite dilution of the dissolved gas [49,176-177,181].

From the above literature review on viscosity, interfacial tension, and mutual diffusion coefficient, it is clear that reliable measurement techniques, as well as experimental data, are available in the literature for systems consisting of liquids with dissolved gases. However, a major limitation of the available database is the limited variation of solvent and solute components. To gain a fundamental understanding of how the solute gases affect the thermophysical properties of the solvent, systematic variation of the

solvent, including variation in carbon chain length, branching, and hydroxylation, and the solute, including gases with different molar mass, size, sphericity, and polarity, is required. In addition, a wide variation of thermodynamic states, covering a wide temperature range up to process relevant conditions, as well as composition, is important but still lacking in the literature.

2.2.2 Computer Simulations

Due to the large number of combinations of solvent and solute components in combination with a wide range of thermodynamic states for which thermophysical properties are relevant for technical applications, it is hardly possible to perform experimental investigations for all possible systems and thermodynamic states. Therefore, other methods are required to determine the thermophysical properties. These methods include theoretical and empirical models, but also computer simulations, which can be used to predict the thermophysical properties. Here, computer simulations are the main focus of research into thermophysical properties, driven by the steadily increasing computing power of stand-alone work stations and computer clusters. Simulations are based on a physical description of the inter- and intramolecular interaction at the electronic, atomistic, or molecular level. By describing the interactions at the subatomic level on the basis of electrons and nuclei, as is the case with quantum-chemical ab initio methods, the highest level of detail can be achieved. They provide access to molecular structure, as well as potential energy surfaces for molecule pairs, and can be combined with theories of statistical mechanics to determine equilibrium properties of pure components or mixtures, as has been shown, for example, for the solubility of CO or CO_2 in water [196]. Due to the high level of detail, quantum-chemical ab initio calculations require a lot of computational power and are only suitable for relatively small systems with usually less than 10^3 atoms [197]. The resulting potential energy surface can be used to develop atomistic force fields (FF), which are used in computer simulations at the atomistic level. Here, pairwise potential energy functions between atoms are used to describe the inter- and intramolecular interactions, resulting in lower computational costs. Therefore, much larger systems with 10^3 to 10^5 atoms can be simulated. The potential energy U_{ij} between two atoms i and j at a distance of r_{ij} is shown in Figure 2.5 and can be further distinguished into bonded and non-bonded interactions, which is exemplified using an *n*-hexane and CO_2 molecule. In the group of bonded interactions, bonds, bond angles, and dihedral angles between two, three, or four atoms, respectively, connected by a covalent bond are contained.

Here, the parameters b_0 and Θ_0 denote the equilibrium bond length and the bond angle.

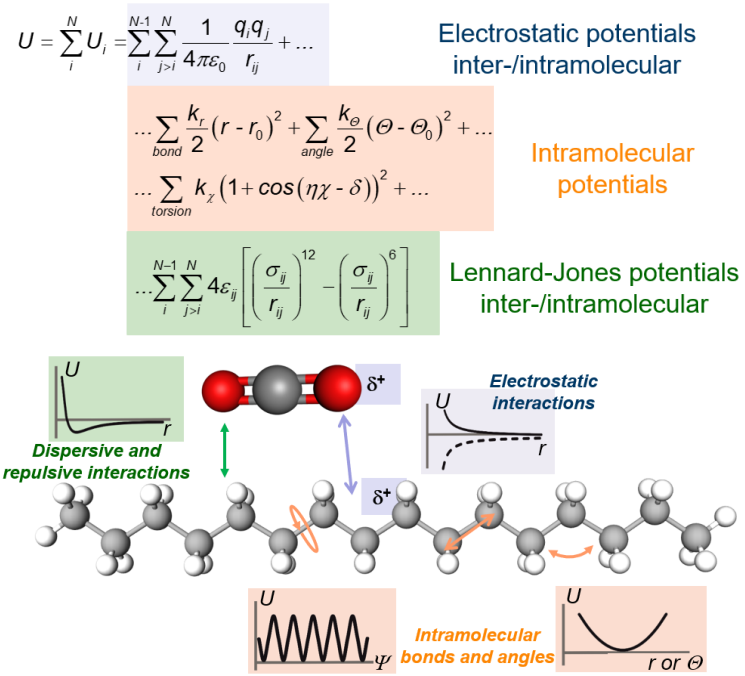

Figure 2.5: Potential Energy U in a System with N Atoms as well as a Schematic Representation of the Interaction Within and Between n-Hexadecane and CO_2.

Non-bonded interactions include electrostatic interactions described by constant partial charges q_i, as well as repulsive and dispersive interactions in the form of Lennard-Jones (LJ) 12-6 potentials described by the atom-specific LJ parameter ε_{ii} and σ_{ii}. To calculate LJ interactions between dissimilar atoms, combinations rules for the LJ parameter, such as the Lorentz-Berthelot mixing rules [198], must be applied. . A possible extension of the potential energy function shown in Figure 2.5 is the inclusion of quadrupolar moments in the electrostatic interactions [199]. Atomistic simulations can be further distinguished into Monte Carlo (MC) and Molecular Dynamics (MD) simulations. In the purely stochastic MC approach, a series of different molecular configurations are generated in a statistical ensemble by randomly moving and rotating atoms and molecules, starting from an initial configuration [200]. By averaging over the different con-

figurations, equilibrium properties such as density, isothermal compressibility, and interfacial tension can be calculated [39,201-202]. In contrast to MC simulations, MD simulations, which are of interest in this work, are able to describe the dynamics in a statistical ensemble of molecules and therefore allow access to dynamical properties as well. They are based on the solutions of Newton's equations of motion in a time-discretized manner that gives access to the positions, velocities, forces, and energies of the particles in the ensemble [38-40]. A variety of thermophysical properties, including viscosity, interfacial tension, and various diffusivities of interest within this work, can be calculated from the recorded trajectories and energies. MD simulations can be performed either in macroscopic thermodynamic equilibrium (EMD) or outside of the macroscopic thermodynamic equilibrium (NEMD), which is often used in simulations of transport properties [41]. Further details on the evaluation of various thermophysical properties by MD simulations are given in Chapter 4. In addition to providing access to thermophysical properties, atomistic simulations provide insight into the fluid structure of the simulated ensemble and can contribute to the development of structure-property relations discussed later in this chapter.

Molecular simulations are closely related to atomistic simulations and describe the interactions in a statistical ensemble of molecules using potential energy functions. In this process, the different atoms of a molecule or a functional group are combined in a single interaction site. This leads to a greatly reduced computational cost at the expense of losing the individual contributions of the atoms to the interactions and the exact molecular geometry. The degree of coarseness can vary widely between approaches with united atoms, in which mainly hydrogen atoms are combined with neighboring heavier atoms to form a single interaction site [36,45,203], and coarse-grained approaches, in which up to nine atoms are combined to form a single interaction site [37]. As with atomistic simulations, molecular simulations can be conducted using MC or MD simulation software. Due to the lower amount of computational cost compared to atomistic simulations, much longer simulations times can be achieved in the case of MD simulations or much larger systems in the case of MC simulations [41].

In the following, an overview of the aforementioned simulation techniques for the determination of the thermophysical properties viscosity, interfacial tension, and diffusion coefficient for systems consisting of liquids with dissolved gases will be given.

Viscosity

The dynamic viscosity can be calculated by EMD simulations from fluctuations of the off-diagonal pressure elements in a homogenous phase via the Green-Kubo method. Further details on this approach can be found in Chapter 4 or in the relevant literature [38-40]. However, this method requires relatively long simulation times in the range of 100 ns, especially for large molecules, until the calculated dynamic viscosity converges to a stable value [41,48]. Alternatively, Zhang et al. [204] proposed the time-decomposition approach, where the viscosity is evaluated not from a single long simulation run, but from up to 100 different short simulations in the range of (2 to 5) ns, evaluated by the Green-Kubo method and fitted to a double exponential function. An indirect method for calculating the viscosity has been reported by Jamali et al. [205], where the viscosity is accessible via the dependence of the self-diffusion coefficients on the system size. Here, the authors take advantage of the fact that the system-size correction for the diffusion coefficient, first determined by Yeh and Hummer for the self-diffusion coefficient [206] and later used by Jamali et al. on the mutual diffusion coefficient of binary and multicomponent mixtures [207-208], depending on the system viscosity. Therefore, the viscosity of a system can be calculated from self-diffusion coefficients of at least two different simulation runs with different system sizes.

With NEMD, the viscosity can be calculated using the relationship between the momentum flux and the velocity gradient described in Eq. 2.3, earlier in this chapter. Here, either the linear velocity profile can be specified [209-210] or a momentum flux can be applied to obtain the velocity gradient [211]. Alternatively, a periodic external force can be applied, and the viscosity can be calculated from the resulting oscillatory velocity field according to the Navier-Stokes equation [41,212].

For systems consisting of liquids with dissolved gases, there are still hardly any computer simulations for the determination of viscosity. Of the few publications available, most deal with the viscosity of mixtures based on the solvent CO_2. Here, solvents such as acetonitrile [213-214], methanol [214], brines [53], or linear and cyclic alkanes [53,214-215] are investigated. With the exception of the research from Zheng et al. [215], who studied the binary mixtures of CO_2 and *n*-decane or *n*-hexadecane up to temperatures of 473.15 K, and Aminian and ZareNezhad [53], who studied binary mixtures of CO_2 dissolved in brines and ternary mixtures of CO_2 dissolved in brines and *n*-decane up to 573.15 K, the investigations are limited to near-ambient temperatures. In all cases where experimental reference data were avail-

able, deviations between the simulated and experimental viscosity up to 50% were found by the authors. In many cases, the deviations could be attributed to the failure of the applied FFs to predict the viscosity of the pure solvent and solute [214-215]. For systems consisting of liquids with dissolved gases other than CO_2, two further publications can be found in the literature. Pisarev and Mistry [216] studied the viscosity of binary mixtures of methane dissolved in *n*-butane at 360 K and over a wide composition range using NEMD simulations. By comparing their simulated results with experimental ones, the authors found good agreement within 10% of the experimental values. Velásquez and Hoyos [217] simulated the viscosity of binary mixtures of *n*-heptane dissolved in toluene using both NEMD and EMD simulations. In all cases, similar deviations from experimental reference values within 10% were reported.

Typical uncertainties reported for the simulated viscosities are in the range of (5 to 15)% (k =2), while NEMD methods usually have slightly smaller uncertainties compared with EMD simulations.

Interfacial Tension

The interfacial tension can be determined using computer simulations either via MC or MD simulations. The most commonly applied approach to access the interfacial tension using either simulation method is the Irving-Kirkwood definition, which expresses the interfacial tension from the diagonal elements of the pressure tensor [218-219]. Further approaches to determine the interfacial tension from computer simulations are summarized by Biscay et al. [220]. Of special importance for the calculation of the interfacial tension is the way long-ranging van der Waals interactions are treated. To save computational power, interactions between atoms are often calculated explicitly only within a certain cut-off radius. Long-ranging dispersive interactions beyond the cut-off are approximated using long-range correction algorithms [38,221]. Since such corrections usually use the average density in the simulation volume, they lead to systematic deviations in VLE simulations, where the density of the liquid and vapor phase differ strongly. Papavasileiou et al. [41] performed a systematic study on the influence of long-range dispersive corrections on the interfacial tension and found that the Particle Mesh Ewald (PME) algorithm for LJ interactions (LJ-PME) [222] is able to accurately account for long-range LJ interactions.

Computer simulations for the determination of the interfacial tension of mixtures consisting of liquids with dissolved gases are available in the literature for many different classes of solvents and solutes. They are moti-

vated by systems and applications related to refrigeration technologies [223-224], CO_2 absorption and storage [225-227], enhanced oil recovery [226,228], chemical and energy engineering [55,227,229-230], or fundamental research [231-232], to mention only a few.

Typical uncertainties for the simulated interfacial tension from MC and MD simulations range between (3 and 10)% (k = 2). For most systems, agreement between simulations for interfacial tension and experimental reference data are within 10%. However, in some specific cases, deviations up to 50% are possible [227]. With the exception of a few publications, e.g., the research of Eckelsbach and Vrabec [231], where the authors determined the interfacial tension of binary mixtures of acetone, nitrogen (N_2), and O_2 up to a temperature of 450 K, the investigations are limited to a temperature range between (273.15 and 373.15) K.

Diffusion Coefficient

Different approaches are available to determine mutual diffusion coefficients of a binary mixture from MD simulations. In EMD simulations, the Fick diffusion coefficient D_{11} can be directly calculated using the Fourier correlation method [233-234]. Using this approach, D_{11} can be calculated from Fick's second law of diffusion by analyzing fluctuations in the local species concentration in the Fourier domain [234]. Thereby, D_{11} can be calculated as function of the wavenumber and extrapolated to zero wavenumber. Alternative approaches based on EMD simulations are able to access the Maxwell-Stefan diffusion coefficient $Đ_{12}$ from molecular trajectories via the Green-Kubo [235-236] method or Onsager's reciprocal relationships for multicomponent mass transfer [194-195]. To compare $Đ_{12}$ from EMD simulations with experimental values for D_{11}, they might by converted to D_{11} via the thermodynamic factor Γ_{11} via

$$D_{11} = Đ_{12} \cdot \Gamma_{11} \,. \tag{2.7}$$

Γ_{11} can be calculated either directly from EMD simulations using Kirkwood-Buff integrals [237-238] or from activity coefficients [239]. The approach of calculating D_{11} from EMD simulations via $Đ_{12}$ and Γ_{11} is also applied in this work and described in more detail in Chapter 4.

Using NEMD simulations, D_{11} can directly be accessed by solving Fick's first law of diffusion. While classical NEMD create a steady-state concentration gradient in the simulation volume and determine the diffusive mass flux to access D_{11}, reverse NEMD simulations apply a diffusive mass flux using a

mass exchange algorithm and analyze the concentration gradient under steady-state conditions to determine D_{11}.

Special care has to be taken, when calculating mutual diffusion coefficients for electrolyte systems, because these systems contain free-moving ions. Since electrolytic components, like ILs or salts in solutions, disassociate into two species, namely anions and cations, a species-based derivation of the mutual diffusion coefficient must be performed [161]. In the case of binary mixtures of an electrolyte and a non-electrolyte, as it is the case for all electrolyte systems in this work, this means that three different species are present. While the diffusive mass transport in a mixture with three species is usually defined by a 2x2 diffusion coefficient matrix, the electroneutrality condition, which links the motion of anions and cations [240], reduces the number of independent mass fluxes by one. Therefore, only one single mutual diffusion coefficient is required to describe the diffusive mass transport in binary mixtures of an electrolyte and non-electrolyte [161]. More details on the determination mutual diffusion coefficients in electrolyte systems are given in Chapter 4.

Available publications on the diffusion coefficient in mixtures consisting of liquids with dissolved gases can be differentiated in investigations close to and outside of infinite dilution. The investigation of mutual diffusion coefficients close to infinite dilution have the advantage that the self-diffusion coefficient of the infinitely diluted component converges to the mutual diffusion coefficient [241]. The computational effort for calculating the self-diffusion coefficient is smaller compared to the mutual diffusion coefficient, so only the self-diffusion coefficient of the diluted component is calculated. Therefore, multiple investigations of the diffusion coefficient close to infinite dilution, mainly for binary mixtures based on CO_2 as the solute are available in the literature [47,242-246]. For further binary mixtures which are not based on CO_2 as the solute, the research of Makrodimitri et al. [48], who studied the self-diffusion coefficient of H_2, CO, or H_2O dissolved in *n*-alkanes, and Koller at el. [49], who studied the self-diffusion coefficients of various light gases in an IL, can be mentioned.

Typical statistical uncertainties related to the self-diffusion coefficient at infinite dilution range between (5 and 20)% (k = 2). The deviation of simulated self-diffusion coefficients from experimental D_{11} data are highly dependent on the underlying FF and range between less than 10% and up to a factor of two and more. With the exception of a few publications [47-48,246], the investigations are limited to temperatures below 373 K.

For the mutual diffusion coefficient of binary mixtures of liquids with dissolved gases, only a few publications are available in the literature [51,233,247]. Zabala et al. [51] investigated D_{11} in binary mixtures consisting of CO_2 dissolved in various linear alkanes up CO_2 mole fractions of 0.7 at temperatures between (298 and 373) K. The authors used EMD simulations to access $Đ_{12}$ with average statistical uncertainties of 10 % and used the theoretical perturbed chain statistical associating fluid theory (PC-SAFT) model to calculate Γ_{11} from fugacity coefficients of CO_2. The agreement with available experimental data was strongly dependent on the system. In the case of CO_2 dissolved in *n*-hexadecane, agreement within 15% with respect to the experimental data was found, while the results for CO_2 dissolved in *n*-decane deviated up to a factor of two from the experimental reference [51]. Dos Santos et al. [233] used a modified approach to directly calculate D_{11} using the Fourier correlation method and validated their method by comparing simulated D_{11} data for mixtures consisting of CO_2 dissolved in *n*-hexane or *n*-octane for temperatures up to 373 K and CO_2 mole fractions up to 0.62. The simulated data with a statistical uncertainty between (5 and 10)% (k = 2) agree within 30% with the experimental data at infinite dilution of the dissolved CO_2 but deviate up to 80% over a wide concentration range [233]. Krishna and van Baten [247] calculated $Đ_{12}$ in binary, ternary and quaternary mixtures of linear alkanes at temperatures between (308 and 333) K and a pressure of 30 MPa, covering the entire composition range. The specified statistical uncertainty for $Đ_{12}$ is approximately 5% (k = 1). Since, however, no experimental data for the mutual diffusion coefficient was available, the authors compare the self-diffusion coefficients of both components in a binary mixture of CH_4 dissolved in *n*-hexane or *n*-octane to experimental reference values. Here, the authors find good agreement within 10% between the simulated and experimental self-diffusivities over the entire composition range [247].

In summary, the literature review for the thermophysical properties viscosity, interfacial tension, and mutual diffusivity of liquids with dissolved gases accessed by computer simulations shows considerable shortcomings. Considering the investigated systems, an imbalance of investigated solutes towards CO_2 is obvious. To get a fundamental understanding on how the dissolved gas influences the thermophysical properties of the mixture, a wide range of different solutes should be investigated in the same solvent, which is only done partially so far. Here, the solutes should show variations in molecular size, weight, and polarity. Furthermore, also a systematic variation of the solvent molecule must be performed to investigate the influence of the solvent size, structure, and polarity. While investigations of

thermophysical properties, for example, were performed for systems consisting of CO_2 dissolved in various hydrocarbons, including alcohols, only a systematic investigation based on CO_2 dissolved in a linear alkane, its branched isomer, and its corresponding primary alcohol can answer how the molecular structure of the solvent influences the thermophysical properties. A further limitation of the available literature data is the lack of overlapping thermodynamic states. To use available literature data to investigate how solute and solvent characteristics influence thermophysical properties, the investigations must be performed at comparable thermodynamic states, which at the moment is not the case. Finally, the available thermophysical properties research using computer simulations is often limited to temperatures below 400 K. Technical applications with systems of liquids with dissolved gases are often conducted at higher temperatures, so the use of available literature data is strongly limited.

3 Aim of this Thesis

The aim of this thesis is the characterization of binary systems consisting of liquids with dissolved gases by the determination of their thermophysical properties viscosity, interfacial tension, and mutual diffusion coefficient. Therefore, light scattering experiments performed in the bulk of the liquid phase and at the vapor-liquid interface, which are able to determine the aforementioned thermophysical properties under saturation conditions in macroscopic thermodynamic equilibrium, are combined with EMD simulations, which are able to access the same thermophysical properties in macroscopic thermodynamic equilibrium at or close to saturation conditions.

To get a fundamental understanding on how the molecular characteristics of both components influence the thermophysical properties of the mixture, a systematic variation of solute and solvent molecules is included. The different solvent classes contain, therefore, linear and branched alkanes and alcohols with a varying number of carbon atoms, as well as imidazolium based ILs with a variation of the carbon chain length attached to the imidazolium ring. To determine the influence of the carbon chain length on the thermophysical properties of the mixture, mixtures based on linear alkanes with a varying carbon chain length are investigated. The influence of branching and hydroxylation is analyzed by investigating binary mixtures based on a linear alkane, as well as its branched isomer or alcohol with the same number of carbon atoms. As solutes, different gases with varying size, weight, and polarity are investigated. Therefore, the gases H_2, helium (He), CH_4, water, CO, N_2, CO_2, and Krypton (Kr) were selected.

The SLS method, which can be applied up to high, process-relevant temperature of 573 K was used for the simultaneous determination of the viscosity and interfacial tension of the binary mixture consisting of liquids with dissolved gases at macroscopic thermodynamic equilibrium. To experimentally investigate the influence of the dissolved gas on the thermophysical properties of the solvent, SLS experiments are additionally performed for the pure solvents under saturation conditions up to 573 K. Furthermore, the influence of possible co-solvents that can be formed in technical applications via side-reactions, is determined through the investigation of binary and ternary liquid mixtures consisting of the long linear alkane *n*-octacosane with shorter linear or branched alkanes, alcohols, or acids. DLS experiments, which are able to access the Fick diffusion coefficient and the thermal diffusivity simultaneously in macroscopic thermo-

dynamic equilibrium, are performed under saturation conditions up to a temperature of 423 K. The DLS experiments were performed by co-authors in the respective publications. The resulting data for the Fick diffusion coefficients are included in this work, however, to validate the EMD simulations and to discuss the influence of the molecular characteristics of the solute and solvent on the diffusion coefficient.

For all investigations of thermophysical properties of liquids with dissolved gases, the light scattering experiments are combined with EMD simulations, which are able to access all three thermophysical properties that are of interest in this work in macroscopic thermodynamic equilibrium at or close to saturation conditions. Additionally, EMD simulations are used to get an insight into the fluid structure on a molecular level and analyze structure-property relationships, which in turn can help to get a fundamental understanding of how the fluid structure influence the thermophysical properties and can help to develop prediction models build on a strong physical basis. Therefore, EMD simulations are performed for all systems consisting of liquids with dissolved gases at comparable thermodynamic states as the light scattering experiments up to a temperature of 573 K. With respect to the shortcomings of available FFs for the prediction of thermophysical properties up to high temperatures, also an assessment and modification of available FFs is performed. Based on the best-performing FF for the prediction of the thermophysical properties for the pure solvents, a modification of the FF is presented, which removes the temperature dependency of the prediction accuracy. By applying the modified FF to systems consisting of liquids with dissolved gases, the influence of molecular characteristics of the components on the thermophysical properties of the mixture can be analyzed using EMD simulations over a wide temperature range.

Based on the results from light scattering experiments and EMD simulations, a predictive engineering model for the binary diffusion coefficient in mixtures consisting of liquids with dissolved gases close to infinite dilution of the gas is developed and validated using experimental reference data from the literature. This model only depends on the thermodynamic state and the thermophysical and chemical properties of the pure solvent and solute and can, therefore, be applied to arbitrary systems.

4 Applied Strategy and Used Methods

In this chapter, the strategy and an overview on the most important methods for investigating the thermophysical properties of systems consisting of liquids with dissolved gases are given. At first, the molecules investigated in this work will be summarized. More details for the used methods are given in the respective publications that are part of this work. First, the SLS and DLS methods for the experimental investigation of the viscosity, interfacial tension, and mutual diffusion coefficient are described. Thereafter, the basic concept of EMD simulations with a focus on the prediction of the aforementioned thermophysical properties is given.

4.1 Model Systems of Interest

The solvents and solutes investigated by light scattering experiments and EMD simulations as part of this work are summarized in Figure 4.1. As solvents, seven linear alkanes with a carbon number ranging between 6 and 40 are included to investigate the influence of the carbon chain length on the thermophysical properties. By including primary alcohols with a carbon number ranging between 2 and 16, the influence of the carbon chain length can be analyzed also for primary alcohols and the influence of hydroxylation can be studied by comparing the results for primary and one diol to the corresponding linear alkanes. To analyze the influence of branching on the thermophysical properties, additionally branched alkanes and alcohols with the same number of carbon atoms as the investigated linear alkanes and alcohols are included. Furthermore, imidazolium-based ILs with varying carbon chain length at the cation ($[C_xC_1IM]$, x = 2, 6, or 10) and bis(trifluoromethane)sulfonimide as the anion $[NTf_2]$ are included in the investigations of the mutual diffusion coefficient in liquids with dissolved gases. By including ILs as solvents, the range of molecular mass and viscosity of the solvents is considerably extended. Further, the influence of the strong charge localization in ILs on the diffusive mass transport can be investigated. The two acids included as solvents are not investigated in mixtures with dissolved gases, but are rather investigated in mixtures with the long linear alkane *n*-octacosane since such acids, together with short linear and branched alkanes as well as alcohols, can be formed during the synthesis of linear alkanes.

As solutes, the gases H_2, He, CH_4, water, CO, N_2, CO_2, and Kr were chosen for their wide range of molecular weight, size, and polarity. Of special

interest are, for example, the two gases CO and N_2, which have nearly identical molecular weights but strongly differ in their polarity and are therefore suitable candidates to analyze the influence of the solute polarity on the thermophysical properties of the mixture when dissolved in liquids. Another solute pair that is of great interest especially for the investigation of diffusion coefficients in systems consisting of liquids with dissolved gases, is H_2 and He. Since He is the heavier molecule of the two but has a smaller molecule size, investigations of mixtures containing the two molecules help to get a better understanding of how the molecule size and weight influence the mutual diffusion coefficient.

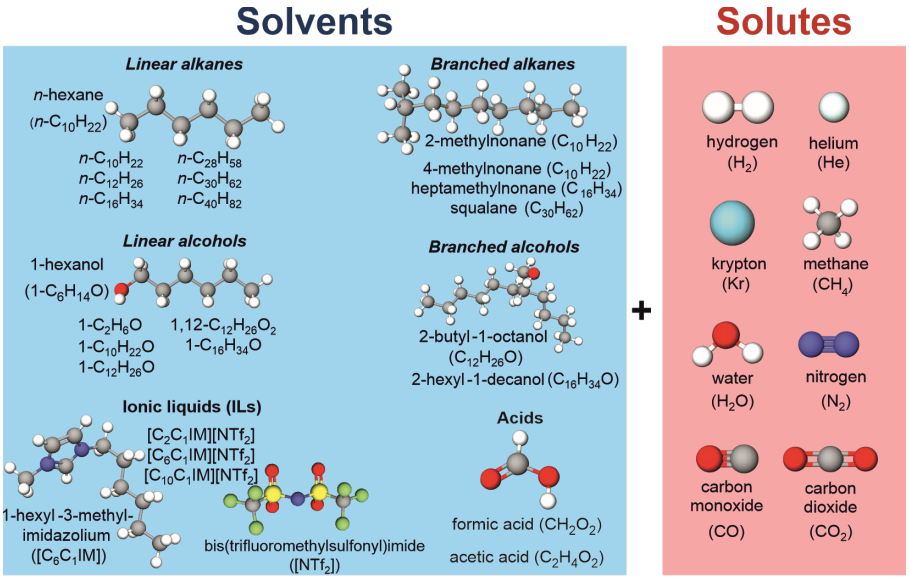

Figure 4.1: Solvents and solutes investigated in this work.

4.2 Dynamic Light Scattering

4.2.1 Surface Light Scattering – Viscosity and Interfacial Tension

The SLS technique is applied in this work to measure the viscosity and interfacial tension of pure solvents, binary and ternary solvent mixtures, as well as binary systems consisting of liquids with dissolved gases under saturation conditions in macroscopic thermodynamic equilibrium. Unlike

various conventional methods, the SLS technique is able to determine both properties from microscopic fluctuations at the interface between to fluid phases and, therefore, does not rely on imposing any macroscopic gradients. Further advantages of the technique are its contact-less measuring principle and that no calibration must be performed.

In this section, the basic principles of the techniques, the data evaluation, and the experimental setup are briefly introduced. For more detailed information on the SLS technique, the reader is referred to previous publication of Fröba et al. [116,120,248-249].

Theoretical Background

The SLS technique is based on the detection and evaluation of light scattered from microscopic fluctuations at a liquid surface, also referred to as surface or capillary waves. Such fluctuations are caused by the Brownian motion of molecules and are always present at a liquid surface. By irradiating the surface wave with coherent laser light, which interacts with the surface fluctuations, information on the dynamics of the surface waves is contained in the scattered light. A schematic representation of the scattering geometry in a SLS measurement is given in Figure 4.2 a). By fixing the angle of the incident light Θ_E and the detection direction, the scattering angle Θ_S is defined. Thereby, also the scattering vector $\vec{q} = \vec{k}_I' - \vec{k}_S'$ is defined, where $\vec{k}_I'$ and $\vec{k}_S'$ are the projections of the wave vectors of the refracted and scattered light into the plane of the surface. Consequently, the wave number of the surface vibration mode is determined [116].

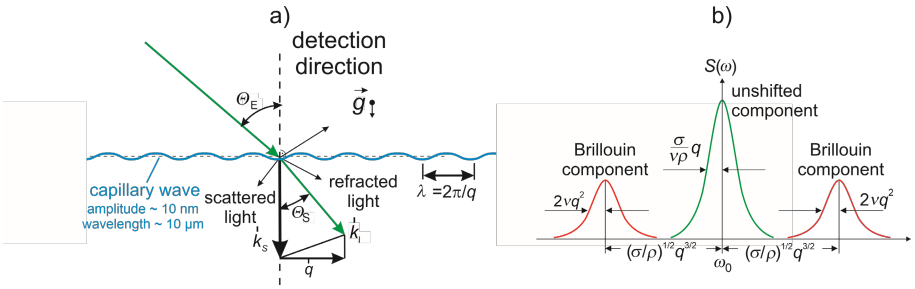

Figure 4.2: a) Schematic representation of the scattering geometry. b) Spectrum of the scattered light from SLS experiments. First order approximation for the relationship between line broadening and frequency shift are given within the spectrum.

A schematic representation of the spectrum of the scattered light is shown in Figure 4.2 b). Here, using the capillary number $Y = \sigma\rho/(4\eta^2 q)$, two different cases can be identified. For $Y \leq 0.145$, which is usually observed for

systems with a large viscosity and/or small interfacial tension, an overdamped behavior of the related surface waves and a frequency-unshifted Rayleigh line is observed. For systems that have a small viscosity and/or large surface tension and $Y < 0.145$, an oscillatory behavior of the surface wave leading to a frequency shift and, therefore, a Brillouin doublet can be observed [116].

Using a first-order approximation, which is also shown in Figure 4.2 b), the viscosity and interfacial tension of the liquid phase can be determined from the half-width at half-maximum and frequency shift of the Brillouin doublet in the case of an oscillatory behavior. In the case of an overdamped behavior, only the ratio of the interfacial tension to the viscosity can be determined from the half-width at half-maximum, using the first-order approximation. In this case, additional knowledge of either the viscosity or interfacial tension is required to access the other thermophysical property. However, these first-order approximations do not reliably give access to the thermophysical properties. Therefore, an exact description of the dynamics of free surface waves in the form of the Navier-Stokes equation for incompressible fluids, neglecting the influence of gravitational forces, is used to get accurate results for the thermophysical properties using the damping and frequency of the surface waves [116]. Next to the damping and frequency of the surface waves, further input parameters that are required for solving the working equation are the density of the liquid and vapor phase, as well as the viscosity of the vapor phase.

Data Evaluation

Due to the relatively small line width in the SLS spectrum, analyzing the scattered light in the frequency domain is still challenging. An alternative approach, which is also applied in the case of SLS, is the evaluation of the scattered light in the time domain using photon correlation spectroscopy. Here, the second-order correlation function (CF) of the scattered light intensity is calculated in a post-detection arrangement using a correlator. Two different cases for the CF can be determined, the homodyne and heterodyne detection conditions. Under homodyne conditions, solely the light scattered from the surface fluctuations is analyzed. Due to residual stray light in the experimental setup or reflected light from dust or the cell windows, however, homodyne detection conditions can often not be realized. Using heterodyne detection conditions, the intensity of coherent reference light, which might origin from stray light or is actively superimposed to the scattered light, is of much higher intensity. For all measurements in this work, heterodyne measuring conditions were ensured by superimposing

coherent, unscattered laser light with the light scattered from the surface fluctuations.

Using the heterodyne measurement conditions, the normalized CF $g^2(\tau)$ as function of the correlation time τ for the overdamped case has the form

$$g^2(\tau) = a_g + b_g \cdot \exp(-\tau / \tau_C). \quad (4.1)$$

Here, a_g and b_g are experimental constants depending on the measurement conditions and are not directly required to get access to the thermophysical properties. The mean decay time of the exponential function τ_C however, is the inverse of the damping of the surface wave and enters directly in the working equations. As discussed before, in this case the ratio between the interfacial tension and the viscosity can be accessed. If the surface waves show an oscillating behavior however, $g^2(\tau)$ has the form

$$g^2(\tau) = a_g + b_g \cdot \exp(-\tau / \tau_C) \cdot \cos(\omega_R \tau - c_g). \quad (4.2)$$

Here, ω_R is the propagation frequency of the surface waves and the parameter c a correction which accounts for deviations from the Lorentzian form of the spectrum. In this case, both τ_C and ω_R are determined and used as input parameters in the working equation to get access to the viscosity and interfacial tension simultaneously

To determine τ_C and ω_R, the calculated CF is then fitted using either Equation 4.1 or 4.2, depending whether an overdamped or oscillatory behavior is observed. Exemplary CFs for the overdamped and oscillatory case are shown in Figure 4.3. For the pure solvent 2-hexyl-1-decanol, an overdamped behavior of the surface waves can be found at low temperatures and is shown in Figure 4.3 a) for a temperature of 298.15 K. At temperatures above 348.15 K, an oscillatory behavior of the surface waves can be observed, as shown in Figure 4.3 b) at a temperature of 573.15 K. To determine the uncertainties related to the viscosity and interfacial tension from SLS experiments, at least six different measurements with different Θ_S are performed at each thermodynamic state. The expanded experimental uncertainties are then calculated by performing a Gaussian error propagation using the first-order approximation for both properties. Here, the uncertainty in determining τ_C and ω_R in the form of the double standard deviations from the different measurements, as well as the uncertainty from further input parameters like the density of the liquid and vapor phase, the vapor phase viscosity, and the angle determination are included. For more information on the data evaluations and the determination of the uncertainties, the

reader is referred to the publications, which are part of this work [14,16,250-252].

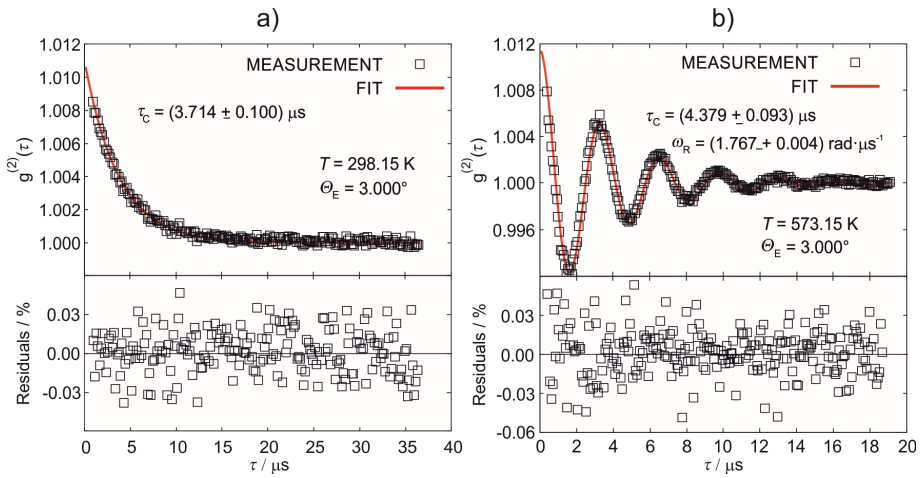

Figure 4.3: CFs determined for pure 2-hexyl-1-decanol showing an overdamped behavior of the surface waves at 298.15 K (a)) and showing an oscillatory behavior of the surface waves at 573.15 K (b)). The solid lines refer to the theoretical description of the CF according to Equations 4.1 and 4.2.

Experimental Setup and Sample Preparation

For the SLS experiments, a Nd:YVO_4-laser (Coherent Verdi-V2) with a laser wave length in vacuo of 532 nm was used. The laser light was focused at the vapor-liquid interface using a lens with a focal length of 2 m. A combination of a polarization beam-splitter and a half-wave plate is used to adjust the laser power of the incident and reference light.

The samples to investigate were prepared with PTFE filters with a pore size of (200 or 450) nm before degassing for at least 2 hours. Afterwards, approximately 40 ml of the solvent or liquid mixture were filled in a stainless-steel measurement cell, which has four windows for optical access. In the case of pure solvents or solvent mixtures, the vapor phase above the samples were flushed multiple times with He. Afterwards, the vapor phase of the cell was filled with He at ambient pressure to avoid water and air in the cell. In case of a mixture of a liquid with a dissolved gas, the vapor phase and the periphery tubing were flushed with He before adding the solute gas. In order to allow measurements up to 573 K, the measurement cell, as well as the periphery tubing and the pressure sensor, which was used to adjust the necessary pressure in the cell, were placed in an insulation

housing and heated up to the required temperature using resistant-heating wires. The temperature was measured using a PT-100 resistance probe.

The scattered light was detected in transmission direction through the transparent liquid layer and was superimposed by the coherent reference light after the measurement cell. The distance between the measurement cell and the detector in the form of photomultiplier tubes was more than 4 m to guarantee a well-defined scattering geometry. The signal from the detector was fed into a correlator with a linear spacing between the correlator channels and a maximum of 256 channels.

For further information on the sample preparation and experimental setup, the reader is referred to the publications as part of this work [14,16,250-252].

4.2.2 Dynamic Light Scattering from Bulk Fluids – Diffusion Coefficient

Results for the Fick diffusion coefficient from DLS experiments are included in this work for the validation of EMD simulations as well as for the analysis of how the molecular characteristics of the solvent and solute molecules influence the thermophysical properties. Since the measurements were performed by other scientific staff at the Institute of Advanced Optical Technologies – Thermophysical Properties, the experimental investigation of diffusivities by DLS are not directly part of this work. Since the results will be discussed later, the theoretical background and data evaluation are important, and a brief introduction into the technique will be given in the following. For further information on the DLS technique, the reader is referred to the publications within this work [33,42,253-256] as well as the literature [181,193,257-258].

Both the SLS and DLS technique are based on the analysis of light scattered by microscopic fluctuations, and, therefore, share the same advantages towards conventional measurement techniques. These are, for example, the nature to determine thermophysical properties in a contact-less way in macroscopic thermodynamic equilibrium without the need of a calibration.

The DLS technique is based on the analysis of light scattered in the bulk of a fluid phase by microscopic fluctuations in temperature, pressure, and, in the case of mixture, the composition while the sample is at macroscopic thermodynamic equilibrium. According to work of Onsager, who formulated his hypothesis of regression [194-195], microscopic gradients in temperature, pressure, and composition relax in the same manner as macroscopic gradients. Therefore, the transport properties related to gradients in

the aforementioned state properties can be determined from the analysis of microscopic fluctuations. As it is the case for SLS, by defining the angle of the incident light and the angle under which the scattered light is detected, fluctuations related to a defined wave vector are studied. A schematic representation of the spectrum of the scattered light of a binary mixture from DLS is shown in Figure 4.4.

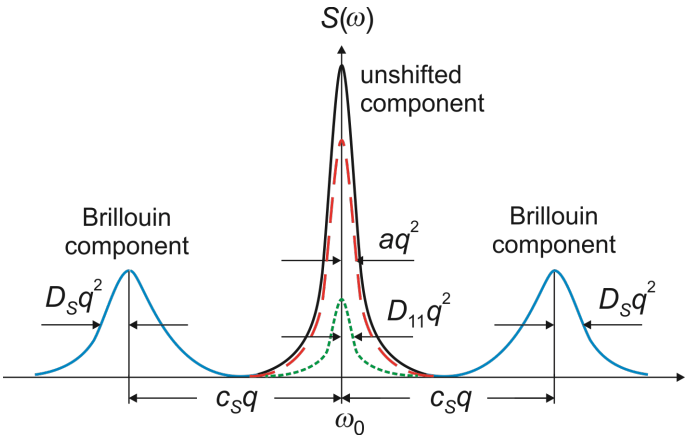

Figure 4.4: Spectrum of the scattered light from DLS experiments for a binary mixture.

In the central frequency-unshifted component, two different contributions related to fluctuations in temperature (red) and composition (green) can be found. In both cases, the damping, i.e. half-width at half-maximum, can directly be related to the corresponding transport properties thermal diffusivity a, in the case of temperature fluctuations, and D_{11}, in the case of fluctuation in composition. Propagating fluctuations in pressure, which lead to a Brillouin-doublet in the spectrum of the scattered light and allow the determination of the speed of sound c_S and sound attenuation D_S, are not of interest in this work and are, therefore, not further discussed. For more information on the analysis of scattered light caused by fluctuations in pressure, the reader is referred to the literature [156,259].

Applying photon correlation spectroscopy in a heterodyne detection scheme, as it was done for all investigations in this work, the normalized CF $g^2(\tau)$ is described by

$$g^2(\tau) = a + b \cdot \exp\left(-\tau / \tau_{C,t}\right) + c \cdot \exp\left(-\tau / \tau_{C,c}\right). \qquad (4.3)$$

Here, $\tau_{C,t}$ and $\tau_{C,c}$ are the characteristic decay times of fluctuations related to fluctuations in temperature and composition, which can be accessed by fitting the experimentally determined correlation function to the theoretical model in Equation 4.3. The two transport properties can then be determined using

$$a = \frac{1}{\tau_{C,t} q^2} \text{ and } D_{11} = \frac{1}{\tau_{C,c} q^2}. \tag{4.4}$$

The experimental setup for DLS measurements is nearly identical to the one described in the previous section for the SLS measurements. For DLS experiments in this work, however, the laser light is focused in the bulk of the liquid phase to get access to a and D_{11}. For more details on the theoretical background, experimental setup, and data evaluation, the reader is referred to the publications that are part of this work [33,42,253-256].

4.3 Equilibrium Molecular Dynamics Simulations

In the following, the strategy, computational details, and data evaluation for the EMD simulations performed in this work to get access to the liquid viscosity, mutual diffusivity, and the interfacial tension are given. Details on the applied FFs and, if necessary, FF developments and optimizations are given together with the results in Chapter 5.

All EMD simulations in this work were performed with the GROMACS simulation package [221] and the leap frog algorithm was used to include the equations of motion. The simulations with fully flexible molecules were performed with a time step of 1 fs, while a time step of 2 fs was used in the case that the bonds connecting the light hydrogen atoms were constraint with the linear constraint solver (LINCS) [260]. In a first step, the solvent molecules adding up to between (10,000 and 40,000) atoms were randomly added in a cubic simulation box with a volume corresponding to the saturation liquid density at the given temperature. While for small molecules 10,000 atoms were enough to obtain approximately 500 molecules, the number of atoms was increased for the larger molecules like long linear and branched alkanes and alcohols or ILs. To find a stable configuration to start dynamic simulations, an energy minimization was preformed, using the steepest decent minimization algorithm, which is included in the GROMACS software package. Once the potential energy of the system converged to a stable value, the temperature of the system was defined by

assigning randomized velocities, corresponding to the desired temperature to the atoms and molecules. The temperature was equilibrated in a short simulation run of approximately 1 ns in the canonical ensemble (*NVT*). In a consecutive simulation, the pressure of the system was adjusted in a 5 ns isobaric-isothermal ensemble (*NpT*), where the box size was varied to achieve the desired pressure. While the first part of this simulation run is neglected for equilibration of temperature and pressure, the latter part of the simulation was used to determine the liquid density. Since liquid density data are available in the literature for most of the solvents studied in this work, a comparison of the calculated densities with experimental reference value served as a first validation of the simulations. After the *NpT* simulation run, the production run in an *NVT* ensemble in the slightly compressed liquid phase, in the case of the viscosity and diffusion coefficients, or in VLE, in the case of the interfacial tension, were performed. The simulations in the compressed liquid phase were performed at 0.1 MPa, when the saturation pressure was below 0.05 MPa. In the case of a saturation pressure above 0.05 MPa, the simulations were performed at 0.2 MPa above the pressure value. With this procedure a phase separation is avoided, which might occur due to the inability of the FFs to accurately predict the saturation pressure. For simulations in VLE, the simulation box was extended in one coordinate direction to create two interfaces. Afterwards, further molecules corresponding to the vapor density at the given thermodynamic state were randomly added.

For binary mixtures consisting of liquids with dissolved gases, the fully equilibrated ensemble at the end of the *NpT* run was used to add the desired number of solute molecules to the liquid phase. Afterwards, the energy minimization and equilibration of temperature and pressure, as described before, was repeated. For VLE simulations, both solvent and solute molecules were added into the vapor phase after extending the box size. The necessary number of solute molecules in the vapor phase was calculated using the vapor density of the gas at the given temperature and partial pressure. The partial pressure was taken from solubility data from the literature.

In all simulations, periodic boundary conditions in all directions were used. The temperature and pressure were controlled using the Nosé-Hoover thermostat [261-262] and Parrinello-Rahman barostat [263-264] with coupling constants of (1 and 14) ps, respectively. Electrostatic interactions were calculated using the particle-mesh Ewald (PME) algorithm [265]. The cut-off for both LJ and electrostatic interactions in the compressed liquid phase was set to 1.6 nm except for simulations with the ILs, where the FF specifies

a cutoff of 1.2 nm [266]. The contribution of LJ interactions to the energy and pressure in the compressed liquid phase were calculated using a standard dispersion correction algorithm included in GROMACS. However, since this dispersion correction is based on the average density in the simulation box, it leads to a strong dependency of the cutoff radius on the calculated interfacial tension. For the binary mixture of *n*-hexane with CO_2, a systematic study of the relationship between the cutoff radius and the interfacial tension has shown that a cutoff of at least 2.0 nm has to be chosen for VLE simulation when using the long-range dispersion corrections. Alternatively, a PME algorithm for long-range LJ interactions called LJ-PME algorithm [222] can be used. Since this algorithm does not rely on the average box density, no cutoff-dependency of the interfacial tension for cutoffs above 1.6 nm could be found. For all systems except the binary mixture of *n*-hexane and CO_2, therefore, the LJ-PME algorithm was used to treat long-ranging LJ interactions.

The final production runs were performed at the high-performance computer (HPC) cluster at the Erlangen Regional Computing Center (RRZE) at the Friedrich-Alexander-University Erlangen-Nürnberg (FAU). The simulations and the post-processing were parallelized on up to five computer nodes, each equipped with 20 physical computer cores, in order to improve the statistics of the simulations or to accelerate the post-processing. In all cases, at least three independent simulations were performed for each thermophysical property and the results from the independent runs were averaged and used to calculate the statistical uncertainty via the double standard deviation.

4.3.1 Viscosity

In this work, the dynamic viscosity η in the slightly compressed liquid is calculated using the Green-Kubo formalism [235-236]

$$\eta = \frac{V}{k_B T} \lim_{\tau' \to \infty} \int_0^{\tau'} \left\langle p_{ij}(\tau + t_0) \cdot p_{ij}(t_0) \right\rangle d\tau \quad \text{with } (i \neq j). \tag{4.5}$$

Here, k_B, T, and V denote the Boltzmann constant, temperature and simulation volume, respectively. The autocorrelation function of the off-diagonal elements of the pressure tensor, i.e. p_{xy}, p_{xz}, and p_{yz}, as a function of the correlation time τ and the angle bracket denote the ensemble average of all possible time origins t_0.

The viscosity as a function of τ as calculated by Equation 4.5 is shown exemplary for the two pure solvents *n*-hexane and *n*-decane at a temperature of 423.15 K in Figure 4.5. In the case of *n*-hexane, the viscosity reaches a plateau after approximately 10 ps. For *n*-decane, which has a larger viscosity, the plateau is reached after approximately 45 ps. In both cases, very strong fluctuations of the calculated viscosity at $\tau < 5$ ps are present. These fluctuations are related to the vibrations of bonds and angles in fully flexible molecules. If the off-diagonal elements of the pressure tensor are saved very frequently, these high-frequency oscillations do not contribute to the calculation of the viscosity. For the simulations in this work, a saving frequency of ≤10 fs was found to be large so that the calculated viscosity is independent of the saving frequency. The final value for the viscosity was calculated by averaging over the plateau. However, since the starting point of the plateau has to be manually fixed, this method is subjective to the person who does the post-processing.

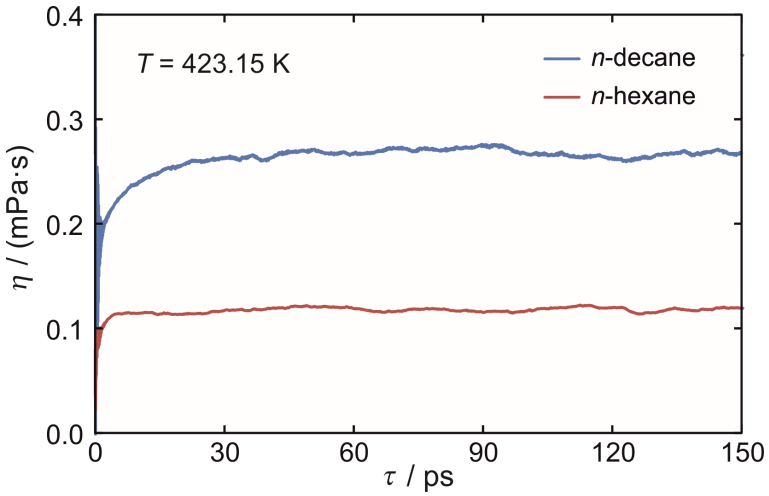

Figure 4.5: Liquid viscosity of n-hexane and n-decane as function of the correlation time τ at a temperature of 423.15 K.

An alternative approach was suggested by Zhang et al. [204], who fitted the viscosity as a function of the correlation time using the sum of two exponential functions. The authors further suggest to perform up to 100 short simulations of (1 to 4) ns instead of performing a long simulation in the range of 100 ns. Both approaches were tested in this work and have shown to give similar results within combined uncertainties. Since in this work,

diffusion coefficients and the viscosity were calculated from the same simulation run, long simulation runs of about (60 to 150) ns were performed. The specified statistical uncertainties are the double standard deviations of the three to five independent simulations. Typical uncertainties related to the calculation of the viscosity depend on the system on investigation and are between 5% (k = 2), in the case of CO_2 dissolved in *n*-hexane, and about 10% (k = 2), in the case of different gases dissolved in *n*-hexadecane.

To accelerate the viscosity calculation, a post-processing script based on the programming language FORTRAN was developed, which allowed the parallelization of the computational effort on multiple computer cores.

For more details on the calculation of viscosities from EMD simulations, the reader is referred to the publications in this work [14,16,252,255-256] and basic literature on the subject [38-40].

4.3.2 Interfacial Tension

To determine the interfacial tension of a system using EMD simulations, VLE simulations must be performed. To ensure that the dimensions of the liquid layer do not influence the calculated interfacial tension, a systematic study on the influence of the liquid layer thickness and the interfacial area on the interfacial tension was performed for the binary mixture of *n*-hexane and CO_2. Here, a liquid layer thickness of at least 4 nm and an interfacial area of at least 4.5 nm x 4.5 nm were found to be sufficient. For binary mixtures based on long linear alkanes and alcohols, however, the liquid layer thickness was further increased to ensure that molecules in the liquid phase do not interact with both interfaces simultaneously. This led to a number of atoms between (20,000 and 40,000) for the investigations in this work.

For the evaluation of the interfacial tension, the approach to Kirkwood and Buff [219], which is based on the analysis of the diagonal element of the pressure tensor, i.e. p_{xx}, p_{yy}, and p_{zz}, was applied. In this approach, the interfacial tension σ is calculated by averaging the diagonal elements of the pressure tensor normal (p_N) and tangential (p_T) to the vapor-liquid interface according to

$$\sigma = \frac{L_N}{2}\left\langle p_N(t) - p_T(t)\right\rangle . \tag{4.6}$$

Here, L_N is the length of the simulation box in the direction normal to the interface. The angle brackets denote averaging over simulation time t. The running average of the interfacial tension, as well as p_N and p_T as a function

of the simulation time are exemplarily shown in Figure 4.6 for the binary mixture of *n*-hexadecane and CO_2 at a CO_2 mole fraction of 0.2 and a temperature of 423.15 K.

The results in Figure 4.6 show a relatively fast convergence of the surface tension within the first 1.6 ns of the simulation run. Typical lengths of the simulations to access the interfacial tension with a statistical uncertainty of about 5% (k = 2) are (20 to 30) ns, while the first 3 ns are excluded from the data evaluation for equilibration purposes. The reason for the shorter simulations and smaller uncertainties for the interfacial tension, compared to the viscosity, is the fact that equilibrium properties are calculated on the basis of averaging over many different time frames, while dynamic and transport properties rely on the evaluation of statistical fluctuations.

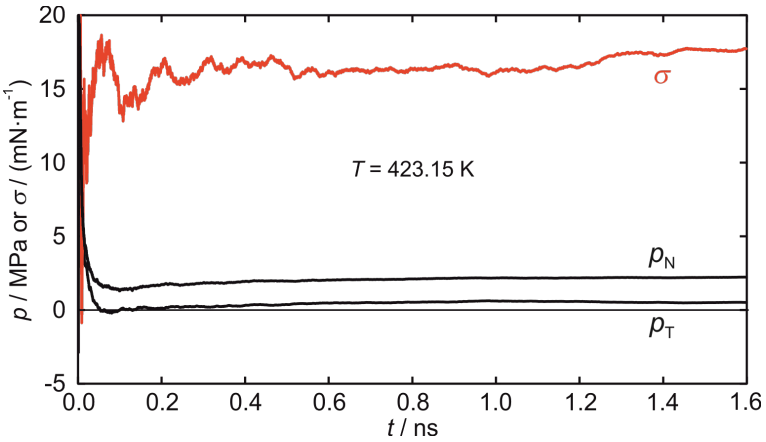

Figure 4.6: Running average of the interfacial tension σ and the normal and tangential diagonal components of the pressure tensor as a function of simulation time t for a binary mixture consisting of n-hexadecane and CO_2 with a CO_2 mole fraction of 0.2 at a temperature of 423.15 K.

Further information on the calculation of the interfacial tension via EMD simulations can be found in the publications from this work [14,16,252,255-256] and basic literature on the subject [38-40].

4.3.3 Diffusion Coefficients

In the following, the strategy and methods for calculating the self-diffusion coefficient of the mixture components, as well as the mutual diffusion coefficient in binary non-electrolyte and electrolyte mixtures are briefly

introduced. For more information on the calculation of diffusion coefficients, the reader is referred to the publications from this work [33,42,253-256] or the literature [161-162,241,247,267-268].

Self-diffusion Coefficient

The self-diffusion coefficient of pure solvents can be used for the validation and development of the underlying FFs, as it was done in this work for pure ILs and linear alkanes [14,255]. In mixtures, the self-diffusion coefficients of the components can be used for the prediction of the mutual diffusion coefficient [161,268]. For binary mixtures, where the solute concentration is in the range of infinite dilution, the Maxwell-Stefan ($Đ_{12}$) and Fick (D_{11}) diffusion coefficient can be approximated by the self-diffusion coefficient of the solute. Using the relationship between $Đ_{12}$ and D_{11} according to Equation 2.7 and the relationship between $Đ_{12}$ and the Onsager coefficients Λ_{ij} [269] one can write for a binary non-electrolyte mixture

$$D_{11} = Đ_{12}\Gamma_{11} = \Gamma_{11}\left(\frac{x_2}{x_1}\Lambda_{11} + \frac{x_1}{x_2}\Lambda_{22} - 2\Lambda_{12}\right). \tag{4.7}$$

Λ_{ij} can be directly calculated from the motion of the molecules according to [247]

$$\Lambda_{ij} = \frac{1}{3N}\lim_{\tau'\to\infty}\int_0^{\tau'}\left\langle \sum_{k=1}^{N_i} v_{k,i}(\tau + t_0)\cdot\sum_{l=1}^{N_j} v_{l,j}(t_0)\right\rangle d\tau\,. \tag{4.8}$$

In this equation, N refers to the total number of molecules, N_i to the number of molecules of type i, and $v_{k,i}$ to the velocity of the k^{th} molecule of component i. If the approach from Equation 4.8 is now applied to calculate the Onsager coefficient of one component with respect to itself, i.e. Λ_{11} and Λ_{22}, we can see that the double summation in Equation 4.8 contains the multiplication of the velocity of each molecule at the time $\tau + t_0$ with the velocity of itself at the time t_0 as well as cross-correlations between molecules of the same type. Λ_{ii} can be rewritten using the self-diffusion coefficient of component i D_i as [268]

$$\Lambda_{ii} = x_i D_i + x_i^2 N\cdot \mathrm{CC}_{ii}\,. \tag{4.9}$$

In this equation, CC_{ii} refers to the cross-correlation of different molecules of component i. Following the same approach, Λ_{ij} can be rewritten as [268]

$$\Lambda_{ij} = x_i x_j N \cdot \mathrm{CC}_{ij} . \tag{4.10}$$

When combining Equations 4.7, 4.9, and 4.10, the Fick diffusion coefficient can be written as

$$D_{11} = \Gamma_{11} \left(x_2 D_1 + x_1 D_2 + x_2 x_1 N \left(CC_{11} + CC_{22} - 2CC_{12} \right) \right). \tag{4.11}$$

At the limit of infinite dilution of component 2 in a binary mixture, we find $x_2 \approx 0$ and $x_1 \approx 1$. Furthermore, Γ_{11} reaches unity at the limits of infinite dilute so that we can write

$$D_{11} = Đ_{12} = D_2 . \tag{4.12}$$

At the infinite dilution of the solute in a binary mixture, both D_{11} and $Đ_{12}$ can, therefore, be approximated with the self-diffusion coefficient of the solute. In this work, this approximation was applied for binary mixtures where the mole fraction of the solute was below 0.03.

To calculate D_i in this work, the Einstein relation based on the mean squared displacement of component i $(\mathrm{MSD})_i$ as function of τ was applied

$$D_i = \frac{1}{6} \lim_{\tau \to \infty} \frac{d}{d\tau} \left\langle r_i \left(\tau + t_0 \right) - r_i \left(t_0 \right) \right\rangle = \frac{1}{6} \lim_{\tau \to \infty} \frac{d\left(\mathrm{MSD}\right)_i}{d\tau} . \tag{4.13}$$

In this equation, r_i refers to the position of component i and the angle brackets denote an ensemble average of all possible t_0 and molecules of component i. The final value of D_i can be calculated from the linear regime between the MSD and τ. Since the statistics for the self-diffusion coefficient of the molecule at infinite dilution are poor, typical simulation times for the calculation of D_i at infinite dilution are (30 to 60) ns, depending on the number of solute molecules, were performed. Typical statistical uncertainties for D_i are 10% (k = 2), for the diluted component, and 3% (k = 2) for the component that is in majority.

Since D_i shows a strong dependency of the simulation box size, all D_i values in this work were corrected using the method introduced by Yeh and Hummer [206].

Mutual Diffusion Coefficient in Binary Non-Electrolyte Mixtures

The mutual diffusion coefficients were calculated according to Equation 4.7. Λ_{ij} were calculated via the summation of the collective displacement of components i and j according to

$$\Lambda_{ij} = \frac{1}{6N} \lim_{\tau \to \infty} \frac{d}{d\tau} \left\langle \sum_{k=1}^{N_i} \left(r_{k,i}(\tau + t_0) - r_{k,i}(t_0) \right) \cdot \sum_{l=1}^{N_j} \left(r_{l,j}(\tau + t_0) - r_{l,j}(t_0) \right) \right\rangle . \quad (4.14)$$

In this equation, $r_{k,i}(t)$ refers to the position of the k^{th} molecule of component i at a given time t. In analogy to D_i, Λ_{ij} was determined in the linear regime of the relationship between the summation of the collective displacement and the correlation time. The box size-dependency of D_{11} and $Đ_{12}$ was corrected using the method described by Jamali et al. [207-208] in the case of the binary mixture of CO_2 dissolved in 1-hexanol. In the investigation of CO_2 dissolved in *n*-hexane, which was performed before the publication of the work of Jamali et al., no box size correction for D_{11} and $Đ_{12}$ was performed.

Due to the collective nature of Λ_{ij}, much longer simulation runs are required to determine Λ_{ij} in comparison to D_i. In this work, simulation runs between (180 and 600) ns were performed to acquire $Đ_{12}$ with typical uncertainties of 10% (k = 2).

The thermodynamic factor Γ_{11}, which is required for the comparison of D_{11} from DLS experiments and $Đ_{12}$ from EMD simulations was determined from EMD simulations via the Kirkwood-Buff (KB) coefficients G_{ij} or the activity coefficient γ according to

$$\Gamma_{11} = 1 + x_1 \left(\frac{\partial \ln(\gamma_1)}{\partial x_1} \right)_{T,p} = \frac{1}{1 + c_t x_1 x_2 \left(G_{11}^{\infty} + G_{22}^{\infty} - 2G_{12}^{\infty} \right)} . \quad (4.15)$$

Here, c_t is the total number density of the binary mixture. The superscript ∞ of G_{ij}^{∞} indicates that the KB coefficients must be independent of the system size. Both methods of calculating Γ_{11} have been applied in this work. Values for γ_i of both components in the mixture were taken from the literature. G_{ij}^{∞} was calculated from radial distribution functions $g_{ij}(r_{ij})$ between the center of mass (COM) of molecules. For the extrapolation of $g_{ij}(r_{ij})$ to the thermodynamic limit, two different approaches were tested and applied. Following the method by Schnell et al. [239], $g_{ij}(r_{ij})$ was calculated for at least two different simulation box sizes. Afterwards, $g_{ij}(r_{ij})$ at each r_{ij} was extrapolated to infinite box sizes assuming a linear relationship between $g_{ij}(r_{ij})$ and the box size. Alternatively, the approach from Ganguly and van der Vegt [270] allows the calculation of $g_{ij}(r_{ij})$ at the thermodynamic limit from a single simulation run using an empirical correction. G_{ij}^{∞} can then be calculated by integrating $g_{ij}(r_{ij})$ over r_{ij} and extrapolating to the

thermodynamic limit using the methodology described by Krüger et al. [237]. Typical statistical uncertainties for the calculation of Γ_{11} from EMD simulations based on the standard deviation of at least 3 independent simulations are approximately 3% (k = 2).

Mutual Diffusion Coefficient in Binary Electrolyte Mixtures

Electrolyte mixtures consisting of one electrolyte (1) and one non-electrolyte (2) component, which were investigated in this work, contain three different species, namely the non-electrolyte (species 2) and the anion (species 1–) and cation (species 1+) of the electrolyte. For the calculation of D_{11} and $Đ_{12}$ from EMD simulation, such systems are considered in a first step as a ternary mixture. Following Equation 4.14, this means that in this case six different Onsager coefficients can be calculated, $\Lambda_{1+,1+}$, $\Lambda_{1+,1-}$, $\Lambda_{1+,2}$, $\Lambda_{1-,1-}$, $\Lambda_{1-,2}$, and $\Lambda_{2,2}$. Following the relationships for the Maxwell-Stefan diffusivity for a ternary system [161,247], $Đ_{1+,1-}$, $Đ_{1+,2}$, and $Đ_{1-,2}$ can be calculated. Due to the electroneutrality condition for electrolyte systems, the movement of both ions of the IL are coupled. This means that the diffusive mass transport for this system in the absence of an external electric field can be described using a single mutual diffusion coefficient. By applying the electroneutrality condition, $Đ_{12}$ for this system can be written as

$$Đ_{12} = \frac{Đ_{1+,2} Đ_{1-,2} \left(z_{1+} - z_{1-} \right)}{z_{1+} Đ_{1+,2} - z_{1-} Đ_{1-,2}} \text{ [161,271].} \tag{4.16}$$

In this equation, z_{1+} and z_{1-} are the charge number of the cation and anion. The statistical uncertainties for $Đ_{12}$ from simulations of approximately 400 ns are 14% (k = 2) on average. The final values for $Đ_{12}$ were corrected for finite-size effects using the method of Jamali et al. [207-208].

In analogy to $Đ_{12}$, Γ_{11} from EMD simulations for the electrolyte systems are calculated on the basis of the three different species. Either the species-based radial distribution functions or the species-based KB integrals are then combined into component-based functions or values assuming a pseudo-pure IL component [272-275] and Γ_{11} can be calculated by Equation 4.15. Both methods were applied for calculating Γ_{11} as function of the CO_2 mole fraction for the binary mixture of [HMIM][NTf_2] and CO_2 at a temperature of 298.15 K and gave identical values within combined uncertainties. Typical statistical uncertainties for Γ_{11} from the same simulations performed for the calculation of $Đ_{12}$ are 3% (k = 2).

5 Results and Discussion

In this section, the most important findings from this work with respect to determination of the thermophysical properties of liquids with dissolved gases will be summarized. The different publications will be discussed in the context of this work to determine thermophysical properties of liquids with dissolved gases by light scattering experiments and EMD simulations. For a complete discussion of the results from this work, the reader is referred to the publications in the Appendix. First, the determination of the viscosity and interfacial tension of binary mixtures consisting of liquids with dissolved gases, as well as the pure solvents, which are required for the discussion of the influence of the dissolved gas on the thermophysical properties of the mixture and the validation of the EMD simulations, will be given. Thereafter, the most important findings of the determination of the mutual diffusion coefficient of binary mixtures consisting of liquids with dissolved gases will be discussed.

5.1 Viscosity and Interfacial Tension

To get a fundamental understanding on how the molecular characteristics of the solvent and solute molecules influence the viscosity and interfacial tension of liquids with dissolved gases, accurate data for the pure solvents are necessary for comparison purposes. Therefore, the experimental determination of the liquid viscosity and interfacial tension of the pure solvents by SLS will be discussed first. Afterwards, the determination of both properties by EMD simulation, including a FF development that relies on the experimental results for the validation, is given. Finally, the investigation of the viscosity and interfacial tension of systems consisting of liquids with dissolved gases by SLS experiments and EMD simulations will be presented for binary mixtures consisting of different gases dissolved in *n*-hexadecane and the binary mixture of *n*-hexane and CO_2.

Viscosity and Interfacial Tension of Pure Solvents by SLS Experiments

SLS experiments were applied to determine the viscosity η and interfacial tension σ of 13 different pure solvents, including six linear alkanes with a wide range of carbon number, two branched alkanes, three linear alcohols, and two branched alcohols, for temperatures between (283 and 573) K and ambient pressure. This allowed the investigation of the influence of carbon

chain length, branching, and hydroxylation on the thermophysical properties.

The experimental results for η and σ of the six linear alkanes *n*-hexane, *n*-octane, *n*-decane, *n*-hexadecane, *n*-triacontane, and *n*-tetracontane as a function of the temperature are shown in Figure 5.1. For legibility purposes, no error bars corresponding to the experimental uncertainties are given in the Figure. The experimental results and the related uncertainties can be found in the respective publications [14,251]. Typical expanded experimental uncertainties for η and σ are (2.0 and 2.3)% (k = 2). For each substance, the viscosity and interfacial tension with respect to the temperature were correlated using a Vogel-type equation and the modified van der Waals equation [14,251].

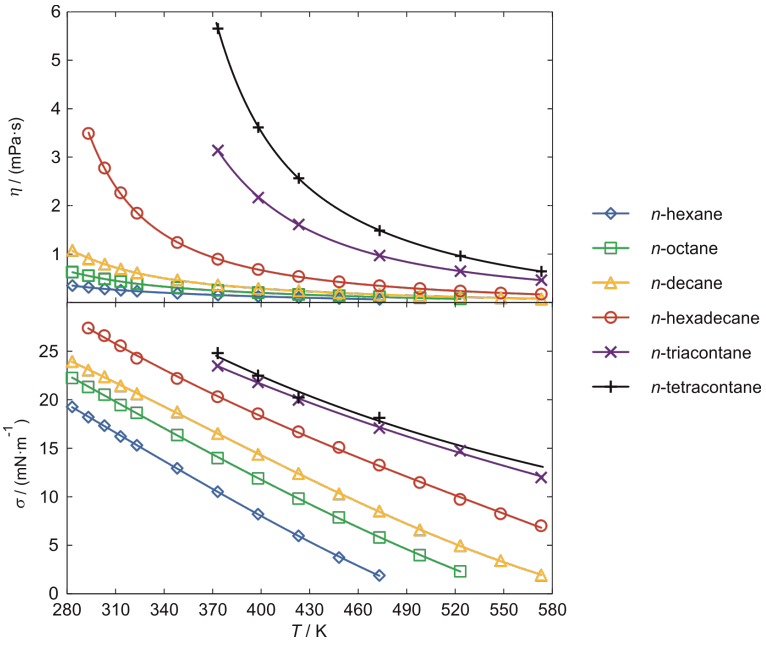

Figure 5.1: Experimental results for η and σ (symbols) as well as the temperature-dependent correlations (lines) of six linear alkanes as a function of temperature at ambient pressure.

A comparison with available data from the literature as well as reference correlations has shown agreement within combined uncertainties. For the two longest alkanes *n*-triacontane and *n*-tetracontane, no experimental data are available in the literature. For these substances, but also for the high temperature range for the shorter *n*-alkanes, the experimental results

from this work greatly contribute to the improvement of available literature data.

Based on the experimental data from this work for the linear alkanes *n*-hexane, *n*-octane, *n*-decane, and *n*-hexadecane and the experimental data for *n*-dodecane and *n*-octacosane, which were also investigated using the SLS technique [13], a predictive equation for η and σ of linear alkanes as a function of temperature and number of carbon atoms could be developed [251]. Using the prediction model, η and σ of the six linear alkanes could be reproduced within the experimental uncertainties with an average absolute relative deviation (AARD) of (1.9 and 1.6)%. For further validation, the prediction model was applied to a training set consisting of four linear alkanes which were not considered in the development of the model. Here, η and σ could be predicted with AARD of (4.8 and 2.3)%.

The experimental results for η and σ of linear alcohols, as well as the branched alkanes and alcohols, as a function of temperature are shown in Figure 5.2. For legibility purposes, no error bars corresponding to the experimental uncertainties are given in Figure 5.2. The experimental results and the related uncertainties can be found in the respective publication [14]. Typical expanded experimental uncertainties for η and σ are (2.1 and 2.6)% (k = 2). For each substance, the viscosity and the interfacial tension with respect to the temperature were correlated using a Vogel-type equation and the modified van der Waals equation [14].

The comparison with literature data has shown a lack of available experimental data especially for long and branched alcohols [14]. Here, the experimental results for η and σ extend the database to further substances and to high temperatures. The systematic variation of the solvent molecules presented in Figures 5.1 and 5.2 allows the investigation of the influence of the molecular characteristics, such as carbon chain length, branching, and hydroxylation, on the thermophysical properties. A detailed discussion of these influences is given in Ref [14]. In the following, a brief summary of the main findings will be given.

The influence of the carbon chain length on η and σ follows the expected trend of an increase of both properties with increasing chain length. Hydroxylation, which was investigated by comparing the linear alkanes with the linear alcohols with the same number of carbon atoms, leads to an increase of both properties. This can be explained by the strong contribution of hydrogen bonds between the hydroxyl group of the alcohols. For the influence of branching, the two isomers *n*-hexadecane and HMN have an

identical η within combined uncertainties, while the branched squalane has a (2 to 17)% smaller viscosity compared to the linear *n*-triacontane. For the branched alcohols, agreement within combined uncertainties between the branched and linear isomers can be explained by the predominant contribution of the hydroxyl groups to the intermolecular interactions. All branched alkanes and alcohols show a smaller σ compared to the linear isomers. This can be explained by weaker intermolecular interactions of the branched isomers due to steric behavior of the methyl groups.

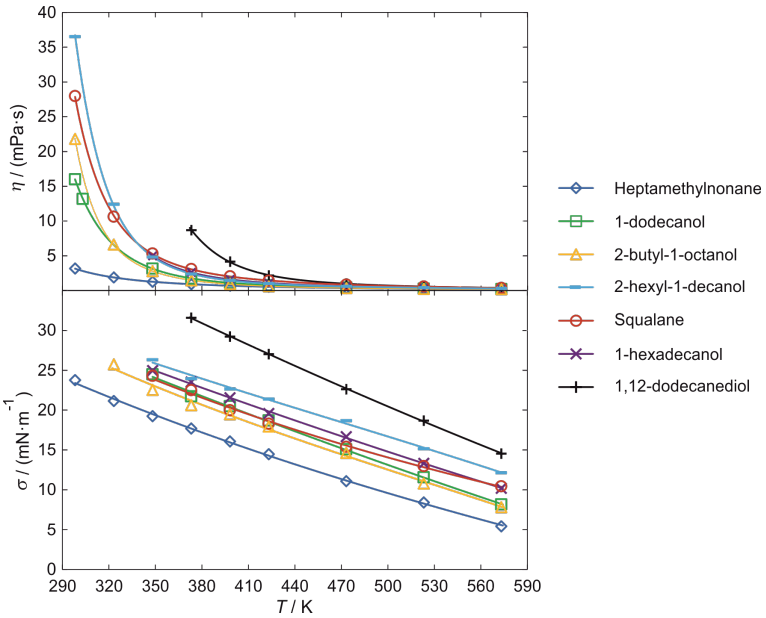

Figure 5.2: Experimental results for η and σ (symbols) as well as the temperature-dependent correlations (lines) of seven different linear alcohols, as well as branched alkanes and alcohols as a function of temperature at ambient pressure.

Further experimental investigations of η and σ for systems without dissolved gases were performed for binary and ternary mixtures of *n*-octacosane with common co-solvents that might be formed during the synthesis of linear alkanes [250]. The co-solvents include linear and branched alkanes, alcohols, or acids. The investigations include temperature-dependent experiments covering a range between (373.15 and 523.15) K and concentration-dependent investigations up to a mole fraction of the co-solvent of 0.6 at a temperature of 423.15 K. The η and σ of the mixtures were predicted using linear mixing rules based on the pure component proper-

ties. Here, a very strong influence of 2-methylnonane and 4-methylnonane on σ in binary mixtures with *n*-octacosane was found even at very low mole fractions of the co-solvent below 0.03.

Prediction of the Viscosity and Interfacial Tension of Pure Solvents Using EMD Simulations

EMD simulations for the prediction of η and σ of the pure solvents discussed in the previous section were made to investigate whether EMD simulations are able to predict the influence of the carbon chain length, branching, and hydroxylation correctly. Furthermore, suitable FFs for the simulation of binary mixtures of liquids with dissolved gases should be identified. For the validation of the EMD simulations for the prediction of η and σ, the experimental results presented in the previous section are used. For the comparison of the liquid density ρ from EMD simulations with experimental results, data from the literature and experiments performed by co-workers at AOT-TP using a U-tube densimeter are applied.

To compare the ability of different FFs available in the literature to capture the influence of the carbon chain length, branching and hydroxylation, EMD simulations were performed to predict ρ, η, and σ of *n*-dodecane, *n*-octacosane, HMN, and 1-dodecanol. Here, commonly applied FFs from the literature, namely the all-atom L-OPLS FF [43-44], the united-atom TraPPE FF [36,45,203], and the coarse-grained MARTINI FF [37] were applied. The best agreement with experimental reference values, especially at low temperatures, was found for the L-OPLS FF [14]. It was therefore chosen for all further EMD simulations. However, since the L-OPLS FF shows a strong temperature-dependent drift in the accuracy for the prediction of the thermophysical properties [41], a modification of the FF was performed. This was done on the basis of ρ of *n*-dodecane for the temperature range between (298.15 and 573.15) K. Here, the liquid density was chosen because of its low computational costs and the accuracy of available reference data. While the original L-OPLS FF predicted ρ with deviations up to 13% from the reference correlation of Lemmon and Huber [276], as shown in Figure 5.3, it was possible to remove the temperature-dependent drift of the predicted values from the correlation by introducing a temperature-dependency in the ε_{ii} LJ parameter according to

$$\varepsilon_{ii}(T) = \varepsilon_{ii,\text{L-OPLS}}\left(1 + \sum_{n=0}^{2} C_n T^n\right) \text{ [14].} \tag{5.1}$$

In this equation, $\varepsilon_{ii,\text{L-OPLS}}$ refers to the temperature-independent ε_{ii} parameter given in the original L-OPLS FF [43-44]. The parameters C_n can be found in reference [14]. Using the modification given in Equation 5.1, ρ of *n*-dodecane could be reproduced with 1.5% of the reference correlation, as shown in Figure 5.3.

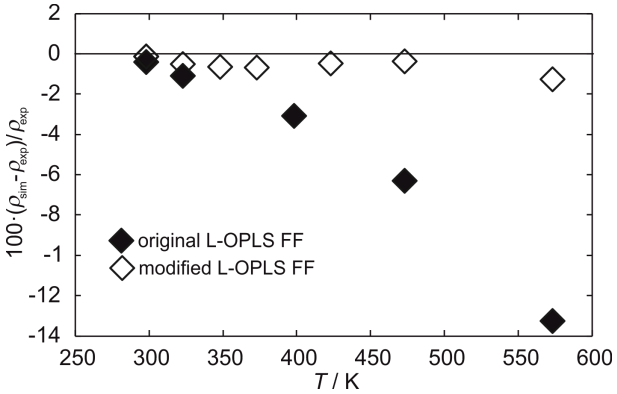

Figure 5.3: Deviations between the predicted liquid density of n-dodecane from EMD simulation as a function of temperature using the original and modified L-OPLS FF and the experimental reference correlation according to Lemmon and Huber [276].

The modification described in Equation 5.1 was then applied for the prediction of ρ, η, and σ of 12 different linear or branched alkanes and alcohols in the temperature range between (298.15 and 573.15) K [14]. The results for ρ, η, and σ from EMD simulations as well as the deviations from experimental reference correlations are shown in Figure 5.4.

Average statistical uncertainties for ρ, η, and σ from EMD simulations are (0.07, 14, and 1.9)% (k = 2), respectively. ρ of the 12 pure solvents was predicted with the modified L-OPLS FF with and AARD from experimental data of 1.1%. Especially for the linear alkanes, a good transferability of the modification in Equation 5.1 from *n*-dodecane to other pure solvents was found. For larger molecules, an increasing deviation with increasing temperature suggest that using the reduced temperature in Equation 5.1 could be more appropriate. For η, the modified L-OPLS FF was able to improve the prediction accuracy and allowed the determination of η of the 12 pure solvents with an AARD of 17%. Considering relative deviations, the prediction of σ still shows a temperature dependency, as shown in Figure 5.4. The modified L-OPLS FF is, however, able to predict the interfacial tension of

all 12 pure solvents with an almost constant absolute deviation from the experimental reference correlation and an AARD of 11%. Here, the constant offset between the simulations and the correlations might be due to the standard LJ corrections, which were used in the original development of the L-OPLS FF, but not in this work for reasons explained in Chapter 4.

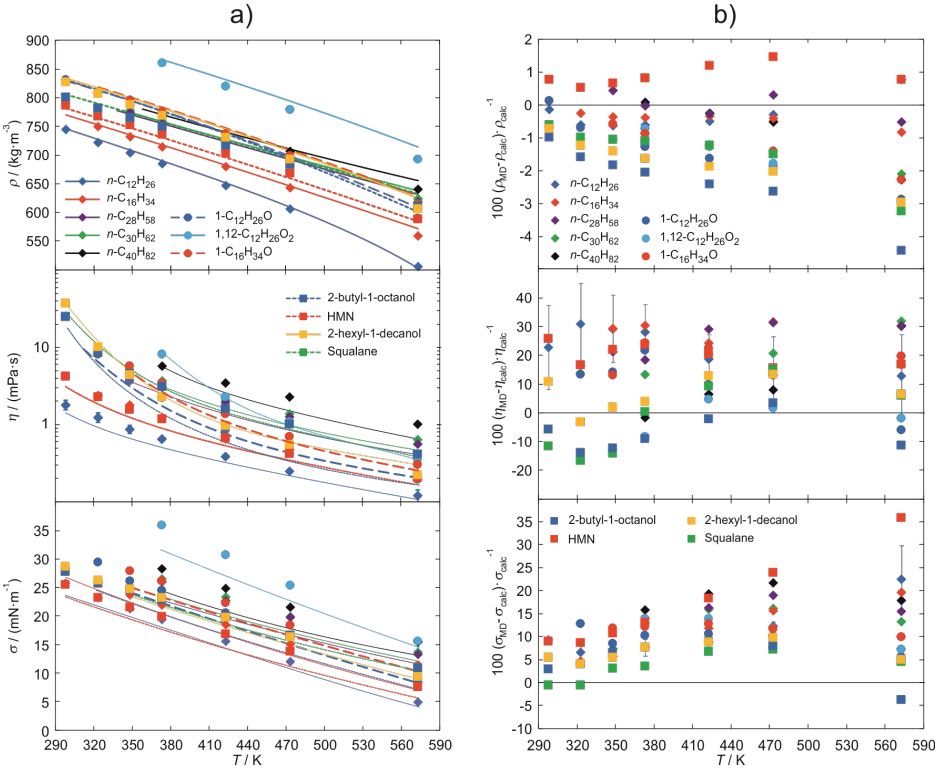

Figure 5.4: a) Results for ρ, η, and σ for the 12 studied linear and branched alkanes and alcohols from EMD simulations as a function of temperature. b) Relative deviations of the simulated properties as a function of temperature from the experimental reference correlations. For visibility purposes, only exemplary error bars, representing the statistical uncertainties (k = 2), are shown for n-dodecane. The figure was adapted from the respective publication [14].

Viscosity and Interfacial Tension of Binary Mixtures Consisting of Liquids with Dissolved Gases

The η and σ of binary mixtures consisting of liquids with dissolved gases were determined in this work for binary mixtures consisting of six gases dissolved in *n*-hexadecane for the temperature range between (298.15 and

573.15) and for the binary mixture of CO_2 dissolved in *n*-hexane at 298.15 K using SLS experiments and EMD simulations. The experimental results for η and σ of the *n*-hexadecane-based mixtures are shown as a function of the temperature in Figure 5.5. The experimental results and the related uncertainties can be found in the respective publication [252]. For comparison purposes, also η of pure *n*-hexadecane as function of temperature at ambient pressure is shown in Figure 5.5 [251]. Due to the limitation of the experimental setup to a pressure of 7.0 MPa, the binary mixtures containing He, H_2, or N_2 could not be investigated at a constant solute mole fraction of 0.1. These mixtures were therefore investigated at a pressure of (3.5 and 7.0) MPa. All other mixtures were investigated at a constant mole fraction of 0.05 and 0.1 or 0.1 and 0.2. The average experimental uncertainties related to η and σ are (2.3 and 1.9)% (k = 2).

A detailed interpretation of the influence of the dissolved gases on η and σ is given in the respective publication [252]. For the two lightest gases He and H_2, only a small influence on the thermophysical properties of pure *n*-hexadecane was found. The largest deviation is present for η of the binary mixture of *n*-hexadecane and He at 573.15 K and 7.0 MPa, where the viscosity of the mixture is approximately 13% larger than the viscosity of pure *n*-hexadecane at ambient pressure. For all other mixtures, the presence of the dissolved gas leads to a reduction of the viscosity at the lowest investigated temperature. This reduction generally increases with increasing mole fraction of the solute and with increasing molar mass of the solute. With increasing temperature, the difference between the binary mixture and pure *n*-hexadecane gets smaller and even converges to values within the combined uncertainties in many cases. This might be caused by two competing effects. The effect of the dissolved gas leads to a reduction of η. The effect of the pressure leads to an increase in η with increasing pressure. Since the intermolecular interactions between *n*-hexadecane molecules decrease with increasing temperature, caused by a decrease in density and a stronger bending of the linear alkane, the influence of the gas molecules of the intermolecular interactions gets weaker. The influence of the pressure on η, however, gets stronger with increasing temperature. The interplay of the two counterbalancing effects leads to the temperature-dependent trend seen in Figure 5.5.

For the binary mixture of *n*-hexadecane with the two lightest gases He and H_2, σ is within combined uncertainties of pure *n*-hexadecane for almost the entire temperature range. In the case of all other mixtures, the presence of the dissolved gases leads to a clear reduction of σ, compared to pure *n*-

hexadecane. Also, the reduction increases with increasing mole fraction of the solute. However, at a comparable mole fraction of the solute, N_2 seems to have a stronger influence on the interfacial tension in comparison to CH_4. This difference will be further discussed later on in combination with the EMD simulations for these systems.

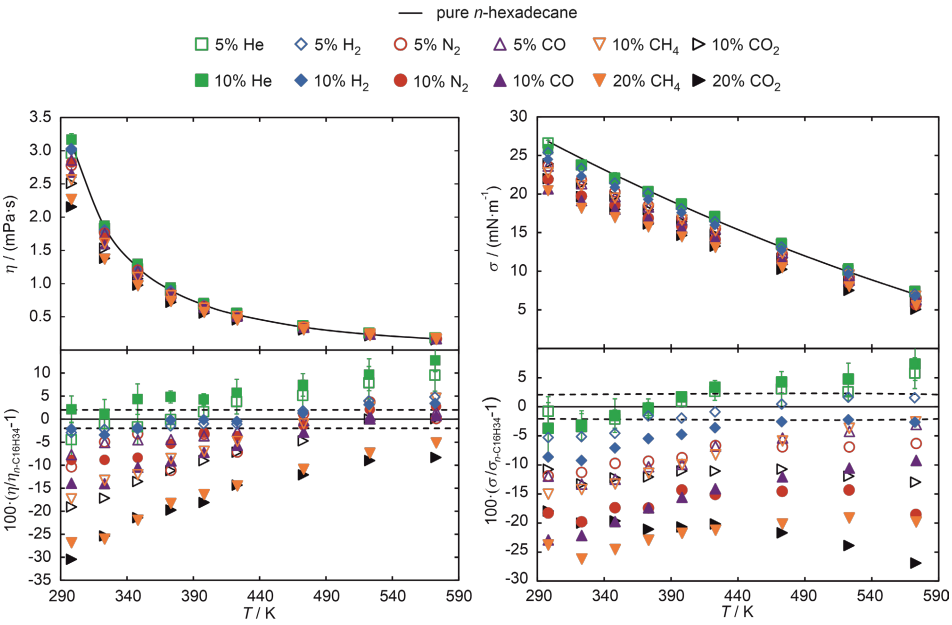

Figure 5.5: Results for η (a)) and σ (b)) for binary mixtures consisting of n-hexadecane with the dissolved gases He, H_2, N_2, CO, CO_2, or CH_4 as a function of temperature. The viscosity of pure n-hexadecane is given for comparison purposes. For visibility reasons, exemplary error bars, representing the statistical uncertainties (k = 2), are shown only for the binary mixtures containing He. The dotted lines mark the average expanded experimental uncertainty (k = 2) of pure n-hexadecane. The mole fractions of the dissolved gas given in the legend are approximate values. The real composition at each temperature can be taken from reference [252]. The Figure was taken from the original publication [252].

The modified L-OPLS FF was used to calculate η and σ for the same binary mixtures that were studied via SLS experiments. For further information on the applied FFs for the solutes and simulation details, the reader is referred to the original publication [252]. In Figure 5.6, the deviations between η and σ of the binary mixtures and pure *n*-hexadecane determined by EMD simulations are shown as function of the temperature. Here, the comparison to the thermophysical properties of pure *n*-hexadecane from EMD simulations [14] was chosen to investigate whether the FFs are able to predict

the influence of the gas on the thermophysical properties of the pure solvent.

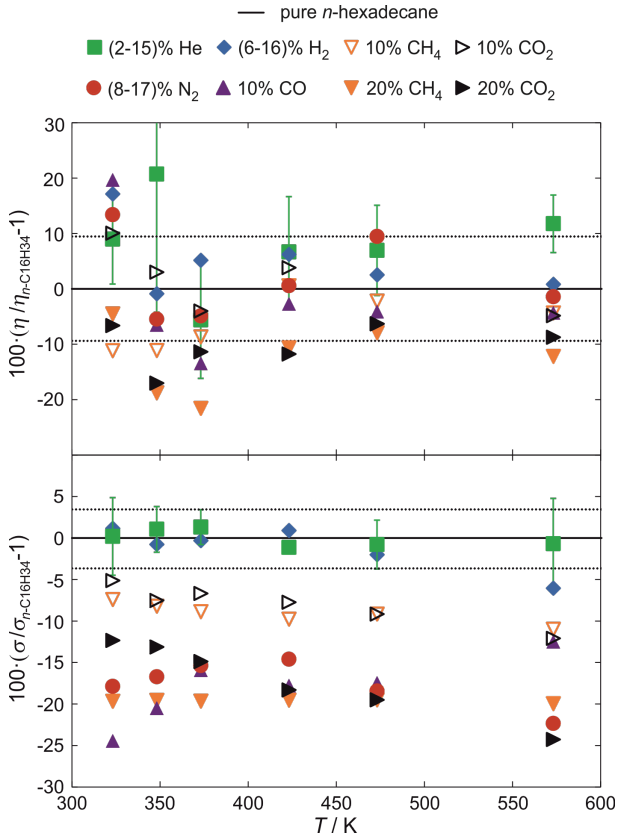

Figure 5.6: Deviations between η or σ of the binary mixtures from the values for pure n-hexadecane, which was also investigated using EMD simulations [14], as a function of the temperature. The mole fractions of the dissolved gas given in the legend are approximate values. The real composition at each temperature can be taken from reference [252]. The Figure was taken from the original publication [252].

Due to the relatively large statistical uncertainties of η of about 11% (k = 2), most data points fall within combined uncertainties of pure *n*-hexadecane. Especially at low temperature ≤ 373.15 K, the EMD simulations do not predict a lower η for the binary mixture in comparison to the pure solvent, as it was present in the results from SLS experiments. At larger temperatures, the general trend of decrease in η of about (10 to 20)% for binary mixtures containing CO_2 and CH_4, and very small deviations for mixtures containing

He, H_2, or N_2, is in good agreement with the experimental results. Also for σ of the binary mixtures, EMD simulations were able to predict the general trend for the influence of the dissolved gas on σ of pure *n*-hexadecane. Here, both the magnitude of the reduction in σ of up to 25% and the almost temperature-independent trend of the deviations could be predicted [252].

Because of the agreement between SLS experiments and EMD simulations for the influence of the dissolved gases on σ of pure *n*-hexadecane, EMD simulations were used to calculate the surface enrichment of the dissolved gas molecules to get a better understanding on why different gases show a different influence on σ of pure *n*-hexadecane at comparable mole fractions. Therefore, the spatially-resolved partial number density ρ_N for the solute and solvent molecular across the vapor-liquid interface was determined and used to calculate the relative adsorption $\Gamma_i^{(j)}$ [56]. Using the calculated $\Gamma_i^{(j)}$ for the binary mixture in this work, for example, the larger influence of N_2, in comparison to CH_4 at comparable mole fractions, on σ of pure *n*-hexadecane could be related to a larger enrichment of N_2 at the vapor-liquid interface [252]. Such structure-property relationships are helpful understand how the molecular characteristics of the solute and solvent influence thermophysical properties and can further be used in the development of prediction models.

Further investigations of systems consisting of liquids with dissolved gases were performed for the binary mixture of *n*-hexane with dissolved CO_2 at a temperature of 303.15 K over a wide range of composition using SLS experiments and EMD simulations [16]. The results for η and σ from experiments and simulations as a function of CO_2 mole fraction x_{CO_2} are shown in Figure 5.7.

The SLS experiments performed up to $x_{CO_2} = 0.755$ show a small plateau for $x_{CO_2} < 0.08$, followed by a decreasing trend for both properties with increasing x_{CO_2}. The results from EMD simulations predict a slightly stronger concentration dependent trend for η than the experimental results, which leads to a small overprediction at low x_{CO_2} and an underprediction at larger x_{CO_2}. The AARD of the simulated viscosities from a polynomial fit of the experimental data with respect to x_{CO_2} is 10.8%. EMD simulations give consistently lower values for σ compared to the experimental results. This led to an AARD of the simulated results for σ from a polynomial fit of the experimental results with respect to x_{CO_2} of 13.7%.

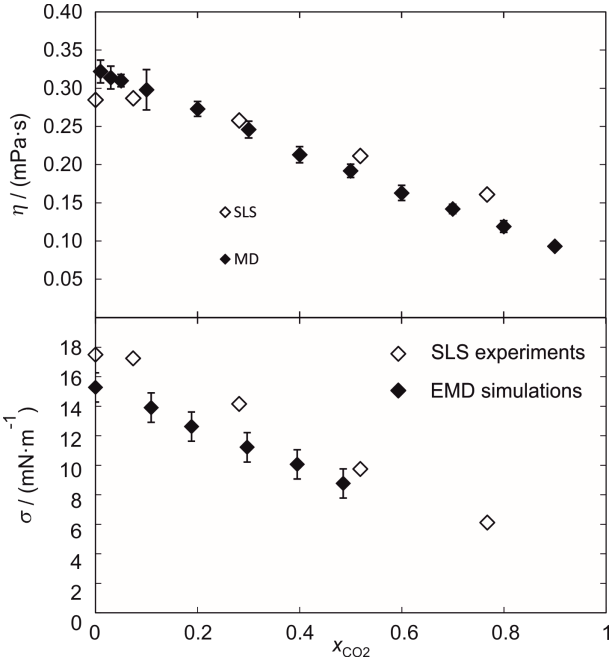

Figure 5.7: Results for η and σ of the binary mixture of n-hexane and CO_2 from SLS experiments and EMD simulations as a function of CO_2 mole fraction at a temperature of 303.15 K.

5.2 Mutual Diffusion Coefficients in Binary Mixtures Consisting of Liquids with Dissolved Gases

In this section, mutual diffusion coefficients calculated from EMD simulations for binary mixtures consisting of *n*-alkanes, primary alcohols, or ILs as solvents and He, H_2, N_2, CO, CO_2 or Kr as the solutes are presented. In most of the cases, D_{11} measured by DLS experiments from co-workers at AOT-TP serve as the reference to compare and validate the simulations. First, the results from investigations at infinite dilution of the gaseous solutes are presented. Based on these results, a predictive model for D_{11} of binary mixtures consisting of liquids with dissolved gases close to infinite dilution could be developed and is presented here. Afterwards, results for D_{11} over a wide composition range are shown for three binary mixtures consisting of CO_2 dissolved in *n*-hexane, 1-hexanol, or [HMIM][NTf_2]. Next to the results for D_{11} from EMD simulations, also $Đ_{12}$ and Γ_{11} are discussed to get a better understanding of their influence on D_{11}.

Mutual Diffusion Coefficients at the Limit of Infinite Dilution

For all investigations performed at infinite dilution of the gas, D_{11} was approximated by the self-diffusion coefficient of the gas according to Equation 4.12.

The results for D_{11} for binary mixtures consisting of He, H_2, N_2, or CO dissolved in *n*-hexane or *n*-decane by EMD simulations and DLS experiments as function of the temperature are shown in Figure 5.8 [33].

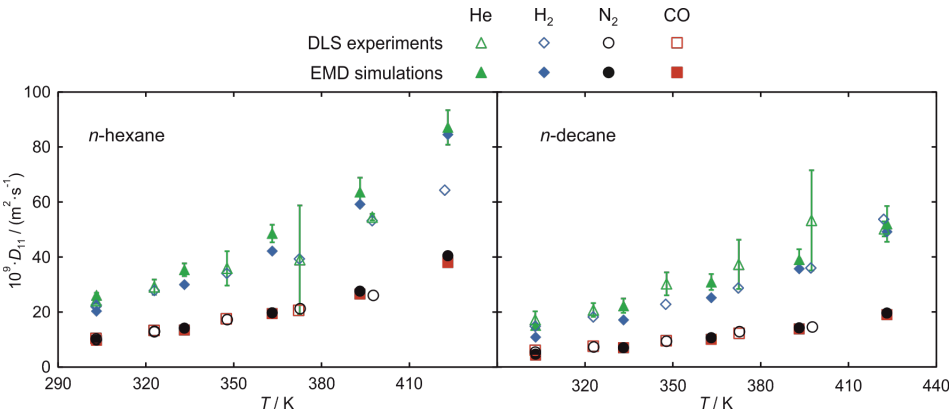

Figure 5.8: Mutual diffusivity D_{11} as a function of temperature from DLS experiments and EMD simulations for binary mixtures of n-hexane or n-decane with dissolved gases.

The average statistical uncertainty of D_{11} determined for EMD simulations is 7% (k = 2). For the comparison between experiments and simulations, the simulation results, which cover a wider temperature range for some systems, were correlated with respect to the temperature using an Arrhenius-type equation [33]. The AARD between the experimental and simulated results for D_{11} are (8.3 and 18.2)% for the two solvents *n*-hexane and *n*-decane. The much larger AARD for the *n*-decane is due to a strong underprediction of D_{11} from EMD simulations at low temperatures, which is in agreement with the general overprediction of η of pure *n*-decane [33].

Further investigations were performed for binary mixtures consisting of ethanol, 1-hexanol, or 1-decanol as the solvent and He, H_2, N_2, CO, or CO_2 as the solute at temperatures between (303.15 and 423.15) K [42]. Similar as for the *n*-alkanes based systems, the EMD simulations were able to describe the temperature-dependent trend of D_{11} well, but give slightly smaller D_{11} values at low temperatures. This can also be explained by the tendency of

the L-OPLS FF to overpredict the viscosity of linear alcohols, as shown in the previous section. The AARD between the simulated and experimental results for the 15 investigated systems is 14% [42].

Based on the investigations of D_{11} in binary mixtures consisting of *n*-alkanes or 1-alcohols as solvents at the infinite dilution of the dissolved gases, a predictive model for D_{11} was developed [42]. This model is able to predict D_{11} in a binary mixture of the solute (1) and solvent (2) at infinite dilution according to

$$D_{11,\mathrm{calc}} = 5.249 \cdot 10^{-17} \cdot \frac{T\left(\Psi M_2\right)^{1/2}}{\nu_2^{\,0.8}\left[M_1\left(0.45+\omega_1\right)\right]^{0.25}} \cdot \tag{5.2}$$

In this equation, M, ν, and ω refer to the molar mass, kinematic viscosity, and the acentric factor, respectively. The association factor Ψ was introduced to accurately predict D_{11} in alcohol-based mixtures and can be calculated according to

$$\Psi = 1 + 1.338 \cdot 10^{6} \cdot \frac{\nu_2^{\,0.3} \cdot \mu_2}{M_2 \cdot T} . \tag{5.3}$$

Here, μ refers to the dipole moment. The model was developed using the experimental data from the publications as part of this work [33,42] as well as further experimental data from the literature on D_{11} in binary mixtures consisting of *n*-alkanes with dissolved gases. The transferability of the model to data that were not included in the development was investigated using a testing set of 101 experimental and simulated data for D_{11}. A generally good agreement between the predicted data and the testing set with an AARD of 12% was found. A comparison between the 305 data points in the training and testing set and the predicted values using Equation 5.2 is shown in Figure 5.9.

Finally, investigations of binary mixtures consisting of the ILS [EMIM]-[NTf_2], [HMIM][NTf_2], and [DMIM][NTf_2] as solvents and He, H_2, N_2, CO, CO_2, and Kr as solutes were performed using DLS experiments and EMD simulations for temperatures between (298.15 and 348.15) K [255]. To identify suitable FFs for the ILs, different FFs from the literature were applied for the prediction of the liquid density, viscosity, and ion self-diffusivity of the pure ILs and the results were compared to experimental reference data. While the FF of Neumann et al. [266] showed the best agreement for both static and dynamic properties, the deviations of the simulated data from experimental reference values were increasing with an increasing carbon

chain length of the alkyl group attached to the imidazolium ring of the cation. Following the findings of Logotheti et al. [277], who found that the effective charge of the anion and cation are smaller than +1 and –1 for ILs in the liquid phase using QM calculations, an empirical model for the effective charge of the ions with respect to the alkyl chain length was developed [255]. This led to an effective charge of 1.00, 0.96, and 0.90 for the anions and cations in [EMIM][NTf_2], [HMIM][NTf_2], and [DMIM][NTf_2], respectively [255].

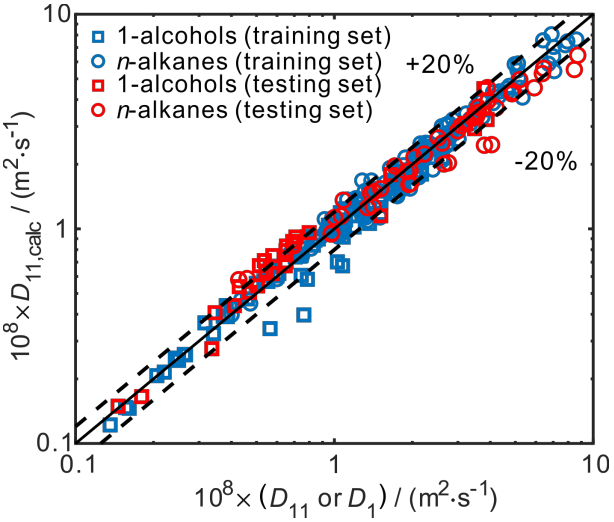

Figure 5.9: Comparison between the 305 D_{11} data points contained in the training and testing set with the calculated values using Equation 5.2. The Figure was taken from the original publication [42].

The modified Neumann FF was than applied for the prediction of D_{11} in the binary mixtures with dissolved gases. The results for D11 from EMD simulation and DLS experiments are shown in Figure 5.10. The average statistical uncertainty related to the investigation of D_{11} from EMD simulations is 8% (k = 2). The AARD between the simulated and experimental D_{11} data are (9.8, 11, and 14)% for binary mixtures based on EMIM][NTf_2], [HMIM]-[NTf_2], and [DMIM][NTf_2], respectively. The most important finding from this work is that D_{11} is almost not influenced by the viscosity of the solvent, as can be seen in Figure 5.10 for H_2-based mixtures. This ultimately led to a failure of the prediction model in Equation 5.2, which considers the solvent viscosity with the power of –0.8 in the prediction of D_{11}. As an extension of this work, further investigations including solvents with a wide range of

viscosities, therefore, have to be performed and the prediction model has to be further refined.

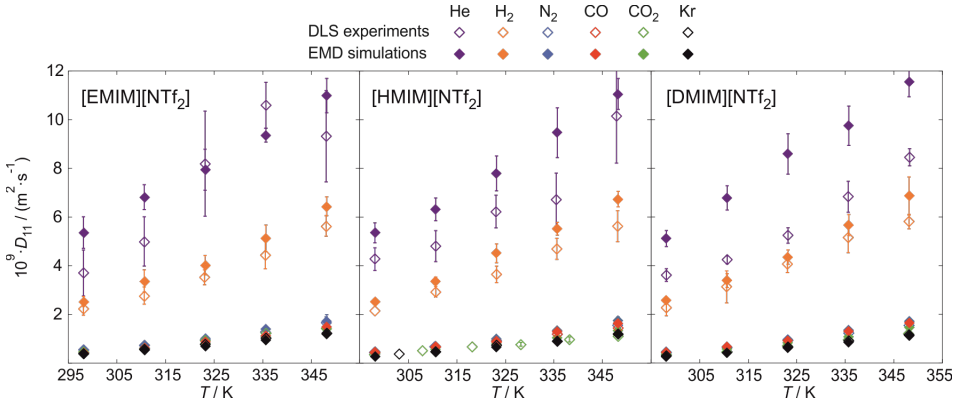

Figure 5.10: Fick diffusion coefficient D_{11} as a function of temperature of different binary mixtures of [EMIM][NTf_2], [HMIM][NTf_2], and [DMIM][NTf_2] with dissolved gases.

Mutual Diffusion Coefficient as a Function of the Composition

EMD simulations and DLS experiments were performed for three binary mixtures consisting of CO_2 dissolved in *n*-hexane, 1-hexanol, or [HMIM][NTf_2] to study D_{11} over a wide composition range [253-254,256]. $Đ_{12}$ was calculated with a typical statistical uncertainty of 10% (k = 2) in all cases based on the approaches detailed in Chapter 4. For the binary mixtures based on *n*-hexane and [HMIM][NTf_2], Γ_{11} was calculated from EMD simulations via KB integrals. For the binary mixture of 1-hexanol with dissolved gases, Γ_{11} was calculated from EMD simulations and activity coefficients in the mixture via the non-random two-liquid (NRTL) model [84]. Neither approach was able to predict the convergence of Γ_{11} to zero when approaching the VLE to VLLE transition. With the knowledge of the location of the spinodal for each investigated temperature, a new set of NRTL parameters was determined. The final data for D_{11} in the case of the binary mixture of 1-hexanol and CO_2 were calculated with Γ_{11} from the improved NRTL model. Typical statistical uncertainties for Γ_{11} calculated from EMD simulations are 3% (k = 2). The uncertainty of Γ_{11} calculated from the NRTL model was assumed to be 10%, based on the empirical nature of the modification. Results for D_{11} from EMD simulations and DLS experiments for all three mixtures at a temperature of 303.15 K, in the case of the *n*-hexane- and 1-hexanol-

based systems, and 298.15 K, for the binary mixture based on [HMIM]–[NTf_2], as a function of composition are shown in Figure 5.11.

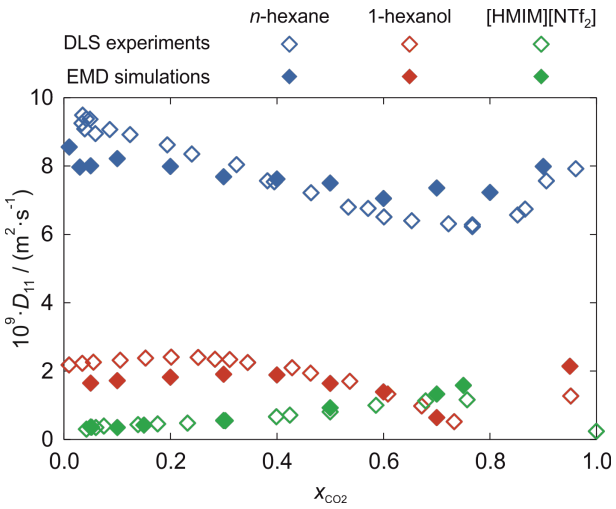

Figure 5.11: Comparison between D_{11} from EMD simulations and DLS experiments for the binary mixtures of CO_2 dissolved in n-hexane, 1-hexanol, or [HMIMNTf_2] at (303.15 or 298.15) K as a function of composition.

For all three mixtures, a non-ideal concentration dependency of D_{11} was found. For the mixture of *n*-hexane with CO_2, the decrease of D_{11} up to x_{CO_2} ≈ 0.75 and the subsequent increase could be related to a solute-solvent transition. Here, the break-down of the *n*-hexane network was studied by EMD simulations using radial distribution functions between the center of mass of the two components and was confirmed by polarization-difference Raman spectroscopy (PDRS) experiments performed simultaneously with the DLS experiments [253]. The two mixtures based on 1-hexanol and [HMIM][NTf_2] show a VLE to VLLE transition at the lowest temperatures studied, which explains the decrease of D_{11} approaching the transition point in the case of the 1-hexanol-based system [254]. For the binary mixture based on [HMIM][NTf_2], a steady increase of D_{11} with increasing x_{CO_2} and a leveling-off at x_{CO_2} ≈ 0.7 was found [256]. The reason why D_{11} does not decrease approaching the VLE to VLLE transition, but merely levels-off, might be related to the distance between the spinodal and binodal. Since no data on the location of the spinodal and binodal exist for this mixture, this could not be confirmed.

EMD simulations were able to predict the composition-dependent trend for D_{11} for all three mixtures investigated in this work. The AARD between the simulated and experimentally investigated D_{11} data shown in Figure 5.11 is 13%. For a detailed discussion of the influence of the temperature on D_{11} over a wide composition range, the reader is referred to the respective publications [253-254,256].

To get a better understanding on how the fluid structure influences D_{11}, the contributions to D_{11} from EMD simulations were investigated separately. In Figure 5.12, composition-dependent results for $Đ_{12}$ and Γ_{11} are shown for the three binary mixtures at the same temperatures as shown in Figure 5.11.

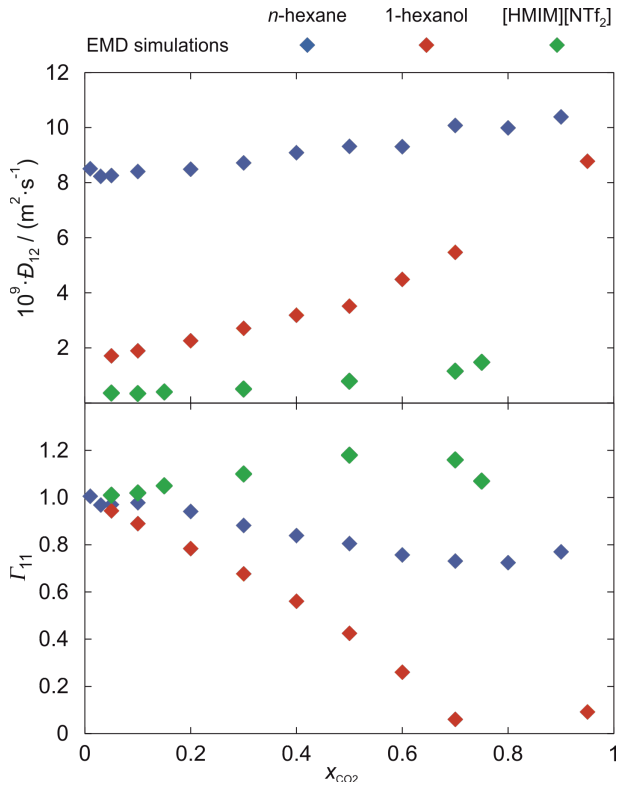

Figure 5.12: Results for $Đ_{12}$ and Γ_{11} from EMD simulations and DLS experiments for the binary mixtures of CO_2 dissolved in n-hexane, 1-hexanol, or [HMIMNTf$_2$] at (303.15 or 298.15) K as a function of composition.

The results in Figure 5.12 show an increase of $Đ_{12}$ with increasing x_{CO_2} for all three mixtures. This can be related to an increase in mobility of the com-

ponents with increasing CO_2 mole fraction. For Γ_{11}, on the other hand, the composition-dependent behavior varies strongly for the three investigated systems. For the binary mixture of *n*-hexane with CO_2, Γ_{11} decreases up to a $x_{CO_2} \approx 0.8$ and increases afterwards, which could be related to the solvent-solute transition [253]. The data for Γ_{11} for the binary mixture of 1-hexanol with CO_2 from the NRTL model with the adjusted parameters show a steady decrease up to the VLE to VLLE transition [254]. For the mixture of [HMIM][NTf_2] with CO_2, Γ_{11} first increases with increasing x_{CO_2} up to $x_{CO_2} \approx 0.6$ and decreases afterwards [256]. This behavior shows that EMD simulations for this mixture are able to predict the presence of the VLE to VLLE transition. In all three cases, a strong influence of the fluid structure, which is directly contained in Γ_{11}, on D_{11} is obvious. To get a deeper understanding of the complex and non-ideal composition-dependency of D_{11}, EMD simulations with their ability to decompose D_{11} into $Đ_{12}$ and Γ_{11} are a valuable tool. For a more detailed discussion of the influence of $Đ_{12}$ and Γ_{11} on D_{11} and derived structure-property relationships, the reader is referred to the respective publications from this work [253-254,256].

6 Conclusions and Prospect

The present thesis contributes to a fundamental understanding of the thermophysical properties viscosity, interfacial tension, and mutual diffusion coefficient of systems consisting of liquids with dissolved gases. Since such systems are relevant working fluids in many fields of chemical and energy engineering, accurate data for the aforementioned properties are required for the efficient design and optimization of related processes and apparatuses. Due to the wide range of possible working fluids in combination with different gases and the wide range of thermodynamic states that are of interest for their application, not only accurate thermophysical properties are required, but also a fundamental understanding of how the molecular characteristics of the components influence them. This helps with the selection of suitable working fluids. Light scattering experiments and EMD simulations were combined in this work for the determination of the thermophysical properties as well as the investigation of how the mixture components influence the properties. Here, accurate data from the experiments help to validate the simulations, while EMD simulations allow an insight in the fluid structure on a molecular level and help to interpret the thermophysical properties.

To gain a fundamental understanding of how the molecular characteristics of the solvent and solute influence the thermophysical properties, solvent molecules with a wide range of molecular and structural characteristics were investigated. This includes linear and branched alkanes and alcohols with varying carbon chain length, as well as imidazolium-based ILs with a varying chain length of the alkyl-tail attached to the imidazolium ring. To capture the influence of the solute, different dissolved gases with varying size, weight, and polarity were included. A wide investigated temperature range between (283 and 573) K was chosen for the investigations by experiments and simulations to determine thermophysical properties at process-relevant conditions.

To determine the viscosity and interfacial tension of the binary mixtures and the pure solvents, SLS experiments were used in this work. They allow the determination of both properties with typical experimental uncertainties of 2.2% (k = 2) by analyzing the light scattered from microscopic fluctuations at the vapor-liquid interface in a contact-less manner and without the need of calibration. The experimental results from this work for the pure solvents could contribute to an improvement of available data for both properties and could extend the temperature range for many substances up

to high, process-relevant conditions. SLS experiments for binary mixtures consisting of liquids with dissolved gases present the first systematic study of the influence of different solute molecules on the thermophysical properties of the solvent over a wide temperature range. DLS experiments based on the analysis of microscopic fluctuations in the bulk-fluid phase are able to determine the mutual diffusion coefficient in mixtures at macroscopic thermodynamic equilibrium with typical experimental uncertainties between (3 and 10)% (k = 2), depending on the thermodynamic state. Results from DLS experiments performed by co-workers at AOT-TP are used in the work for the validation of EMD simulations and for the discussion of the influence of the solvent and solute characteristics on the mutual diffusion coefficient.

EMD simulations are able to predict multiple thermophysical properties in macroscopic thermodynamic equilibrium by the analysis of microscopic fluctuations. They were applied in this work to determine the viscosity, interfacial tension, and mutual diffusion coefficient at the same thermodynamic states as investigated by the light scattering experiments. Due to a strong temperature-dependency in the accuracy of predicting the liquid density and viscosity, as well as the interfacial tension of pure solvents modeled with the commonly applied L-OPLS FF [43-44], a temperature correction in the form of a temperature-dependent description for the ε_{ii} parameter of the LJ interactions was developed. This correction was based solely on the liquid density of *n*-dodecane and was applied to all other pure solvents and the solvents in binary mixtures with dissolved gases. For the prediction of the mutual diffusion coefficient in binary mixtures consisting of ILs with dissolved gases, the FF by Neumann et al. [266] was modified by scaling of the effective charges of the anion and cation of the ILs. Typical statistical uncertainties for the prediction of the viscosity, interfacial tension, and mutual diffusion coefficient are (10, 3, and 10)% (k = 2).

Using the results from SLS experiments for mixtures consisting of *n*-hexadecane with dissolved gas, the influence of the dissolved gases on the viscosity and interfacial tension of pure *n*-hexadecane could be resolved. For the light gases He and H_2, the viscosity and interfacial tension are mostly within combined uncertainties of pure *n*-hexadecane. For all other gases, a reduction of the viscosity and interfacial tension compared to pure *n*-hexadecane with deviations up to 30% was found. With the exception of He and H_2, this reduction increases with increasing mole fraction and molecular weight of the solute. The comparison between EMD simulations and SLS experiments for the viscosity and interfacial tension of pure solvents and liquids with dissolved gases has shown a general overprediction of both

properties by approximately (15 and 10)%. When comparing the interfacial tension of the simulated mixture to that of simulated *n*-hexadecane, similar deviations as shown by the experiments can be found. For the viscosity, however, the EMD simulations were not able to accurately predict the influence of the dissolved gas on the viscosity of pure *n*-hexadecane at temperatures below 373.15 K. EMD simulations could further be used to develop structure-property relationships between the surface enrichment of the solutes and their influence on the interfacial tension of the mixture.

The mutual diffusion coefficient in binary mixtures consisting of different gases dissolved in *n*-alkanes, 1-alcohols, or ILs at infinite dilution of the dissolved gas by EMD simulations and DLS experiments were presented. The results from EMD simulations agree with the DLS experiments with an AARD of approximately 14% and are often within combined uncertainties. Based on the results for binary mixtures of different gases dissolved in *n*-alkanes or 1-alcohols, an empirical prediction model for the mutual diffusion coefficient at infinite dilution could be developed. This model requires only thermophysical and molecular properties of the pure solvent and solutes and was able to predict the mutual diffusion coefficients of a testing set containing 101 data points with and AARD of 12%.

Finally, the mutual diffusion coefficient in binary mixtures of *n*-hexane, 1-hexanol, or [HMIM][NTf_2] with dissolved CO_2 from EMD simulations and DLS experiments were presented. The composition-dependent trend of the mutual diffusion coefficient from DLS experiments could be predicted by EMD simulation with an AARD of approximately 14%. By decomposing the mutual diffusion coefficient into the Maxwell-Stefan diffusion coefficient and the thermodynamic factor, the composition-dependent trend for the mutual diffusion coefficient could be related to the structural arrangements in the fluid phase.

In summary, the combination of light scattering experiments and EMD simulations have been shown to be a powerful tool in thermophysical property research of liquids with dissolved gases. The combination of both techniques allows the accurate determination of thermophysical properties by experiments and the development of a fundamental understanding for the influence of the solute and solvents on the properties. In this work, the viscosity and interfacial tension of binary mixtures based only on *n*-hexadecane have been presented. For further research, this approach can be applied to binary mixtures based on further solvents with different molecular characteristics, such as longer or branched alkanes and alcohols. Such data can be correlated with the properties of the solute and solvent molecules

to develop a predictive model for the viscosity and interfacial tension of liquids with dissolved gases. The failure of the empirical model to predict the mutual diffusion coefficient in binary mixtures based on ILs suggests that further investigations with solvents covering a wide viscosity range should be performed. Finally, the results from this work for the mutual diffusion coefficient by EMD simulations and DLS experiments can be used for the development of a prediction model that is based on the prediction of the thermodynamic factor and the Maxwell-Stefan diffusion coefficient in order to predict a non-ideal concentration-dependent behavior of the mutual diffusion coefficient.

References

(1) Lee, S.; Sardesai, A. Liquid Phase Methanol and Dimethyl Ether Synthesis from Syngas. *Top. Catal.* **2005,** *32*, 197-207.

(2) Li, B.; Jens, K.-J. Low-Temperature and Low-Pressure Methanol Synthesis in the Liquid Phase Catalyzed by Copper Alkoxide Systems. *Ind. Eng. Chem. Res.* **2014,** *53*, 1735-1740.

(3) Maitlis, P. M.; de Klerk, A. *Greener Fischer-Tropsch Processes for Fuels and Feedstocks*. Wiley-VCH Verlag GmbH & Co. KGaA Weinheim, Germany, 2013.

(4) Pöhlmann, F.; Jess, A. Interplay of Reaction and Pore Diffusion During Cobalt-Catalyzed Fischer–Tropsch Synthesis with CO_2-Rich Syngas. *Catalysis Today* **2016,** *275*, 172-182.

(5) Scovazzo, P. Determination of the Upper Limits, Benchmarks, and Critical Properties for Gas Separations Using Stabilized Room Temperature Ionic Liquid Membranes (SILMs) for the Purpose of Guiding Future Research. *J. Membr. Sci.* **2009,** *343*, 199-211.

(6) Srikhirin, P.; Aphornratana, S.; Chungpaibulpatana, S. A Review of Absorption Refrigeration Technologies. *Renew. Sust. Energ. Rev.* **2001,** *5*, 343-372.

(7) Bajerlein, M.; Karpiuk, W.; Smolec, R. Use of Gas Desorption Effect in Injection Systems of Diesel Engines. *Energies* **2021,** *14*,

(8) Farajzadeh, R.; Eftekhari, A. A.; Dafnomilis, G.; Lake, L. W.; Bruining, J. On the sustainability of CO_2 storage through CO_2 – Enhanced oil recovery. *Appl. Energy* **2020,** *261*, 114467.

(9) Schäfer, R.; Merten, C.; Eigenberger, G. Bubble Size Distributions in a Bubble Column Reactor Under Industrial Conditions. *Exp. Therm. Fluid Sci.* **2002,** *26*, 595-604.

(10) Michailidou, E. K.; Assael, M. J.; Huber, M. L.; Perkins, R. A. Reference Correlation of the Viscosity of *n*-Hexane from the Triple Point to 600 K and up to 100 MPa. *J. Phys. Chem. Ref. Data* **2013,** *42*, 033104.

(11) Mazee, W. M. Some Properties of Hydrocarbons Having More than Twenty Carbon Atoms. *Recl. Trav. Chim. Pays-Bas* **1948,** *67*, 197-213.

(12) Doolittle, A. K.; Peterson, R. H. Preparation and Physical Properties of a Series of *n*-Alkanes. *J. Am. Chem. Soc.* **1951,** *73*, 2145-2151.

(13) Koller, T. M.; Klein, T.; Giraudet, C.; Chen, J.; Kalantar, A.; van der Laan, G. P.; Rausch, M. H.; Fröba, A. P. Liquid Viscosity and Surface Tension of *n*-Dodecane, *n*-Octacosane, Their Mixtures, and a Wax between 323 and 573 K by Surface Light Scattering. *J. Chem. Eng. Data* **2017,** *62*, 3319-3333.

(14) Klein, T.; Lenahan, F. D.; Kerscher, M.; Rausch, M. H.; Economou, I. G.; Koller, T. M.; Fröba, A. P. Characterization of Long Linear and Branched Alkanes and Alcohols for Temperatures up to 573.15 K by Surface Light Scattering and Molecular Dynamics Simulations. *J. Phys. Chem. B* **2020,** *124*, 4146-4163.

(15) Berstad, D. A. *Viscosity and Density of n-Hexane, Cyclohexane and Benzene, and Their Binary Mixtures with Methane*. Ph.D. thesis, Universitetet i Trondheim, Institutt for Uorganisk Kjemi Norges Tekniske Hegskole, 1989.

(16) Koller, T. M.; Yan, S.; Steininger, C.; Klein, T.; Fröba, A. P. Interfacial Tension and Liquid Viscosity of Binary Mixtures of *n*-Hexane, *n*-Decane, or 1-Hexanol with Carbon Dioxide by Molecular Dynamics Simulations and Surface Light Scattering. *Int. J. Thermophys.* **2019,** *40*, 79.

(17) Mulero, A.; Cachadiña, I. Recommended Correlations for the Surface Tension of Several Fluids Included in the REFPROP Program. *J. Phys. Chem. Ref. Data* **2014,** *43*, 023104.

(18) Baidakov, V. G.; Khotienkova, M. N. Capillary Constant and Surface Tension of Propane (R-290) with Helium Dissolved in it. *Int. J. Refrig.* **2019,** *98*, 261-265.

(19) He, M.; Peng, S.; Zhang, Y.; Zhang, S.; Liu, X. Mutual Diffusion Coefficients of Isopropanol+*n*-heptane and isobutanol+*n*-Heptane. *J. Chem. Thermodyn.* **2016,** *96*, 127-133.

(20) Păez, S.; Guevara-Carrion, G.; Hasse, H.; Vrabec, J. Mutual Diffusion in the Ternary Mixture of Water + Methanol + Ethanol and its Binary Subsystems. *Phys. Chem. Chem. Phys.* **2013,** *15*, 3985-4001.

(21) Köhler, W.; Müller, B. Soret and Mass Diffusion Coefficients of Toluene/*n*-Hexane Mixtures. *J. Chem. Phys.* **1995,** *103*, 4367-4370.

(22) Ramprasad, G.; Das, T. R.; Mukherjee, A. K. Mutual Diffusion Coefficients of Some Binary Liquid Systems: Toluene-*n*-alkyl Alcohol. *J. Chem. Eng. Japan* **1991,** *24*, 389-391.

(23) Zubeir, L. F.; Romanos, G. E.; Weggemans, W. M. A.; Iliev, B.; Schubert, T. J. S.; Kroon, M. C. Solubility and Diffusivity of CO_2 in the Ionic Liquid 1-Butyl-3-Methylimidazolium Tricyanomethanide within a Large Pressure Range (0.01 MPa to 10 MPa). *J. Chem. Eng. Data* **2015,** *60*, 1544-1562.

(24) Moya, C.; Palomar, J.; Gonzalez-Miquel, M.; Bedia, J.; Rodriguez, F. Diffusion Coefficients of CO_2 in Ionic Liquids Estimated by Gravimetry. *Ind. Eng. Chem. Res.* **2014,** *53*, 13782-13789.

(25) Turnaoglu, T.; Shiflett, M. B. 110th Anniversary: The First Thermodynamic and Kinetic Analysis of Ammonia in Imidazolium-Based Ionic Liquids Using a Gravimetric Microbalance. *Ind. Eng. Chem. Res.* **2019,** *58*, 4644-4655.

(26) Liu, X.; Pan, P.; He, M. Vapor-Liquid Equilibrium and Diffusion Coefficients of R32 + [HMIM][FEP], R152a + [HMIM][FEP] and R161 + [HMIM][FEP]. *J. Mol. Liq.* **2018,** *253*, 28-35.

(27) Assael, M. J.; Dymond, J. H.; Papadaki, M. Viscosity coefficients of binary *n*-heptane+*n*-alkane mixtures. *Fluid Phase Equilibr.* **1992,** *75*, 287-297.

(28) Grunberg, L.; Nissan, A. H. Mixture Law for Viscosity. *Nature* **1949,** *164*, 799.

(29) Macleod, D. B. On a Relation between Surface Tension and Density. *Trans. Faraday Soc.* **1923,** *19*, 38-41.

(30) Sastri, S. R. S.; Rao, K. K. A Simple Method to Predict Surface Tension of Organic Liquids. *Chem. Eng. J. Biochem. Eng. J.* **1995,** *59*, 181-186.

(31) Wilke, C. R.; Chang, P. Correlation of Diffusion Coefficients in Dilute Solutions. *AIChE J.* **1955,** *1*, 264-270.

(32) Arnold, J. H. Studies in Diffusion. II. A Kinetic Theory of Diffusion in Liquid Systems. *J. Am. Chem. Soc.* **1930,** *52*, 3937-3955.

(33) Giraudet, C.; Klein, T.; Zhao, G.; Rausch, M. H.; Koller, T. M.; Froba, A. P. Thermal, Mutual, and Self-Diffusivities of Binary Liquid Mixtures Consisting of Gases Dissolved in *n*-Alkanes at Infinite Dilution. *J. Phys. Chem. B* **2018,** *122*, 3163-3175.

(34) Goeppert-Mayer, M.; Sklar, A. L. Calculations of the Lower Excited Levels of Benzene. *J. Chem. Phys.* **1938,** *6*, 645-652.

(35) Jorgensen, W. L.; Tirado-Rives, J. The OPLS [Optimized Potentials for Liquid Simulations] Potential Functions for Proteins, Energy Minimizations for Crystals of Cyclic Peptides and Crambin. *J. Am. Chem. Soc.* **1988,** *110*, 1657-1666.

(36) Martin, M. G.; Siepmann, J. I. Transferable Potentials for Phase Equilibria. 1. United-Atom Description of *n*-Alkanes. *J. Phys. Chem. B* **1998,** *102*, 2569-2577.

(37) Marrink, S. J.; Risselada, H. J.; Yefimov, S.; Tieleman, D. P.; de Vries, A. H. The MARTINI Force Field: Coarse Grained Model for Biomolecular Simulations. *J. Phys. Chem. B* **2007,** *111*, 7812-7824.

(38) Allen, M. P.; Tildesley, D. J. *Computer Simulation of Liquids*. Oxford University Press: New York, 1987.

(39) Frenkel, D.; Smit, B. *Understanding Molecular Simulation: from Algorithms to Applications* Academic Press: San Diego, 2002.

(40) Rapaport, D. C. *The Art of Molecular Dynamics Simulation*. 2 ed.; Cambridge University Press: Cambridge, U.K., 2004.

(41) Papavasileiou, K. D.; Peristeras, L. D.; Bick, A.; Economou, I. G. Molecular Dynamics Simulation of Pure *n*-Alkanes and Their Mixtures at Elevated Temperatures Using Atomistic and Coarse-Grained Force Fields. *J. Phys. Chem. B* **2019,** *123*, 6229-6243.

(42) Wu, W.; Klein, T.; Kerscher, M.; Rausch, M. H.; Koller, T. M.; Giraudet, C.; Fröba, A. P. Diffusivities in 1-Alcohols Containing Dissolved H_2, He, N_2, CO, or CO_2 Close to Infinite Dilution. *J. Phys. Chem. B* **2019,** *123*, 8777-8790.

(43) Pluhackova, K.; Morhenn, H.; Lautner, L.; Lohstroh, W.; Nemkovski, K. S.; Unruh, T.; Böckmann, R. A. Extension of the LOPLS-AA Force Field for Alcohols, Esters, and Monoolein Bilayers and its Validation by Neutron Scattering Experiments. *J. Phys. Chem. B* **2015,** *119*, 15287-15299.

(44) Siu, S. W. I.; Pluhackova, K.; Böckmann, R. A. Optimization of the OPLS-AA Force Field for Long Hydrocarbons. *J. Chem. Theory Comput.* **2012,** *8*, 1459-1470.

(45) Martin, M. G.; Siepmann, J. I. Novel Configurational-Bias Monte Carlo Method for Branched Molecules. Transferable Potentials for Phase Equilibria. 2. United-Atom Description of Branched Alkanes. *J. Phys. Chem. B* **1999,** *103*, 4508-4517.

(46) Jorgensen, W. L.; Maxwell, D. S.; Tirado-Rives, J. Development and Testing of the OPLS All-Atom Force Field on Conformational Energetics and Properties of Organic Liquids. *J. Am. Chem. Soc.* **1996,** *118*, 11225-11236.

(47) Moultos, O. A.; Tsimpanogiannis, I. N.; Panagiotopoulos, A. Z.; Trusler, J. P. M.; Economou, I. G. Atomistic Molecular Dynamics Simulations of Carbon Dioxide Diffusivity in *n*-Hexane, *n*-Decane, *n*-Hexadecane, Cyclohexane, and Squalane. *J. Phys. Chem. B* **2016,** *120*, 12890-12900.

(48) Makrodimitri, Z. A.; Heller, A.; Koller, T. M.; Rausch, M. H.; Fleys, M. S. H.; Bos, A. N. R.; van der Laan, G. P.; Fröba, A. P.; Economou, I. G. Viscosity of Heavy *n*-Alkanes and Diffusion of Gases Therein Based on Molecular Dynamics Simulations and Empirical Correlations. *J. Chem. Thermodyn.* **2015,** *91*, 101-107.

(49) Koller, T. M.; Heller, A.; Rausch, M. H.; Wasserscheid, P.; Economou, I. G.; Fröba, A. P. Mutual and Self-Diffusivities in Binary Mixtures of [EMIM][$B(CN)_4$] with Dissolved Gases by Using Dynamic Light Scattering and Molecular Dynamics Simulations. *J. Phys. Chem. B* **2015,** *119*, 8583-8592.

(50) Zhao, X.; Jin, H.; Chen, Y.; Ge, Z. Numerical Study of H_2, CH_4, CO, O_2 and CO_2 Diffusion in Water Near the Critical Point with Molecular Dynamics Simulation. *Comput. Math. Appl.* **2021,** *81*, 759-771.

(51) Zabala, D.; Nieto-Draghi, C.; de Hemptinne, J. C.; López de Ramos, A. L. Diffusion Coefficients in CO_2/*n*-Alkane Binary Liquid Mixtures by Molecular Simulation. *J. Phys. Chem. B* **2008,** *112*, 16610-16618.

(52) Aghaie, M.; Rezaei, N.; Zendehboudi, S. New Insights into Bulk and Interface Properties of [Bmim][Ac]/[Bmim][BF_4] Ionic Liquid/CO_2 Systems — Molecular Dynamics Simulation Approach. *J. Mol. Liq.* **2020,** *317*, 113497.

(53) Aminian, A.; ZareNezhad, B. Molecular Dynamics Simulations Study on the Shear Viscosity, Density, and Equilibrium Interfacial Tensions of CO_2 + Brines and Brines + CO_2 + *n*-Decane Systems. *J. Phys. Chem. B* **2021,** *125*, 2707-2718.

(54) Li, C.; Pu, H.; Zhao, J. X. Molecular Simulation Study on the Volume Swelling and the Viscosity Reduction of *n*-Alkane/CO_2 Systems. *Ind. Eng. Chem. Res.* **2019,** *58*, 8871-8877.

(55) Becker, S.; Werth, S.; Horsch, M.; Langenbach, K.; Hasse, H. Interfacial Tension and Adsorption in the Binary System Ethanol and Carbon Dioxide: Experiments, Molecular Simulation and Density Gradient Theory. *Fluid Phase Equilib.* **2016,** *427*, 476-487.

(56) Stephan, S.; Hasse, H. Enrichment at Vapour–Liquid Interfaces of Mixtures: Establishing a Link Between Nanoscopic and Macroscopic Properties. *Int. Rev. Phys. Chem.* **2020,** *39*, 319-349.

(57) Stephan, S.; Schaefer, D.; Langenbach, K.; Hasse, H. Mass Transfer Through Vapour–Liquid Interfaces: a Molecular Dynamics Simulation Study. *Mol. Phys.* **2021,** *119*, e1810798.

(58) Henry, W.; Banks, J. III. Experiments on the Quantity of Gases Absorbed by Water, at Different Temperatures, and Under Different Pressures. *Philos. Trans. R. Soc. London* **1803,** *93*, 29-274.

(59) Poling, B.; Prausnitz, J. M.; O'Connell, J. P. *The Properties of Gases and Liquids*. 5th ed.; McGraw-Hill: New York, 2001.

(60) Secuianu, C.; Feroiu, V.; Geană, D. High-Pressure Phase Equilibria in the (Carbon Dioxide+1-Hexanol) System. *J. Chem. Thermodyn.* **2010,** *42*, 1286-1291.

(61) van Konynenburg, P. H.; Scott, R. L.; Rowlinson, J. S. Critical Lines and Phase Equilibria in Binary van der Waals Mixtures. *Philos. Trans. R. Soc.* **1980,** *298*, 495-540.

(62) Nasirzadeh, K.; Neueder, R.; Kunz, W. Vapor Pressure Determination of the Aliphatic C_5 to C_8 1-Alcohols. *J. Chem. Eng. Data* **2006,** *51*, 7-10.

(63) Parameswaran, V. R.; Gogate, M. R.; Lee, B. G.; Lee, S. Mass Transfer in the Liquid Phase Methanol Synthesis Process. *Fuel Sci. Technol. Int.* **1991,** *9*, 695-744.

(64) Kölbel, H.; Ralek, M. The Fischer-Tropsch Synthesis in the Liquid Phase. *Catal. Rev.* **1980,** *21*, 225-274.

(65) Lee, S.; Gogate, M. R.; Kulik, C. J. A Novel Single-Step Dimethyl Ether (DME) Synthesis in a Three-Phase Slurry Reactor from CO-Rich Syngas. *Chem. Eng. Sci.* **1992,** *47*, 3769-3776.

(66) Lee, S.; Gogate, M. R.; Kulik, C. J. A Single-Stage, Liquid-Phase Dimethyl Ether Synthesis Process From Syngas II. Ccomparison of Per-Pass Syngas Conversion, Reactor Productivity and Hydrogenation Extent. *Fuel Sci. Technol. Int.* **1991,** *9*, 889-912.

(67) Youssef, A. A.; Al-Dahhan, M. H.; Dudukovic, M. P. Bubble Columns with Internals: A Review. *Int. J. Chem. React. Eng.* **2013,** *11*, 169-223.

(68) Rode, C. V.; Bhattacharya, A.; Chaudhari, R. V. Performance of a Bubble Column Reactor for Oxidation of Ethylene (Wacker Process). *Can. J. Chem. Eng.* **1992,** *70*, 612-617.

(69) Shuqing, W.; Rufong, Z.; Jicheng, W. Mathematical Model of the Process for the Oxidation of Acetaldehyde to Acetic Acid. *Comput. Ind.* **1992,** *18*, 213-219.

(70) Acién Fernández, F. G.; Fernández Sevilla, J. M.; Molina Grima, E. Photobioreactors for the Production of Microalgae. *Rev. Environ. Sci. Biotechnol.* **2013,** *12*, 131-151.

(71) Basha, O. M.; Morsi, B. I. Novel Approach and Correlation for Bubble Size Distribution in a Slurry Bubble Column Reactor Operating in the Churn–Turbulent Flow Regime. *Ind. Eng. Chem. Res.* **2018,** *57*, 5705-5716.

(72) Lübbert, A.; Paaschen, T.; Lapin, A. Fluid Dynamics in Bubble Column Bioreactors: Experiments and Numerical Simulations. *Biotechnol. Bioeng.* **1996,** *52*, 248-258.

(73) Ettelaie, R.; Murray, B. S. Evolution of Bubble Size Distribution in Particle Stabilised Bubble Dispersions: Competition Between Particle Adsorption and Dissolution Kinetics. *Colloids Surf. A Physicochem. Eng. Asp.* **2015,** *475*, 27-36.

(74) Summerfelt, S. T.; Vinci, B. J.; Piedrahita, R. H. Oxygenation and Carbon Dioxide Control in Water Reuse Systems. *Aquac. Eng.* **2000,** *22*, 87-108.

(75) Rausch, M. H.; Schmidt, P. S.; Gall, T. R.; Giraudet, C.; Fröba, A. P. Wetting Behavior and Interfacial Tension of a Refrigerant Oil in Air and Refrigerant Atmospheres. *Int. J. Refrig.* **2019,** *107*, 225-233.

(76) He, M.; Peng, S.; Liu, X.; Pan, P.; He, Y. Diffusion Coefficients and Henry's Constants of Hydrofluorocarbons in [HMIM][Tf_2N], [HMIM][TfO], and [HMIM][BF_4]. *J. Chem. Thermodyn.* **2017,** *112*, 43-51.

(77) Blath, J.; Christ, M.; Deubler, N.; Hirth, T.; Schiestel, T. Gas Solubilities in Room Temperature Ionic Liquids – Correlation between RTiL-Molar Mass and Henry's Law Constant. *Chem. Eng. J.* **2011,** *172*, 167-176.

(78) Park, J.; Robinson, R. L.; Gasem, K. A. M. Solubilities of Hydrogen in Heavy Normal Paraffins at Temperatures from 323.2 to 423.2 K and Pressures to 17.4 MPa. *J. Chem. Eng. Data* **1995,** *40*, 241-244.

(79) Clever, H. L.; Battino, R.; Saylor, J. H.; Gross, P. M. The Solubility of Helium, Neon, Argon and Krypton in Some Hydrocarbon Solvents. *J. Phys. Chem.* **1957,** *61*, 1078-1082.

(80) Hesse, P. J.; Battino, R.; Scharlin, P.; Wilhelm, E. Solubility of Gases in Liquids. 20. Solubility of He, Ne, Ar, Kr, N_2, O_2, CH_4, CF_4, and SF_6 in *n*-Alkanes *n*-C_lH_{2l+2} ($6 \le l \le 16$) at 298.15 K. *J. Chem. Eng. Data* **1996,** *41*, 195-201.

(81) Lay, E. N.; Taghikhani, V.; Ghotbi, C. Measurement and Correlation of CO_2 Solubility in the Systems of CO_2 + Toluene, CO_2 + Benzene, and CO_2 + *n*-Hexane at Near-Critical and Supercritical Conditions. *J. Chem. Eng. Data* **2006,** *51*, 2197-2200.

(82) Beier, A.; Kuranov, J.; Stephan, K.; Hasse, H. High-Pressure Phase Equilibria of Carbon Dioxide + 1-Hexanol at 303.15 and 313.15 K. *J. Chem. Eng. Data* **2003,** *48*, 1365-1367.

(83) Lam, D. H.; Jangkamolkulchai, A.; Luks, K. D. Liquid—Liquid—Vapor Phase Equilibrium Behavior of Certain Binary Carbon Dioxide + *n*-Alkanol Mixtures. *Fluid Phase Equilib.* **1990,** *60*, 131-141.

(84) Pereira, L.; Santos, P. G. d.; Scheer, A. P.; Ndiaye, P. M.; Corazza, M. L. High Pressure Phase Equilibrium Measurements for Binary Systems CO_2 +1-Pentanol and CO_2 +1-Hexanol. *J. Supercrit. Fluids* **2014,** *88*, 38-45.

(85) Ren, W.; Sensenich, B.; Scurto, A. M. High-Pressure Phase Equilibria of {Carbon Dioxide (CO_2) +*n*-Alkyl-Imidazolium Bis(trifluoromethylsulfonyl)amide} Ionic Liquids. *J. Chem. Thermodyn.* **2010,** *42*, 305-311.

(86) IUPAC-NIST SOLUBILITY DATA SERIES - IUPAC-NIST Solubility Database, Version 1.1. https://srdata.nist.gov/solubility/index.aspx (accessed 28.07.2021).

(87) Dong, Q.; Muzny, C. D.; Kazakov, A.; Diky, V.; Magee, J. W.; Widegren, J. A.; Chirico, R. D.; Marsh, K. N.; Frenkel, M. ILThermo: A Free-Access Web Database for Thermodynamic Properties of Ionic Liquids. *J. Chem. Eng. Data* **2007,** *52*, 1141-1159.

(88) Kazakov, A.; Magee, J. W.; Chirico, R. D.; Paulechka, E.; Diky, V.; Muzny, C. D.; Kroenlein, K.; Frenkel, M., NIST Standard Reference Database 147: NIST Ionic Liquids Database - (ILThermo) Version 2.0. National Institute of Standards and Technology, Gaithersburg MD, 20899.

(89) Ciotta, F.; Maitland, G.; Smietana, M.; Trusler, J. P. M.; Vesovic, V. Viscosity and Density of Carbon Dioxide + 2,6,10,15,19,23-Hexamethyltetracosane (Squalane). *J. Chem. Eng. Data* **2009,** *54*, 2436-2443.

(90) Ciotta, F.; Maitland, G.; Smietana, M.; Trusler, J. P. M.; Vesovic, V. Viscosity and Density of Carbon Dioxide + 2,6,10,15,19,23-Hexamethyltetracosane (Squalane). *J. Chem. Eng. Data* **2010,** 55, 4126-4126.

(91) Lewis, J. R. The Viscosity of Liquids Containing Dissolved Gases. *J. Am. Chem. Soc.* **1925,** *47*, 626-640.

(92) Audonnet, F.; Pádua, A. A. H. Viscosity and Density of Mixtures of Methane and *n*-Decane from 298 to 393 K and up to 75 MPa. *Fluid Phase Equilib.* **2004,** *216*, 235-244.

(93) Derevich, I. V.; Gromadskaya, R. S. Effect of Dissolved Gases on the Viscosity of Petroleum. *Theor. Found. Chem. Eng* **2002,** *36*, 583-588.

(94) Mohammed, M.; Ciotta, F.; Trusler, J. P. M. Viscosities and Densities of Binary Mixtures of Hexadecane with Dissolved Methane or Carbon Dioxide at Temperatures from (298 to 473) K and at Pressures up to 120 MPa. *J. Chem. Eng. Data* **2017,** *62*, 422-439.

(95) Hu, R.; Trusler, J. P. M.; Crawshaw, J. P. Effect of CO_2 Dissolution on the Rheology of a Heavy Oil/Water Emulsion. *Energy Fuels* **2017,** *31*, 3399-3408.

(96) Kian, K.; Scurto, A. M. Viscosity of Compressed CO_2-Saturated *n*-Alkanes: CO_2/*n*-Hexane, CO_2/*n*-Decane, and CO_2/*n*-Tetradecane. *J. Supercrit. Fluids* **2018,** *133*, 411-420.

(97) Binti Mohd Taib, M.; Trusler, J. P. M. Viscosity and Density of 1,3-Dimethylbenzene + Carbon Dioxide at Temperatures from 298 to 423 K and at Pressures up to 100 MPa. *J. Chem. Eng. Data* **2020,** *65*, 2186-2193.

(98) McBride-Wright, M.; Maitland, G. C.; Trusler, J. P. M. Viscosity and Density of Aqueous Solutions of Carbon Dioxide at Temperatures from (274 to 449) K and at Pressures up to 100 MPa. *J. Chem. Eng. Data* **2015,** *60*, 171-180.

(99) Calabrese, C.; McBride-Wright, M.; Maitland, G. C.; Trusler, J. P. M. Extension of Vibrating-Wire Viscometry to Electrically Conducting Fluids and Measurements of Viscosity and Density of Brines with Dissolved CO_2 at Reservoir Conditions. *J. Chem. Eng. Data* **2019,** *64*, 3831-3847.

(100) Kariznovi, M.; Nourozieh, H.; Abedi, J. Solubility of Carbon Dioxide, Methane, and Ethane in 1-Butanol and Saturated Liquid Densities and Viscosities. *J. Chem. Thermodyn.* **2013,** *67*, 227-233.

(101) Sih, R.; Armenti, M.; Mammucari, R.; Dehghani, F.; Foster, N. R. Viscosity Measurements on Saturated Gas-Expanded Liquid Systems—Ethanol and Carbon Dioxide. *J. Supercrit. Fluids* **2008,** *43*, 460-468.

(102) Sih, R.; Dehghani, F.; Foster, N. R. Viscosity Measurements on Gas Expanded Liquid Systems—Methanol and Carbon Dioxide. *J. Supercrit. Fluids* **2007,** *41*, 148-157.

(103) Sih, R.; Foster, N. R. Viscosity Measurements on Saturated Gas Expanded Liquid Systems—Acetone and Carbon Dioxide. *J. Supercrit. Fluids* **2008,** *47*, 233-239.

(104) Liu, Z.; Wu, W.; Han, B.; Dong, Z.; Zhao, G.; Wang, J.; Jiang, T.; Yang, G. Study on the Phase Behaviors, Viscosities, and Thermodynamic Properties of CO_2/[C_4mim][PF_6]/Methanol System at Elevated Pressures. *Chem. Eur. J.* **2003,** *9*, 3897-3903.

(105) Morais, A. R. C.; Alaras, L. M.; Baek, D. L.; Fox, R. V.; Shiflett, M. B.; Scurto, A. M. Viscosity of 1-Alkyl-1-methylpyrrolidinium Bis(trifluoromethylsulfonyl)imide Ionic Liquids Saturated with Compressed CO_2. *J. Chem. Eng. Data* **2019,** *64*, 4658-4667.

(106) Lopes, J. M.; Kareth, S.; Bermejo, M. D.; Martín, Á.; Weidner, E.; Cocero, M. J. Experimental Determination of Viscosities and Densities of Mixtures Carbon Dioxide+1-Allyl-3-Methylimidazolium Chloride. Viscosity Correlation. *J. Supercrit. Fluids* **2016,** *111*, 91-96.

(107) Fillion, J. J.; Brennecke, J. F. Viscosity of Ionic Liquid–Ionic Liquid Mixtures. *J. Chem. Eng. Data* **2017,** *62*, 1884-1901.

(108) Kanakubo, M.; Makino, T.; Umecky, T. CO_2 Solubility in and Physical Properties for Ionic Liquid Mixtures of 1-Butyl-3-Methylimidazolium Acetate and 1-Butyl-3-Methylimidazolium Bis(trifluoromethanesulfonyl)-amide. *J. Mol. Liq.* **2016,** *217*, 112-119.

(109) Ren, S.; Hou, Y.; Wu, W.; Liu, Q.; Xiao, Y.; Chen, X. Properties of Ionic Liquids Absorbing SO_2 and the Mechanism of the Absorption. *J. Phys. Chem. B* **2010,** *114*, 2175-2179.

(110) Fan, W.; Zhou, Q.; Sun, J.; Zhang, S. Density, Excess Molar Volume, and Viscosity for the Methyl Methacrylate + 1-Butyl-3-methylimidazolium Hexafluorophosphate Ionic Liquid Binary System at Atmospheric Pressure. *J. Chem. Eng. Data* **2009,** *54*, 2307-2311.

(111) Zhang, Y.; Wang, X.; Yin, J. Viscosity of Saturated Mixtures of 1-Hexyl-3-Methyl-Imidazolium Bis(trifluoromethylsulfonyl)amide with R600a and R152a. *J. Chem. Thermodyn.* **2020,** *141*, 105970.

(112) Nieto de Castro, C. A.; Santos, F. J. V.; Fareleira, J. M. N. A.; Wakeham, W. A. Metrology of Viscosity: Have We Learned Enough? *J. Chem. Eng. Data* **2009,** *54*, 171-178.

(113) Assael, M. J.; Oliveira, C. P.; Papadaki, M.; Wakeham, W. A. Vibrating-Wire Viscometers for Liquids at High Pressures. *Int. J. Thermophys.* **1992,** *13*, 593-615.

(114) Ciotta, F.; Trusler, J. P. M. Improved Understanding of Vibrating-Wire Viscometer–Densimeters. *J. Chem. Eng. Data* **2010,** *55*, 2195-2201.

(115) Diogo, J. C. F.; Caetano, F. J. P.; Fareleira, J. M. N. A. Viscosity and Density Measurements of Compressed Liquid Dimethyl Adipate using Oscillating Body Techniques. *Fluid Phase Equilib.* **2014,** *367*, 85-94.

(116) Fröba, A. P. *Simultane Bestimmung von Viskosität und Oberflächenspannung transparenter Fluide mittels Oberflächenlichtstreuung*. Friedrich-Alexander-University Erlangen-Nürnberg, Doctoral thesis, Erlangen: 2002.

(117) Lucassen-Reynders, E. H.; Lucassen, J. Properties of Capillary Waves. *Adv. Colloid Interfac.* **1970,** *2*, 347-395.

(118) Langevin, D. *Light Scattering by Liquid Surfaces and Complementary Techniques*. Marcel Dekker: New York, 1992.

(119) Fröba, A. P.; Leipertz, A. Accurate Determination of Liquid Viscosity and Surface Tension Using Surface Light Scattering (SLS): Toluene Under Saturation Conditions Between 260 and 380 K. *Int. J. Thermophys.* **2003,** *24*, 895-921.

(120) Fröba, A. P.; Leipertz, A. Viscosity of Diisodecyl Phthalate by Surface Light Scattering (SLS). *J. Chem. Eng. Data* **2007,** *52*, 1803-1810.

(121) Will, S.; Leipertz, A. Thermophysical Properties of Fluids from Dynamic Light Scattering. *Int. J. Thermophys.* **2001,** *22*, 317-338.

(122) Einstein, A. Über die von der molekularkinetischen Theorie der Wärme geforderte Bewegung von in ruhenden Flüssigkeiten suspendierten Teilchen. *Ann. Phys.* **1905,** *322*, 549-560.

(123) Will, S.; Leipertz, A. Viscosity of Liquid *n*-Heptane by Dynamic Light Scattering. *Int. J. Thermophys.* **1997,** *18*, 1339-1354.

(124) Luning Prak, D. J.; Lee, B. G.; Cowart, J. S.; Trulove, P. C. Density, Viscosity, Speed of Sound, Bulk Modulus, Surface Tension, and Flash Point of Binary Mixtures of Butylbenzene + Linear Alkanes (*n*-Decane, *n*-Dodecane, *n*-Tetradecane, *n*-Hexadecane, or *n*-Heptadecane) at 0.1 MPa. *J. Chem. Eng. Data* **2017,** *62*, 169-187.

(125) Luning Prak, D. J. Density, Viscosity, Speed of Sound, Bulk Modulus, Surface Tension, and Flash Point of Binary Mixtures of Butylcyclohexane with Toluene or *n*-Hexadecane. *J. Chem. Eng. Data* **2016,** *61*, 3595-3606.

(126) Luning Prak, D. J.; Lee, B. G.; Cowart, J. S.; Trulove, P. C. Density, Viscosity, Speed of Sound, Bulk Modulus, Surface Tension, and Flash Point of Binary Mixtures of Butylbenzene + Linear Alkanes (*n*-Decane, *n*-Dodecane, *n*-Tetradecane, *n*-Hexadecane, or *n*-Heptadecane) at 0.1 MPa. *J. Chem. Eng. Data* **2016,** *62*, 169-187.

(127) Luning Prak, D. J.; Luning Prak, P. J.; Cowart, J. S.; Trulove, P. C. Densities and Viscosities at 293.15–373.15 K, Speeds of Sound and Bulk Moduli at 293.15–333.15 K, Surface Tensions, and Flash Points of Binary Mixtures of *n*-Hexadecane and Alkylbenzenes at 0.1 MPa. *J. Chem. Eng. Data* **2017,** *62*, 1673-1688.

(128) Luning Prak, D. J.; Ye, S.; McLaughlin, M.; Cowart, J. S.; Trulove, P. C. Density, Viscosity, Speed of Sound, Bulk Modulus, Surface Tension, and Flash Point of Selected Ternary Mixtures of *n*-Butylcyclohexane + a Linear Alkane (*n*-Hexadcane or *n*-Dodecane) + an Aromatic Compound (Toluene, *n*-Butylbenzene, or *n*-Hexylbenzene). *J. Chem. Eng. Data* **2017,** *62*, 3452-3472.

(129) Sage, B. H. Measurement of Viscosities of Liquids Saturated with Gases at High Pressures. *Ind. Eng. Chem. Anal. Ed.* **1933,** *5*, 261-263.

(130) Sage, B. H.; Inman, B. N.; Lacey, W. N. Viscosity of Hydrocarbon Solutions. *Ind. Eng. Chem.* **1937,** *29*, 888-892.

(131) Brock, J. R.; Bird, R. B. Surface Tension and the Principle of Corresponding States. *AIChE J.* **1955,** *1*, 174-177.

(132) Beecher, C. E.; Parkhurst, I. P. Effect of Dissolved Gas upon the Viscosity and Surface Tension of Crude Oil. *Trans. AIME* **1926,** *G-26*, 51-69.

(133) Zuidema, H.; Waters, G. Ring Method for the Determination of Interfacial Tension. *Ind. Eng. Chem. Anal. Ed.* **1941,** *13*, 312-313.

(134) Katz, D. L.; Monroe, R. R.; Trainer, R. P. Surface Tension of Crude Oils Containing Dissolved Gases. *Pet. Technol.* **1943,** *6*, 1-10.

(135) Lv, P.; Stevar, M. S. P.; Trusler, J. P. M. Interfacial Tensions in the (CH_4 + CO_2 + H_2O) System under Two- and Three-Phase Conditions. *Fluid Phase Equilib.* **2020,** *522*, 112760.

(136) Lubetkin, S. D.; Akhtar, M. The Variation of Surface Tension and Contact Angle under Applied Pressure of Dissolved Gases, and the Effects of These Changes on the Rate of Bubble Nucleation. *J. Colloid Interf. Sci.* **1996,** *180*, 43-60.

(137) Cui, J.; Bi, S.; Fröba, A. P.; Wu, J. Viscosity and Interfacial Tension of *n*-Heptane with Dissolved Carbon Dioxide by Surface Light Scattering (SLS). *J. Chem. Thermodyn.* **2021,** *152*, 106266.

(138) Cui, J.; Wu, J.; Bi, S. Liquid Viscosity, Interfacial Tension,Thermal Diffusivity and Mutual Diffusivity of *n*-Tetradecane with Dissolved Carbon Dioxide. *Fluid Phase Equilib.* **2021,** *534*, 112951.

(139) Nowrouzi, I.; Mohammadi, A. H.; Khaksar Manshad, A. Synergic Effects of Dissolved Carbon Dioxide and an Anionic Surfactant Synthesized from Rapeseed oil on Interfacial Tension (IFT) Reduction, Wettability Alteration, and Oil Swelling in the Process of Chemical Water Injection into Carbonate Oil Reservoirs. *Fuel* **2021,** *290*, 120011.

(140) Chow, Y. T. F.; Eriksen, D. K.; Galindo, A.; Haslam, A. J.; Jackson, G.; Maitland, G. C.; Trusler, J. P. M. Interfacial Tensions of Systems Comprising Water, Carbon Dioxide and Diluent Gases at High Pressures: Experimental Measurements and Modelling with SAFT-VR Mie and Square-Gradient Theory. *Fluid Phase Equilib.* **2016,** *407*, 159-176.

(141) Espinoza, D. N.; Santamarina, J. C. Water-CO_2-Mineral Systems: Interfacial Tension, Contact Angle, and Diffusion—Implications to CO_2 Geological Storage. *Water Resour. Res.* **2010,** *46*,

(142) Chalbaud, C.; Robin, M.; Lombard, J. M.; Martin, F.; Egermann, P.; Bertin, H. Interfacial Tension Measurements and Wettability Evaluation for Geological CO_2 Storage. *Adv. Water Resour.* **2009,** *32*, 98-109.

(143) Uhlig, H. H. The Solubilities of Gases and Surface Tension. *J. Phys. Chem.* **1937,** *41*, 1215-1226.

(144) Rice, O. K. The Effect of Pressure on Surface Tension. *J. Chem. Phys.* **1947,** *15*, 333-335.

(145) Li, N.; Zhang, C.-W.; Ma, Q.-L.; Jiang, L.-Y.; Xu, Y.-X.; Chen, G.-J.; Sun, C.-Y.; Yang, L.-Y. Interfacial Tension Measurement and Calculation of (Carbon Dioxide + *n*-Alkane) Binary Mixtures. *J. Chem. Eng. Data* **2017,** *62*, 2861-2871.

(146) Drelich, J.; Fang, C.; White, C. L., Measurement of Interfacial Tension in Fluid-Fluid Systems. In *Encyclopedia of Surface and Colloid Science*, 3 ed.; Hubbard, A. T., Ed. Marcel Dekker Inc.: New York, U.S., 2002; pp 3158-3163.

(147) Vakili-Nezhaad, G. R.; Al-Wadhahi, M.; Al-Haddabi, S.; Vakilinejad, A.; Acree, W. E. Surface Tension of Binary Organic Mixtures Based on a New Dimensionless Number. *J. Chem. Thermodyn.* **2021,** *152*, 106292.

(148) Chang, C.-W.; Hsiung, T.-L.; Lui, C.-P.; Tu, C.-H. Densities, Surface Tensions, and Isobaric Vapor–Liquid Equilibria for the Mixtures of 2-Propanol, Water, and 1,2-Propanediol. *Fluid Phase Equilib.* **2015,** *389*, 28-40.

(149) Tong, J.; Liu, Q.-S.; Xu, W.-G.; Fang, D.-W.; Yang, J.-Z. Estimation of Physicochemical Properties of Ionic Liquids 1-Alkyl-3-Methylimidazolium Chloroaluminate. *J. Phys. Chem. B* **2008,** *112*, 4381-4386.

(150) Ghatee, M. H.; Zolghadr, A. R. Surface Tension Measurements of Imidazolium-Based Ionic Liquids at Liquid–Vapor Equilibrium. *Fluid Phase Equilib.* **2008,** *263*, 168-175.

(151) Koller, T. M.; Rausch, M. H.; Pohako-Esko, K.; Wasserscheid, P.; Fröba, A. P. Surface Tension of Tricyanomethanide- and Tetracyanoborate-Based Imidazolium Ionic Liquids by Using the Pendant Drop Method. *J. Chem. Eng. Data* **2015,** *60*, 2665-2673.

(152) Rowane, A. J.; Mallepally, R. R.; Gavaises, M.; McHugh, M. A. Interfacial Tension of Isomers *n*-Hexadecane and 2,2,4,4,6,8,8-Heptamethylnonane with Nitrogen at High Pressures and Temperatures. *Ind. Eng. Chem. Res.* **2020,** *59*, 9293-9299.

(153) Georgiadis, A.; Llovell, F.; Bismarck, A.; Blas, F. J.; Galindo, A.; Maitland, G. C.; Trusler, J. P. M.; Jackson, G. Interfacial Tension Measurements and Modelling of (Carbon Dioxide+*n*-Alkane) and (Carbon Dioxide+Water) Binary Mixtures at Elevated Pressures and Temperatures. *J. Supercrit. Fluids* **2010,** *55*, 743-754.

(154) Tariq, M.; Carvalho, P. J.; Coutinho, J. A. P.; Marrucho, I. M.; Lopes, J. N. C.; Rebelo, L. P. N. Viscosity of (C_2–C_{14}) 1-Alkyl-3-Methylimidazolium Bis(trifluoromethylsulfonyl)amide Ionic Liquids in an Extended Temperature Range. *Fluid Phase Equilib.* **2011,** *301*, 22-32.

(155) Fröba, A. P.; Pellegrino, L. P.; Leipertz, A. Viscosity and Surface Tension of Saturated *n*-Pentane. *Int. J. Thermophys.* **2004,** *25*, 1323-1337.

(156) Fröba, A. P.; Botero, C.; Leipertz, A. Thermal Diffusivity, Sound Speed, Viscosity, and Surface Tension of R227ea (1,1,1,2,3,3,3-Heptafluoropropane). *Int. J. Thermophys.* **2006,** *27*, 1609-1625.

(157) Graham, T. XXVII. On the Law of the Diffusion of Gases. *London, Edinburgh Dublin Philos. Mag. J. Sci.* **1833,** *2*, 175-190.

(158) Graham, T. X. Liquid Diffusion Applied to Analysis. *Philos. Trans. R. Soc.* **1861,** *151*, 183-224.

(159) Fick, A. Über Diffusion. *Ann. Phys.* **1855,** *170*, 59-86.

(160) Guevara-Carrion, G.; Gaponenko, Y.; Janzen, T.; Vrabec, J.; Shevtsova, V. Diffusion in Multicomponent Liquids: From Microscopic to Macroscopic Scales. *J Phys. Chem. B* **2016,** *120*, 12193-12210.

(161) Liu, X.; Vlugt, T. J. H.; Bardow, A. Maxwell–Stefan Diffusivities in Binary Mixtures of Ionic Liquids with Dimethyl Sulfoxide (DMSO) and H_2O. *J. Phys. Chem. B* **2011,** *115*, 8506-8517.

(162) Krishna, R.; Wesselingh, J. A. The Maxwell-Stefan Approach to Mass Transfer. *Chem. Eng. Sci.* **1997,** *52*, 861-911.

(163) Xu, F.; Jimenez, M.; Dietrich, N.; Hébrard, G. Fast Determination of Gas-Liquid Diffusion Coefficient by an Innovative Double Approach. *Chem. Eng. Sci.* **2017,** *170*, 68-76.

(164) Cadogan, S. P.; Maitland, G. C.; Trusler, J. P. M. Diffusion Coefficients of CO_2 and N_2 in Water at Temperatures between 298.15 K and 423.15 K at Pressures up to 45 MPa. *J. Chem. Eng. Data* **2014,** *59*, 519-525.

(165) Ng, W. Y.; Walkley, J. Diffusion of Gases in Liquids: the Constant Size Bubble Method. *Can. J. Chem.* **1969,** *47*, 1075-1077.

(166) Dietrich, N.; Francois, J.; Jimenez, M.; Cockx, A.; Guiraud, P.; Hébrard, G. Fast Measurements of the Gas-Liquid Diffusion Coefficient in the Gaussian Wake of a Spherical Bubble. *Chem. Eng. Tech.* **2015,** *38*, 941-946.

(167) Ahmadi, H.; Jamialahmadi, M.; Soulgani, B. S.; Dinarvand, N.; Sharafi, M. S. Experimental Study and Modelling on Diffusion Coefficient of CO_2 in Water. *Fluid Phase Equilib.* **2020,** *523*, 112584.

(168) Takeuchi, H.; Fujine, M.; Sato, T.; Onda, K. Simultaneous Determination of Diffusion Coefficient and Solubility of Gas in Liquid by a Diaphragm Cell. *J. Chem. Eng. Japan* **1975,** *8*, 252-253.

(169) Lefortier, S. G. R.; Hamersma, P. J.; Bardow, A.; Kreutzer, M. T. Rapid Microfluidic Screening of CO_2 Solubility and Diffusion in Pure and Mixed Solvents. *Lab Chip* **2012,** *12*, 3387-3391.

(170) Cadogan, S. P.; Hallett, J. P.; Maitland, G. C.; Trusler, J. P. M. Diffusion Coefficients of Carbon Dioxide in Brines Measured Using ^{13}C Pulsed-Field Gradient Nuclear Magnetic Resonance. *J. Chem. Eng. Data* **2015,** *60*, 181-184.

(171) Sheikha, H.; Mehrotra, A. K.; Pooladi-Darvish, M. An Inverse Solution Methodology for Estimating the Diffusion Coefficient of Gases in Athabasca Bitumen from Pressure-Decay Data. *J. Petro. Sci. Eng.* **2006,** *53*, 189-202.

(172) Meng, L.; Sabet, N.; Maini, B.; Dong, M.; Hassanzadeh, H. Estimation of Diffusion Coefficient of Gases in Liquids from Swelling Data – An Analytical Model for Including the Effects of Advection and Density Change. *Fuel* **2019,** *252*, 68-76.

(173) Cadogan, S. P.; Mistry, B.; Wong, Y.; Maitland, G. C.; Trusler, J. P. M. Diffusion Coefficients of Carbon Dioxide in Eight Hydrocarbon Liquids at Temperatures between (298.15 and 423.15) K at Pressures up to 69 MPa. *J. Chem. Eng. Data* **2016,** *61*, 3922-3932.

(174) Taib, M. B. M.; Trusler, J. P. M. Diffusion Coefficients of Methane in Methylbenzene and Heptane at Temperatures between 323 K and 398 K at Pressures up to 65 MPa. *Int. J. Thermophys.* **2020,** *41*, 119.

(175) Khalifi, M.; Sabet, N.; Zirrahi, M.; Hassanzadeh, H.; Abedi, J. Concentration-Dependent Molecular Diffusion Coefficient of Gaseous Ethane in Liquid Toluene. *AIChE J.* **2020,** *66*, e16966.

(176) Heller, A.; Koller, T. M.; Rausch, M. H.; Fleys, M. S. H.; Bos, A. N. R.; van der Laan, G. P.; Makrodimitri, Z. A.; Economou, I. G.; Fröba, A. P. Simultaneous Determination of Thermal and Mutual Diffusivity of Binary Mixtures of *n*-Octacosane with Carbon Monoxide, Hydrogen, and Water by Dynamic Light Scattering. *J. Phys. Chem. B* **2014,** *118*, 3981-3990.

(177) Heller, A.; Fleys, M. S. H.; Chen, J.; van der Laan, G. P.; Rausch, M. H.; Fröba, A. P. Thermal and Mutual Diffusivity of Binary Mixtures of *n*-Dodecane and *n*-Tetracontane with Carbon Monoxide, Hydrogen, and Water from Dynamic Light Scattering (DLS). *J. Chem. Eng. Data* **2016,** *61*, 1333-1340.

(178) Jamialahmadi, M.; Emadi, M.; Müller-Steinhagen, H. Diffusion Coefficients of Methane in Liquid Hydrocarbons at High Pressure and Temperature. *J. Petro. Sci. Eng.* **2006,** *53*, 47-60.

(179) Morgan, D.; Ferguson, L.; Scovazzo, P. Diffusivities of Gases in Room-Temperature Ionic Liquids: Data and Correlations Obtained Using a Lag-Time Technique. *Ind. Eng. Chem. Res.* **2005,** *44*, 4815-4823.

(180) Moganty, S. S.; Baltus, R. E. Diffusivity of Carbon Dioxide in Room-Temperature Ionic Liquids. *Ind. Eng. Chem. Res.* **2010,** *49*, 9370-9376.

(181) Rausch, M. H.; Heller, A.; Herbst, J.; Koller, T. M.; Bahlmann, M.; Schulz, P. S.; Wasserscheid, P.; Fröba, A. P. Mutual and Thermal Diffusivity of Binary Mixtures of the Ionic Liquids [BMIM][$C(CN)_3$] and [BMIM][$B(CN)_4$] with Dissolved CO_2 by Dynamic Light Scattering. *J. Phys. Chem. B* **2014,** *118*, 4636-4646.

(182) Shiflett, M. B.; Harmer, M. A.; Junk, C. P.; Yokozeki, A. Solubility and Diffusivity of 1,1,1,2-Tetrafluoroethane in Room-Temperature Ionic Liquids. *Fluid Phase Equilib.* **2006,** *242*, 220-232.

(183) Asensio-Delgado, S.; Pardo, F.; Zarca, G.; Urtiaga, A. Vapor–Liquid Equilibria and Diffusion Coefficients of Difluoromethane, 1,1,1,2-Tetrafluoroethane, and 2,3,3,3-Tetrafluoropropene in Low-Viscosity Ionic Liquids. *J. Chem. Eng. Data* **2020,** *65*, 4242-4251.

(184) Merkel, N. C.; Römich, C.; Bernewitz, R.; Künemund, H.; Gleiß, M.; Sauer, S.; Schubert, T. J. S.; Guthausen, G.; Schaber, K. Thermophysical Properties of the Binary Mixture of Water + Diethylmethylammonium Trifluoromethanesulfonate and the Ternary Mixture of Water + Diethylmethylammonium Trifluoromethanesulfonate + Diethylmethylammonium Methanesulfonate. *J. Chem. Eng. Data* **2014,** *59*, 560-570.

(185) Nieto de Castro, C. A.; Langa, E.; Morais, A. L.; Lopes, M. L. M.; Lourenço, M. J. V.; Santos, F. J. V.; Santos, M. S. C. S.; Lopes, J. N. C.; Veiga, H. I. M.; Macatrão, M.; Esperança, J. M. S. S.; Marques, C. S.; Rebelo, L. P. N.; Afonso, C. A. M. Studies on the Density, Heat Capacity, Surface Tension and Infinite Dilution Diffusion with the Ionic Liquids $[C_4mim][NTf_2]$, $[C_4mim][dca]$, $[C_2mim][EtOSO_3]$ and [Aliquat][dca]. *Fluid Phase Equilib.* **2010,** *294*, 157-179.

(186) He, X.; Shao, Q.; Kong, W.; Yu, L.; Zhang, X.; Deng, Y. A Simple Method for Estimating Mutual Diffusion Coefficients of Ionic Liquids-Water Based on an Optofluidic Chip. *Fluid Phase Equilib.* **2014,** *366*, 9-15.

(187) Duda, J. L.; Vrentas, J. S. Laminar Liquid Jet Diffusion Studies. *AIChE J.* **1968,** *14*, 286-294.

(188) Hou, Y.; Baltus, R. E. Experimental Measurement of the Solubility and Diffusivity of CO_2 in Room-Temperature Ionic Liquids Using a Transient Thin-Liquid-Film Method. *Ind. Eng. Chem. Res.* **2007,** *46*, 8166-8175.

(189) Secuianu, C.; Maitland, G. C.; Trusler, J. P. M.; Wakeham, W. A. Mutual Diffusion Coefficients of Aqueous KCl at High Pressures Measured by the Taylor Dispersion Method. *J. Chem. Eng. Data* **2011,** *56*, 4840-4848.

(190) Guzmán, J.; Garrido, L. Determination of Carbon Dioxide Transport Coefficients in Liquids and Polymers by NMR Spectroscopy. *J. Phys. Chem. B* **2012,** *116*, 6050-6058.

(191) Etesse, P.; Chapman, W. G.; Kobayashi, R. Nuclear Magnetic Resonance Measurement of Spin-Lattice Relaxation and Self-Diffusion in Supercritical CO_2-*n*-Hexadecane Mixtures. *Mol. Phys.* **1993,** *80*, 1145-1164.

(192) Fröba, A. P.; Will, S.; Leipertz, A. Diffusion Modes of an Equimolar Methane–Ethane Mixture from Dynamic Light Scattering. *Int. J. Thermophys.* **2000,** *21*, 603-620.

(193) Fröba, A. P. *Dynamic Light Scattering (DLS) for the Characterization of Working Fluids in Chemical and Energy Engineering*. Habilitation Thesis, Friedrich-Alexander-Universität Erlangen-Nürnberg, Erlangen, 2009.

(194) Onsager, L. Reciprocal Relations in Irreversible Processes. I. *Phys. Rev.* **1931,** *37*, 405-426.

(195) Onsager, L. Reciprocal Relations in Irreversible Processes. II. *Phys. Rev.* **1931,** *38*, 2265-2279.

(196) Sato, H.; Matubayasi, N.; Nakahara, M.; Hirata, F. Which Carbon Oxide is More Soluble? Ab Initio Study on Carbon Monoxide and Dioxide in Aqueous Solution. *Chem. Phys. Lett.* **2000,** *323*, 257-262.

(197) L.S. Batista, M.; A.P. Coutinho, J.; R.B. Gomes, J. Prediction of Ionic Liquids Properties through Molecular Dynamics Simulations. *Curr. Phys. Chem.* **2014,** *4*, 151-172.

(198) Lorentz, H. A. Ueber die Anwendung des Satzes vom Virial in der kinetischen Theorie der Gase. *Ann. Phys.* **1881,** *248*, 127-136.

(199) Köster, A.; Thol, M.; Vrabec, J. Molecular Models for the Hydrogen Age: Hydrogen, Nitrogen, Oxygen, Argon, and Water. *J. Chem. Eng. Data* **2018,** *63*, 305-320.

(200) Metropolis, N.; Rosenbluth, A. W.; Rosenbluth, M. N.; Teller, A. H.; Teller, E. Equation of State Calculations by Fast Computing Machines. *J. Chem. Phys.* **1953,** *21*, 1087-1092.

(201) Maginn, E. J.; Elliott, J. R. Historical Perspective and Current Outlook for Molecular Dynamics As a Chemical Engineering Tool. *Ind. Eng. Chem. Res.* **2010,** *49*, 3059-3078.

(202) Biscay, F.; Ghoufi, A.; Goujon, F.; Lachet, V.; Malfreyt, P. Calculation of the Surface Tension from Monte Carlo Simulations: Does the Model Impact on the Finite-Size Effects? *J. Chem. Phys.* **2009,** *130*, 184710.

(203) Chen, B.; Potoff, J. J.; Siepmann, J. I. Monte Carlo Calculations for Alcohols and Their Mixtures with Alkanes. Transferable Potentials for Phase Equilibria. 5. United-Atom Description of Primary, Secondary, and Tertiary Alcohols. *J. Phys. Chem. B* **2001,** *105*, 3093-3104.

(204) Zhang, Y.; Otani, A.; Maginn, E. J. Reliable Viscosity Calculation from Equilibrium Molecular Dynamics Simulations: A Time Decomposition Method. *J. Chem. Theory Comput.* **2015,** *11*, 3537-3546.

(205) Jamali, S. H.; Hartkamp, R.; Bardas, C.; Söhl, J.; Vlugt, T. J. H.; Moultos, O. A. Shear Viscosity Computed from the Finite-Size Effects of Self-Diffusivity in Equilibrium Molecular Dynamics. *J. Chem. Theory Comput.* **2018,** *14*, 5959-5968.

(206) Yeh, I.-C.; Hummer, G. System-Size Dependence of Diffusion Coefficients and Viscosities from Molecular Dynamics Simulations with Periodic Boundary Conditions. *J. Phys. Chem. B* **2004,** *108*, 15873-15879.

(207) Jamali, S. H.; Wolff, L.; Becker, T. M.; Bardow, A.; Vlugt, T. J. H.; Moultos, O. A. Finite-Size Effects of Binary Mutual Diffusion Coefficients from Molecular Dynamics. *J. Chem. Theory Comput.* **2018,** *14*, 2667-2677.

(208) Jamali, S. H.; Bardow, A.; Vlugt, T. J. H.; Moultos, O. A. Generalized Form for Finite-Size Corrections in Mutual Diffusion Coefficients of Multicomponent Mixtures Obtained from Equilibrium Molecular Dynamics Simulation. *J. Chem. Theory Comput.* **2020,** *16*, 3799-3806.

(209) Baig, C.; Edwards, B. J.; Keffer, D. J.; Cochran, H. D.; Harmandaris, V. A. Rheological and Structural Studies of Linear Polyethylene Melts Under Planar Elongational Flow Using Nonequilibrium Molecular Dynamics Simulations. *J. Chem. Phys.* **2006,** *124*, 084902.

(210) Baig, C.; Edwards, B. J.; Keffer, D. J.; Cochran, H. D. A Proper Approach for Nonequilibrium Molecular Dynamics Simulations of Planar Elongational Flow. *J. Chem. Phys.* **2005,** *122*, 114103.

(211) Müller-Plathe, F. Reversing the Perturbation in Nonequilibrium Molecular Dynamics: An Easy Way to Calculate the Shear Viscosity of Fluids. *Phys. Rev. E* **1999,** *59*, 4894-4898.

(212) Hess, B. Determining the Shear Viscosity of Model Liquids from Molecular Dynamics Simulations. *J. Chem. Phys.* **2001,** *116*, 209-217.

(213) Houndonougbo, Y.; Laird, B. B.; Kuczera, K. Transport Properties of CO_2-Expanded Acetonitrile from Molecular Dynamics Simulations. *J. Chem. Phys.* **2007,** *126*, 074507.

(214) Li, H.; Maroncelli, M. Solvation and Solvatochromism in CO_2-Expanded Liquids. 1. Simulations of the Solvent Systems CO_2 + Cyclohexane, Acetonitrile, and Methanol. *J. Phys. Chem. B* **2006,** *110*, 21189-21197.

(215) Zheng, L.; Bresme, F.; Trusler, J. P. M.; Müller, E. A. Employing SAFT Coarse-Grained Force Fields for the Molecular Simulation of Thermodynamic and Transport Properties of CO_2–*n*-Alkane Mixtures. *J. Chem. Eng. Data* **2020,** *65*, 1159-1171.

(216) Pisarev, V.; Mistry, S. Volume-Based Mixing Rules for Viscosities of Methane + *n*-Butane Liquid Mixtures. *Fluid Phase Equilib.* **2019,** *484*, 98-105.

(217) Velásquez, A. M.; Hoyos, B. A. Viscosity of Heptane-Toluene Mixtures. Comparison of Molecular Dynamics and Group Contribution Methods. *J. Mol. Model.* **2017,** *23*, 58.

(218) Irving, J. H.; Kirkwood, J. G. The Statistical Mechanical Theory of Transport Processes. IV. The Equations of Hydrodynamics. *J. Chem. Phys.* **1950,** *18*, 817-829.

(219) Kirkwood, J. G.; Buff, F. P. The Statistical Mechanical Theory of Surface Tension. *J. Chem. Phys.* **1949,** *17*, 338-343.

(220) Biscay, F.; Ghoufi, A.; Lachet, V.; Malfreyt, P. Monte Carlo Simulations of the Pressure Dependence of the Water–Acid Gas Interfacial Tensions. *J. Phys. Chem. B* **2009,** *113*, 14277-14290.

(221) Abraham, M. J.; Murtola, T.; Schulz, R.; Páll, S.; Smith, J. C.; Hess, B.; Lindahl, E. GROMACS: High Performance Molecular Simulations Through Multi-Level Parallelism from Laptops to Supercomputers. *SoftwareX* **2015,** *1-2*, 19-25.

(222) Wennberg, C. L.; Murtola, T.; Páll, S.; Abraham, M. J.; Hess, B.; Lindahl, E. Direct-Space Corrections Enable Fast and Accurate Lorentz–Berthelot Combination Rule Lennard-Jones Lattice Summation. *J. Chem. Theory Comput.* **2015,** *11*, 5737-5746.

(223) Li, Y.; Fouad, W. A.; Vega, L. F. Interfacial Anomaly in Low Global Warming Potential Refrigerant Blends as Predicted by Molecular Dynamics Simulations. *Phys. Chem. Chem. Phys.* **2019,** *21*, 22092-22102.

(224) Vilaseca, O.; Llovell, F.; Yustos, J.; Marcos, R. M.; Vega, L. F. Phase Equilibria, Surface Tensions and Heat Capacities of Hydrofluorocarbons and Their Mixtures Including the Critical Region. *J. Supercrit. Fluids* **2010,** *55*, 755-768.

(225) Mejía, A.; Cartes, M.; Segura, H.; Müller, E. A. Use of Equations of State and Coarse Grained Simulations to Complement Experiments: Describing the Interfacial Properties of Carbon Dioxide + Decane and Carbon Dioxide + Eicosane Mixtures. *J. Chem. Eng. Data* **2014,** *59*, 2928-2941.

(226) Cao, F.; Deetz, J. D.; Sun, H. Free Energy-Based Coarse-Grained Force Field for Binary Mixtures of Hydrocarbons, Nitrogen, Oxygen, and Carbon Dioxide. *J. Chem. Inf. Model.* **2017,** *57*, 50-59.

(227) Neyt, J.-C.; Wender, A.; Lachet, V.; Malfreyt, P. Modeling the Pressure Dependence of Acid Gas + *n*-Alkane Interfacial Tensions Using Atomistic Monte Carlo Simulations. *J. Phys. Chem. C* **2012,** *116*, 10563-10572.

(228) Müller, E. A.; Mejía, A. Interfacial Properties of Selected Binary Mixtures Containing *n*-Alkanes. *Fluid Phase Equilib.* **2009,** *282*, 68-81.

(229) Stephan, S.; Becker, S.; Langenbach, K.; Hasse, H. Vapor-Liquid Interfacial Properties of the System Cyclohexane + CO_2: Experiments, Molecular Simulation and Density Gradient Theory. *Fluid Phase Equilib.* **2020,** *518*, 112583.

(230) Algaba, J.; Cartes, M.; Mejía, A.; Míguez, J. M.; Blas, F. J. Phase Equilibria and Interfacial Properties of the Tetrahydrofuran + Methane Binary Mixture from Experiment and Computer Simulation. *J. Phys. Chem. C* **2019,** *123*, 20960-20970.

(231) Eckelsbach, S.; Vrabec, J. Fluid Phase Interface Properties of Acetone, Oxygen, Nitrogen and Their Binary Mixtures by Molecular Simulation. *Phys. Chem. Chem. Phys.* **2015,** *17*, 27195-27203.

(232) Baidakov, V. G.; Protsenko, S. P. Molecular-Dynamics Investigation of Phase Equilibrium and Surface Tension in Argon–Neon System. *J. Phys. Chem. C* **2008,** *112*, 17231-17234.

(233) dos Santos, T. J. P.; Tavares, F. W.; Abreu, C. Fick Diffusion Coefficients via Molecular Dynamics: An Alternative Approach in the Fourier Domain. *J. Mol. Liq.* **2021,** *329*, 115460.

(234) Nichols, J. W.; Wheeler, D. R. Fourier Correlation Method for Simulating Mutual Diffusion Coefficients in Condensed Systems at Equilibrium. *Ind. Eng. Chem. Res.* **2015,** *54*, 12156-12164.

(235) Green, M. S. Markoff Random Processes and the Statistical Mechanics of Time-Dependent Phenomena. II. Irreversible Processes in Fluids. *J. Chem. Phys.* **1954,** *22*, 398-413.

(236) Kubo, R. Statistical-Mechanical Theory of Irreversible Processes. I. General Theory and Simple Applications to Magnetic and Conduction Problems. *J. Phys. Soc. Jpn.* **1957,** *12*, 570-586.

(237) Krüger, P.; Schnell, S. K.; Bedeaux, D.; Kjelstrup, S.; Vlugt, T. J. H.; Simon, J.-M. Kirkwood–Buff Integrals for Finite Volumes. *J. Phys. Chem. Lett.* **2013,** *4*, 235-238.

(238) Schnell, S. K.; Englebienne, P.; Simon, J.-M.; Krüger, P.; Balaji, S. P.; Kjelstrup, S.; Bedeaux, D.; Bardow, A.; Vlugt, T. J. H. How to Apply the Kirkwood–Buff Theory to Individual Species in Salt Solutions. *Chem. Phys. Lett.* **2013,** *582*, 154-157.

(239) Schnell, S. K.; Liu, X.; Simon, J.-M.; Bardow, A.; Bedeaux, D.; Vlugt, T. J. H.; Kjelstrup, S. Calculating Thermodynamic Properties from Fluctuations at Small Scales. *J. Phys. Chem. B* **2011,** *115*, 10911-10918.

(240) Rüther, T.; Bhatt, A. I.; Best, A. S.; Harris, K. R.; Hollenkamp, A. F. Electrolytes for Lithium (Sodium) Batteries Based on Ionic Liquids: Highlighting the Key Role Played by the Anion. *Batteries & Supercaps.* **2020,** *3*, 793-827.

(241) Liu, X.; Schnell, S. K.; Simon, J.-M.; Krüger, P.; Bedeaux, D.; Kjelstrup, S.; Bardow, A.; Vlugt, T. J. H. Diffusion Coefficients from Molecular Dynamics Simulations in Binary and Ternary Mixtures. *Int. J. Thermophys.* **2013,** *34*, 1169-1196.

(242) Feng, H.; Gao, W.; Sun, Z.; Lei, B.; Li, G.; Chen, L. Molecular Dynamics Simulation of Diffusion and Structure of Some *n*-Alkanes in near Critical and Supercritical Carbon Dioxide at Infinite Dilution. *J. Phys. Chem. B* **2013,** *117*, 12525-12534.

(243) Higashi, H.; Iwai, Y.; Arai, Y. Calculation of Self-Diffusion and Tracer Diffusion Coefficients near the Critical Point of Carbon Dioxide Using Molecular Dynamics Simulation. *Ind. Eng. Chem. Res.* **2000,** *39*, 4567-4570.

(244) Higashi, H.; Iwai, Y.; Uchida, H.; Arai, Y. Diffusion Coefficients of Aromatic Compounds in Supercritical Carbon Dioxide Using Molecular Dynamics Simulation. *J. Supercrit. Fluids* **1998,** *13*, 93-97.

(245) Iwai, Y.; Higashi, H.; Uchida, H.; Arai, Y. Molecular Dynamics Simulation of Diffusion Coefficients of Naphthalene and 2-Naphthol in Supercritical Carbon Dioxide. *Fluid Phase Equilib.* **1997,** *127*, 251-261.

(246) Moultos, O. A.; Tsimpanogiannis, I. N.; Panagiotopoulos, A. Z.; Economou, I. G. Atomistic Molecular Dynamics Simulations of CO_2 Diffusivity in H_2O for a Wide Range of Temperatures and Pressures. *J. Phys. Chem. B* **2014,** *118*, 5532-5541.

(247) Krishna, R.; van Baten, J. M. The Darken Relation for Multicomponent Diffusion in Liquid Mixtures of Linear Alkanes: An Investigation Using Molecular Dynamics (MD) Simulations. *Ind. Eng. Chem. Res.* **2005,** *44*, 6939-6947.

(248) Fröba, A. P.; Leipertz, A. Viscosity and Surface Tension of Saturated Toluene from Surface Light Scattering (SLS). *Int. J. Thermophys.* **2001,** *22*, 41-59.

(249) Fröba, A. P.; Will, S., Light Scattering by Surface Waves – Surface Light Scattering. In *Experimental Thermodynamics, Vol. IX: Advances in Transport Properties of Fluids*, Assael, M. J.; Goodwin, A. R. H.; Vesovic, V.; Wakeham, W. A., Eds. Royal Society of Chemistry: Cambridge, U.K., 2014; p 22–35.

(250) Klein, T.; Cui, J.; Kalantar, A.; Chen, J.; Rausch, M. H.; Koller, T. M.; Fröba, A. P. Liquid Viscosity and Interfacial Tension of Binary and Ternary Mixtures Containing *n*-Octacosane by Surface Light Scattering. *J. Chem. Eng. Data* **2019,** *64*, 817-826.

(251) Klein, T.; Yan, S.; Cui, J.; Magee, J. W.; Kroenlein, K.; Rausch, M. H.; Koller, T. M.; Fröba, A. P. Liquid Viscosity and Surface Tension of *n*-Hexane, *n*-Octane, *n*-Decane, and *n*-Hexadecane up to 573 K by Surface Light Scattering. *J. Chem. Eng. Data* **2019,** *64*, 4116-4131.

(252) Klein, T.; Lenahan, F. D.; Kerscher, M.; Jander, J. H.; Rausch, M. H.; Koller, T. M.; Fröba, A. P. Viscosity and Interfacial Tension of Binary Mixtures of *n*-Hexadecane with Dissolved Gases Using Surface Light Scattering and Equilibrium Molecular Dynamics Simulations. *J. Chem. Eng. Data* **2021,** *66*, 3205-3218.

(253) Klein, T.; Wu, W.; Rausch, M. H.; Giraudet, C.; Koller, T. M.; Fröba, A. P. Influence of Liquid Structure on Fickian Diffusion in Binary Mixtures of *n*-Hexane and Carbon Dioxide Probed by Dynamic Light Scattering, Raman Spectroscopy, and Molecular Dynamics Simulations. *J. Phys. Chem. B* **2018,** *122*, 7122-7133.

(254) Wu, W.; Klein, T.; Kerscher, M.; Rausch, M. H.; Koller, T. M.; Giraudet, C.; Fröba, A. P. Mutual and Thermal Diffusivities as well as Fluid-Phase Equilibria of Mixtures of 1-Hexanol and Carbon Dioxide. *J. Phys. Chem. B* **2020,** *124*, 2482-2494.

(255) Klein, T.; Piszko, M.; Lang, M.; Mehler, J.; Schulz, P. S.; Rausch, M. H.; Giraudet, C.; Koller, T. M.; Fröba, A. P. Diffusivities in Binary Mixtures of [AMIM][NTf_2] Ionic Liquids with the Dissolved Gases H_2, He, N_2, CO, CO_2, or Kr Close to Infinite Dilution. *J. Chem. Eng. Data* **2020,** *65*, 4116-4129.

(256) Klein, T.; Piszko, M.; Kankanamge, C. J.; Kasapis, G.; Fröba, A. P. Fick Diffusion Coefficient in Binary Mixtures of [HMIM][NTf_2] and Carbon Dioxide by Dynamic Light Scattering and Molecular Dynamics Simulations. *J. Phys. Chem. B* **2021,** *125*, 5100-5113.

(257) Rausch, M. H.; Hopf, L.; Heller, A.; Leipertz, A.; Fröba, A. P. Binary Diffusion Coefficients for Mixtures of Ionic Liquids [EMIM][$N(CN)_2$], [EMIM][NTf_2], and [HMIM][NTf_2] with Acetone and Ethanol by Dynamic Light Scattering (DLS). *J. Phys. Chem. B* **2013,** *117*, 2429-2437.

(258) Rausch, M. H.; Lehmann, J.; Leipertz, A.; Fröba, A. P. Mutual Diffusion in Binary Mixtures of Ionic Liquids and Molecular Liquids by Dynamic Light Scattering (DLS). *J. Chem. Chem. Phys.* **2011,** *13*, 9525-9533.

(259) Will, S.; Fröba, A. P.; Leipertz, A. Thermal Diffusivity and Sound Velocity of Toluene Over a Wide Temperature Range. *Int. J. Thermophys.* **1998,** *19*, 403-414.

(260) Hess, B.; Bekker, H.; Berendsen, H. J. C.; Fraaije, J. G. E. M. LINCS: A Linear Constraint Solver for Molecular Simulations. *J. Comput. Chem.* **1997,** *18*, 1463-1472.

(261) Nosé, S. A Molecular Dynamics Method for Simulations in the Canonical Ensemble. *Mol. Phys.* **1984,** *52*, 255-268.

(262) Hoover, W. G. Canonical Dynamics: Equilibrium Phase-Space Distributions. *Phys. Rev. A* **1985,** *31*, 1695-1697.

(263) Parrinello, M.; Rahman, A. Polymorphic Transitions in Single Crystals: A new Molecular Dynamics Method. *J. Appl. Phys.* **1981,** *52*, 7182-7190.

(264) Nosé, S.; Klein, M. L. Constant Pressure Molecular Dynamics for Molecular Systems. *Mol. Phys.* **1983,** *50*, 1055-1076.

(265) Darden, T.; York, D.; Pedersen, L. Particle Mesh Ewald: An *N*·log(*N*) Method for Ewald Sums in Large Systems. *J. Chem. Phys.* **1993,** *98*, 10089-10092.

(266) Neumann, J.; Golub, B.; Odebrecht, L.-M.; Ludwig, R.; Paschek, D. Revisiting Imidazolium Based Ionic Liquids: Effect of the Conformation Bias of the [NTf_2] Anion Studied by Molecular Dynamics Simulations. *J. Chem. Phys.* **2018,** *148*, 193828.

(267) Liu, X.; Martín-Calvo, A.; McGarrity, E.; Schnell, S. K.; Calero, S.; Simon, J.-M.; Bedeaux, D.; Kjelstrup, S.; Bardow, A.; Vlugt, T. J. H. Fick Diffusion Coefficients in Ternary Liquid Systems from Equilibrium Molecular Dynamics Simulations. *Ind. Eng. Chem. Res.* **2012,** *51*, 10247-10258.

(268) Liu, X.; Vlugt, T. J. H.; Bardow, A. Predictive Darken Equation for Maxwell-Stefan Diffusivities in Multicomponent Mixtures. *Ind. Eng. Chem. Res.* **2011,** *50*, 10350-10358.

(269) Taylor, R.; Krishna, R. *Multicomponent Mass Transfer*. John Wiley & Sons: New York, USA, 1993.

(270) Ganguly, P.; van der Vegt, N. F. A. Convergence of Sampling Kirkwood–Buff Integrals of Aqueous Solutions with Molecular Dynamics Simulations. *J. Chem. Theory Comput.* **2013,** *9*, 1347-1355.

(271) Richter, J.; Leuchter, A.; Großer, N. Digital Image Holography for Diffusion Measurements in Molten Salts and Ionic Liquids - Method and First Results. *J. Mol. Liq.* **2003,** *103-104*, 359-370.

(272) Weerasinghe, S.; Smith, P. E. A Kirkwood–Buff Derived Force Field for Sodium Chloride in Water. *J. Chem. Phys.* **2003,** *119*, 11342-11349.

(273) Gee, M. B.; Cox, N. R.; Jiao, Y.; Bentenitis, N.; Weerasinghe, S.; Smith, P. E. A Kirkwood-Buff Derived Force Field for Aqueous Alkali Halides. *J. Chem. Theory Comput.* **2011,** *7*, 1369-1380.

(274) Fyta, M.; Netz, R. R. Ionic Force Field Optimization Based on Single-Ion and Ion-Pair Solvation Properties: Going Beyond Standard Mixing Rules. *J. Chem. Phys.* **2012,** *136*, 124103.

(275) Lbadaoui-Darvas, M.; Takahama, S. Water Activity from Equilibrium Molecular Dynamics Simulations and Kirkwood-Buff Theory. *J. Phys. Chem. B* **2019,** *123*, 10757-10768.

(276) Lemmon, E. W.; Huber, M. L. Thermodynamic Properties of *n*-Dodecane. *Energy Fuels* **2004,** *18*, 960-967.

(277) Logotheti, G. E.; Ramos, J.; Economou, I. G. Molecular Modeling of Imidazolium-Based [Tf_2N–] Ionic Liquids: Microscopic Structure, Thermodynamic and Dynamic Properties, and Segmental Dynamics. *J. Phys. Chem. B* **2009,** *113*, 7211-7224.

Appendix: Publications

Publication A

Giraudet, C.; Klein, T.; Zhao, G.; Rausch, M. H.; Koller, T. M.; Fröba, A. P. *Thermal, Mutual, and Self-Diffusivities of Binary Liquid Mixtures Consisting of Gases Dissolved in n-Alkanes at Infinite Dilution*. J. Phys. Chem. B **2018**, *122*, 3163-3175.

Publication B

Klein, T.; Wu, W.; Rausch, M. H.; Giraudet, C.; Koller, T. M.; Fröba, A. P. *Influence of Liquid Structure on Fickian Diffusion in Binary Mixtures of n-Hexane and Carbon Dioxide Probed by Dynamic Light Scattering, Raman Spectroscopy, and Molecular Dynamics Simulations.* J. Phys. Chem. B **2018**, *122*, 7122-7133.

Publication C

Klein, T.; Cui, J.; Kalantar, A.; Chen, J.; Rausch, M. H.; Koller, T. M.; Fröba, A. P. *Liquid Viscosity and Interfacial Tension of Binary and Ternary Mixtures Containing n-Octacosane by Surface Light Scattering*. J. Chem. Eng. Data **2019,** *64*, 817-826.

Publication D

Koller, T. M.; Yan, S.; Steininger, C.; Klein, T.; Fröba, A. P. *Interfacial Tension and Liquid Viscosity of Binary Mixtures of n-Hexane, n-Decane, or 1-Hexanol with Carbon Dioxide by Molecular Dynamics Simulations and Surface Light Scattering*. Int. J. Thermophys. **2019,** *40*, 79.

Publication E

Klein, T.; Yan, S.; Cui, J.; Magee, J. W.; Kroenlein, K.; Rausch, M. H.; Koller, T. M.; Fröba, A. P. *Liquid Viscosity and Surface Tension of n-Hexane, n-Octane, n-Decane, and n-Hexadecane up to 573 K by Surface Light Scattering*. J. Chem. Eng. Data **2019,** *64*, 4116-4131.

Publication F

Wu, W.; Klein, T.; Kerscher, M.; Rausch, M. H.; Koller, T. M.; Giraudet, C.; Fröba, A. P. *Diffusivities in 1-Alcohols Containing Dissolved H_2, He, N_2, CO, or CO_2 Close to Infinite Dilution.* J. Phys. Chem. B **2019,** *123*, 8777-8790.

Publication G

Wu, W.; Klein, T.; Kerscher, M.; Rausch, M. H.; Koller, T. M.; Giraudet, C.; Fröba, A. P. *Mutual and Thermal Diffusivities as well as Fluid-Phase Equilibria of Mixtures of 1-Hexanol and Carbon Dioxide.* J. Phys. Chem. B **2020,** *124*, 2482-2494.

Publication H

Klein, T.; Piszko, M.; Lang, M.; Mehler, J.; Schulz, P. S.; Rausch, M. H.; Giraudet, C.; Koller, T. M.; Fröba, A. P. *Diffusivities in Binary Mixtures of [AMIM][NTf_2] Ionic Liquids with the Dissolved Gases H_2, He, N_2, CO, CO_2, or Kr Close to Infinite Dilution.* J. Chem. Eng. Data **2020,** *65*, 4116-4129.

Publication I

Klein, T.; Lenahan, F. D.; Kerscher, M.; Rausch, M. H.; Economou, I. G.; Koller, T. M.; Fröba, A. P. *Characterization of Long Linear and Branched Alkanes and Alcohols for Temperatures up to 573.15 K by Surface Light Scattering and Molecular Dynamics Simulations.* J. Phys. Chem. B **2020**, 124, 4146-4163.

Publication J

Klein, T.; Piszko, M.; Kankanamge, C. J.; Kasapis, G.; Fröba, A. P. *Fick Diffusion Coefficient in Binary Mixtures of [HMIM][NTf_2] and Carbon Dioxide by Dynamic Light Scattering and Molecular Dynamics Simulations.* J. Phys. Chem. B **2021,** 125, 5100-5113.

Publication K

Klein, T.; Lenahan, F. D.; Kerscher, M.; Jander, J. H.; Rausch, M. H.; Koller, T. M.; Fröba, A. P. *Viscosity and Interfacial Tension of Binary Mixtures of n-Hexadecane with Dissolved Gases Using Surface Light Scattering and Equilibrium Molecular Dynamics Simulations.* J. Chem. Eng. Data **2021**, 66, 3205-3218.

The present thesis aims to get a fundamental understanding of how the molecular characteristics of a solute and solvent influence the thermophysical properties of mixtures consisting of a liquid and a dissolved gas. Due to their relevance as working fluids in chemical and energy engineering, accurate data for the viscosity, interfacial tension, and mutual diffusion coefficient are required for the efficient design and optimization of related processes. In this work, light scattering experiments, which can determine the thermophysical properties in macroscopic thermodynamic equilibrium, are combined with equilibrium molecular dynamics (EMD) simulations at temperatures up to 573 K. EMD simulations are able to predict multiple thermophysical properties by the analysis of the molecular motion in macroscopic thermodynamic equilibrium. The combination of EMD simulations with light scattering experiments allows for the validation of simulations as well as an interpretation of the results by studying the influence of molecular characteristics and the fluid structure on the thermophysical properties.

ISBN 978-3-96147-645-9

FAU UNIVERSITY PRESS 2023